Coupling between epidermis and amphid morphogenesis during embryonic development of *C. elegans*

von
Patricia Kunz
aus Flörsheim am Main, Deutschland

Frankfurt am Main, 2021
D 30

Vom Fachbereich 15 der

Johann Wolfgang Goethe - Universität als Dissertation angenommen.

Dekan: Prof. Dr. Sven Klimpel

Gutachter: Prof. Dr. Stefan Eimer, Prof. Dr. Alexander Gottschalk

Datum der Disputation: 05.07.2022

Declaration

I confirm that all the work presented in this thesis is my original work, including figures and tables in the text. The information derived from other sources has been indicated clearly with references. I certify that this thesis contains no material that has been submitted in the past for the award of a degree or diploma at Goethe University Frankfurt or any other university or similar institution.

Table of Contents

Summary

The amphid (AM) sensilla are the main chemosensory organs with vital roles for multiple developmental and behavioral responses throughout the *C. elegans* life cycle (reviewed in (Sengupta, 2007)). Crucial functions are detection of food sources, preventing proximity to noxious molecules and finding partners for mating. Additionally, pheromone sensation is important, facilitating developmental switches, since high pheromone concentrations and low amounts of food drive entry into a specific larval stage, called Dauer. The bilateral paired adult AM sensilla are composed of lateral nerve bundles (containing 12 bipolar ciliated sensory dendrite trajectories), interfacial AM sheath (AMsh) and socket cells (AMso) (reviewed in (Altun, Z. F. and Hall, D. H., 2010)). AMsh and AMso cells hereby enwrap the AM dendrite bundles at the sensilla ending, thus creating a channel which is opening the AM sensilla to the environmental stimuli through a pore (built by AMso). The AM neural cell bodies are positioned posterior to the nerve ring with their dendrites extending to the anterior tip of the head terminating at the lips in two-fold symmetry either within the AMsh or in the midst of the AM pore. Importantly, adherens junctions interconnect all AM cells at the sensory ending (dendrite tips:AMsh:AMso) and link them to the epidermal sheet ((Ward, S. et al., 1975), (Perkins, L. A. et al., 1986)), thus the AM sensilla are completely embedded within the epidermis. Highly fascinating is the question of how the AM sensilla organs of the adult *C. elegans* gain their extraordinarily elongated shape. This study investigates which morphogenetic and molecular events drive the embryonic morphogenesis of the AM sensilla.

Neurite morphogenesis is described to occur either actively via growth cone mediated elongation ((Tessier-Lavigne, M. and Goodman, C. S., 1996), reviewed in (Huber, A. B. et al., 2003)), retrograde extension (Heiman, M. G. and Shaham, S., 2009) or passively via towing (Gilmour, D. et al., 2004). Besides the common mode of dendrite extension mediated via the growth cone in response to positive or negative guidance signals, head sensilla dendrite extension was recently proposed to occur through retrograde extension, whereby "the presumptive dendritic tip remains stationary while the cell body migrates away..." (Heiman, M. G. and Shaham, S., 2009). Importantly, neurite elongation can also occur passively via connection of neuritic tips to a migrating target tissue which is creating a pulling force and thereby neurite extension, a mode termed towing (Gilmour, D. et al., 2004). Since epidermal migration events are a major driving force for shape changes during early embryogenesis (reviewed in (Altun, Z. F. and Hall, D. H., 2009A), (Chisholm, A. D. and Hardin, J., 2005)), the study in hands investigated if the AM dendrite morphogenesis might correlate with these events. Most common epidermal migration events are dorsal intercalation and ventral enclosure, which lead to covering of dorsal and ventral parts of the embryo's surface. Also, the head region is getting encased by epidermal cells during head enclosure. Moreover, early elongation processes drive the embryonic shape change from lima-bean to 3-fold stage, whereby the tail is getting elongated giving the embryo a worm-like character.

The study in hands investigates the events driving head sensilla morphogenesis (AM, IL, OL, CEP) and additional aspects of head morphogenesis during lima-bean to 1.5-fold embryonic stages of *C. elegans* development. Therefore high resolution live-cell imaging techniques were performed with different markers highlighting AM neural cells (*Pmir-124*), epidermis (VAB-10), sensilla pores (PAR-6), tissues with apical lumen (PAR-6), cell membranes (*Ppie-1::PH(PLCd1)*), non-muscle-myosin components (NMY-2/MLC-4) and pharyngeal cells (PHA-4). In particular, the usage of the AM neural markers *mjIs27 [mir-124p::GFP + lin-15(+)]* and *mjEx142 [mir-124p::mCherry]* (Clark, A. M. et al., 2010) allowed the specific highlighting of the developmental events of AM neural cells. Importantly, RPN-6.1 dsRNA interference was implemented via microinjection techniques, followed by microscopic long-term analysis of F1 embryos. Additionally, UV laser ablation of epidermal tissue next to AM pores or ablation of the pore tissue on one side of an embryo was conducted, to clarify the coherence between AM pore and AM dendrite migration. Also, migration distances of AM pores, length of AM dendrites and lineage-traced migration events of AM and epidermal cells were quantified according to (Sulston, J. E. et al., 1983).

The findings of this dissertation reveal that coupled migration of epidermal sheet, AM pores and AM dendrite tips is crucial for AM sensilla morphogenesis during lima-bean to 1.5-fold embryonic stages (**Figure 3.2, Figure 3.3, Figure 3.4, Figure 3.5**). This conclusion is due to the following observations: Firstly, head enclosure, AM pore migration and AM dendrite tip migration occur concomitantly. Thereby, AM pores are migrating at the leading edge of the epidermal sheet (**Figure 3.2**), AM pores migrate at the tip of AM dendrites (**Figure 3.4**) and, at the same time, AM dendrites elongate with AM neural cell bodies staying stationary. Secondly, UV-laser ablation of one AM pore per embryo strongly impairs AM dendrite elongation on that side (**Figure 3.4B, D, Figure 3.5**). Thirdly, epidermis ablation close to the AM pore leads to disconnection and arrest of the AM pore (parts) from the migrating leading edge (**Figure 3.2C, D**). Thus, cell-cell attachment of AM pores to the epidermis and dendrite tips appears as crucial aspect for AM dendrite extension. Importantly, the findings show that AM neural cell bodies are staying stationary at posterior positions, instead of translocating like AMso, AMsh or epidermal cells (**Figure 3.1B, Figure 3.4A, C**). Additionally, depletion of RPN-6.1 leads to dosage-dependent AM sensilla phenotypes (**Figure 3.6, Figure 3.7**) and intestinal phenotypes (**Figure 3.8**). These include impaired AM pore morphogenesis (stretched, torn apart, loss, **Figure 3.6**), perturbed coupling of AM pore to AM dendrite tips with imprecise spatio-temporal coordination (**Figure 3.6B**, middle bottom panels) and lack of connection between pharynx and prospective mouth (**Figure 3.8**). The author of this study suggests, that stretched and split AM pores indicate pulling forces which they experience during their translocation. Also, the AM pores (partly) disconnect from the migrating epidermis and arrest (**Figure 3.7**) after moderate RPN-6.1 depletion. Importantly, AM dendrite elongation is compromised through impaired AM pore translocation (**Figure 3.6**). Remarkably, other additional sensilla pores translocate in an anterior direction towards the prospective mouth, even when AM morphogenesis is highly impaired after strong RPN-6.1 depletion (**Figure 3.6B**, bottom panels).

Furthermore, the findings show that migration of the IL/OL/CEP sensilla pores occurs collectively towards the prospective mouth during lima-bean to 1.5-fold stage (**Figure 3.1A, Figure 3.2, Figure 3.4, Figure 3.9A**). Remarkably, IL/OL/CEP sensilla pore translocation occurs anteriorly relative to the epidermal leading edge and in constant distance to the AM pores (**Figure 3.9A**). Concurrent with anterior translocation of IL/OL/CEP sensilla pores, the results demonstrate occurrence of bottle-shaped cells (**Figure 3.9B, Figure 3.10B, Figure 3.11B**), accumulation of non-muscle-myosin components and *de novo* enrichment of apical polarity markers (NMY-2/MLC-4; PAR-6/PAR-3, **Figure 3.10, Figure 3.11B**). Remarkably, after modest RPN-6.1 depletion bottle-shape of the anterior-most cells was affected (**Figure 3.9C**), indicating a connection of proteasomal activity to regulation of this morphogenetic event.

The author of this dissertation concludes that physical connection of AM cells to the anteriorly migrating epidermis is crucial for efficient AM dendrite extension. It is known that *C. elegans* apical junctions (CeAJ) are present between AM cells and epidermis ((Ward, S. et al., 1975), (Perkins, L. A. et al., 1986)). Also, recent studies suggest that "these neurons and glia can be viewed as part of an epithelium continuous with the skin, and are shaped by mechanisms shared with other epithelia" (Low, I. I. et al., 2019). Thus the author of this study concludes that the physical attachment of AM pores to epidermis and interconnection of AM cells is enabled by apical junctions. Additionally, the results show that anterior migration of the epidermal sheet is encasing the anterior region of the embryos head, which is confirmed by very recent findings (Grimbert, S. et al., 2020). The author of the study in hands thereby suggests, that anterior epidermis migration drives the translocation of AM pores, which are attached to the epidermal sheet and AM dendrite tips by CeAJ. Thus, anterior migration of the AM pore pulls attached AM dendrite tips anteriorly, while AM neural cell bodies stay posteriorly and AM dendrite tips get elongated by pulling forces. Hence, the conclusion is made that AM dendrite elongation is facilitated by dendrite towing according to ((Gilmour, D. et al., 2004) **Figure 0.1A**), which is driven by head enclosure. Other studies proposed that head sensilla morphogenesis would ensue via retrograde extension (Heiman, M. G. and Shaham, S., 2009). However, recent findings are in stark contrast to this proposed model, suggesting that "…the initial extension of the amphid dendrites is driven by the migrating skin through physical attachment " (Fan, L. et al., 2019). Clearly, the latter description closely resembles the conclusion of AM dendrite extension being facilitated by dendrite towing, which is driven by epidermal head enclosure. Additionally, this study shows that the translocation of the additional IL/OL/CEP head sensilla pores ensues independently of AM sensilla morphogenesis, suggesting apical constriction as a driving force (**Figure 0.1B**). This is due to the fact that bottle-shaped/wedged-shaped cells occur during apical constriction-driven events of gastrulation in *Xenopus laevis* ((Hardin, J. and Keller, R., 1988), reviewed in (Lee, J. Y. and Harland, R. M., 2007)) or during neural tube formation in mammals (Moore, D. C. P. et al., 1987), inferring that apical constriction rather than the previously described formation of cellular rosettes (Fan, L. et al., 2019) contribute to IL/OL/CEP pore translocation.

Also, accumulation of non-muscle-myosin components and apical polarity factors at the anterior most part of the head add more evidence to the suggestion that apical constriction contributes to translocation of the IL/OL/CEP sensilla pores. Moreover, *de novo* collective apical constricting arcade and neural cells were identified at the region close to the prospective mouth, thus leading to the conclusion that collective apical constriction within these cells also facilitates early pharynx development. Besides head enclosure and apical constriction facilitating AM and IL/OL/CEP sensilla morphogenesis during lima-bean to 1.5-fold stage, also diverse additional tissues develop within the embryo's head. Either the development of pharyngeal cyst to pharyngeal tube (Portereiko, M.F. and Mango, S.E., 2001) or the establishment of the nerve ring (reviewed in (Altun, 2017)) ensue within the developing head. The author of this dissertation thereby assumes, that diverse developing tissues within the head during this stage might possibly slightly push AM neural cells in posterior direction after executed AM dendrite towing.

Moreover, this dissertation reveals that the main proteasome activator RPN-6.1 (Pathare, G. R. et al., 2012) enables separation of head enclosure-driven AM sensilla morphogenesis via dendrite towing, from apical constriction-facilitated translocation of IL/OL/CEP sensilla pores, because dosage-dependent depletion of RPN-6.1 has a stronger effect on the first. This study concludes, that RPN-6.1 plays an important role for correct AM pore morphogenesis, precise spatio-temporal coordination of AM pore to AM dendrite tip attachment and AM pore to epidermis coupling, eventually facilitating AM dendrite towing. RPN-6.1 also seems to play a role for correct cell-cell attachment between pharynx and prospective mouth and apical lumen development of the intestine.

Furthermore, this study hypothesizes that the apical extracellular matrix (aECM) components DYF-7 (ZP like domain) and DEX-1 (zonadhesin like domain) (Heiman, M. G. and Shaham, S., 2009) might contribute to AM pore morphogenesis and its attachment to AM dendrite tips, thereby facilitating AM dendrite towing. This is due to following reported findings: Firstly, DYF-7 and DEX-1 are suggested to mediate attachment of AM dendrite tips to the anterior part of the head (Heiman, M. G. and Shaham, S., 2009). Secondly, DYF-7 seems to contribute to AM channel morphogenesis (Low, I. I. et al., 2019) and attachment of AM dendrites to epithelial cells (Fan, L. et al., 2019). Thirdly, DEX-1 was shown to be of importance for excretory pore morphogenesis (resembling AM pore) (Cohen, J. D. et al., 2018). Since recent findings suggest that the CeAJ components DLG-1 and HMR-1 seem to aid in attaching AM dendrites to the epidermis (Fan, L. et al., 2019), the study in hands reasons that they might contribute to interconnect epidermis, AM pore and AM dendrite tips and thereby assist AM dendrite towing. Also, SAX-7 expression occurs all through the AM dendrites (Fan, L. et al., 2019), functions in AM dendrite fasciculation (Yip, Z. C. and Heiman, M. G., 2018) and is suggested to assist dendrite development of another neuron (PVD) ((Salzberg, Y. et al., 2013), (Dong, X. et al., 2013)). This study therefore assumes that SAX-7 could contribute to AM sensilla morphogenesis.

In addition to cell-cell adhesion molecules, also the apical polarity factor PAR-6 might contribute to AM dendrite towing. This assumption was made because the PAR-6 expression pattern was found to resemble DYF-7 expression (Fan, L. et al., 2019) and the author of this dissertation hypothesizes that PAR-6 may act upstream of DYF-7. Remarkably, the study showed impaired AM pore morphogenesis and translocation (marked by PAR-6) after RPN-6.1 depletion (**Figure 3.6B**). The author of the study in hands considers that RPN-6.1 may affect PAR-6 and thereby might be influencing AM pore morphogenesis (possibly through DYF-7 activity). Since PAR-6 is part of the aPAR-complex, which has major roles for apicobasal cell polarity (reviewed in (Von Stetina, S. and Mango, S. E., 2015)), it may aid in correct AM pore apical lumen establishment. Interestingly, also diverse UPS factors have been reported to act upon neuronal development (reviewed in (Hamilton, A. M. and Zito, K., 2013), thus RPN-6.1 might maybe act accordingly.

In summary, the study in hands reveals two force-generating events: On the one hand head enclosure-driven AM sensilla morphogenesis via dendrite towing and, on the other hand, apical constriction-facilitated translocation of additional head sensilla pores. These events occur concurrently with collective *de novo* apical constriction, which seems to create the pharynx-mouth connection and can get separated by setting different thresholds of UPS-mediated protein degradation. Altogether, dendrite towing and apical constriction events enable major morphogenetic developmental aspects of embryonic neuromorphogenesis.
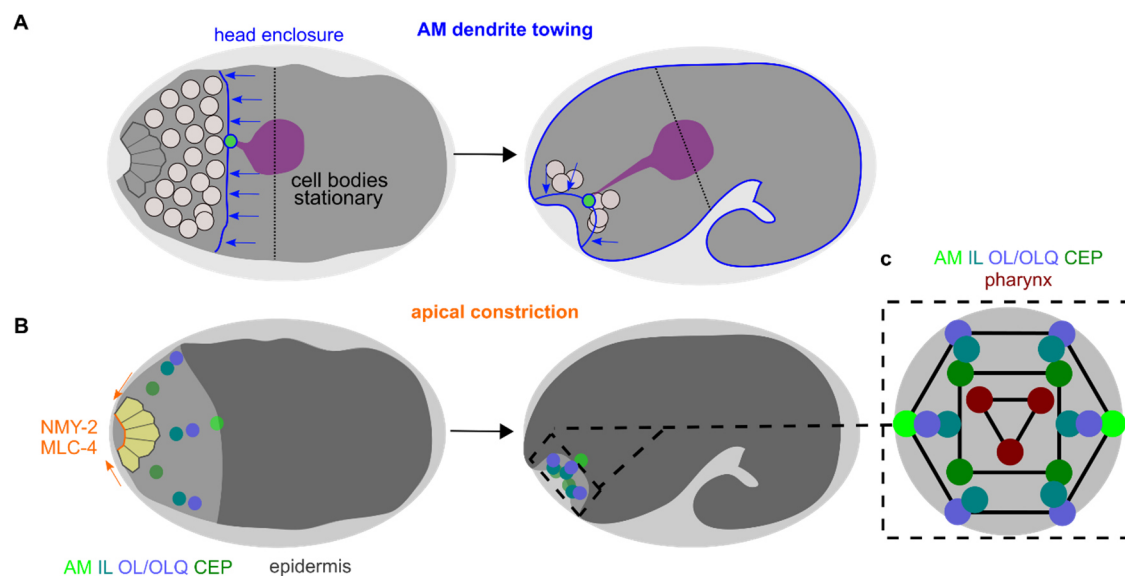
Figure 0.1: Head enclosure drives AM morphogenesis and apical constriction facilitates morphogenesis of IL/OL/CEP sensilla
Schematic illustration depicting morphogenetic events facilitating sensilla morphogenesis in the *C. elegans* embryo. **A**: Epidermal head enclosure facilitates dendrite towing and thus AM sensilla morphogenesis. **B**: Apical constriction contributes to migration of inner labial (IL), outer labial (OL) and cephalic (CEP) sensilla organ cells. **C**: Symmetric positioning of sensilla endings and the pharynx from head-on view. Modified from (Kunz, P. et al., 2021).

Zusammenfassung

Die Amphiden (AM) sind bedeutsame chemosensorische Organe (Sensillen) mit diversen essenziellen Funktionen bezüglich der Entwicklung und des Verhaltens von *C. elegans* (Sengupta, 2007). Hierzu zählen lebensnotwendige Verhaltensweisen wie die Suche nach Futterquellen, das Vermeiden von Gefahrenquellen und das Auffinden von Sexualpartnern, welche durch die Detektion chemosensorischer Reize gesteuert werden. Zudem werden anhand der Rezeption bestimmter Pheromonkonzentrationen spezifische Entwicklungsschritte gesteuert, wie z.B. das Eintreten in das larvale Dauerstadium. Die paarweise angelegten AM-Sensillen bestehen aus je einem lateral verlaufenden Nervenbündel pro Kopfseite, welches jeweils 12 bipolare, ciliierte, sensorische Dendriten beinhaltet (Altun, Z. F. and Hall, D. H., 2010). Die ciliierten Enden der AM-Dendriten werden distal von einer AM-Sockelzelle (AMso) umwickelt, wodurch eine Pore entsteht und der AM-Sensille der Kontakt zu Umweltreizen eröffnet wird. Angrenzend an die Pore umwickelt die AM-Scheidezelle (AMsh) die weiter proximo-distal gelegenen Bereiche der Dendritenden, sodass ein kontinuierlicher AM-Kanal die Enden der AM-Dendriten umgibt. Die Zellkerne der AM-Neuronen befinden sich posterior vom Nervenring, wobei die AM-Dendriten sich über eine verhältnismäßig große Distanz gruppiert in Nervenbündeln bis zur AM-Pore neben der Mundöffnung erstrecken und dort in zweifacher Symmetrie terminieren. Von Bedeutung für die vorliegende Arbeit ist insbesondere, dass die AM-Sensille gänzlich in die Epidermis eingebettet ist, wobei alle Kompartimente des proximalen Endes der Sensille untereinander und mit der Epidermis über *C. elegans* Adhäsionsverbindungen (CeAJ) verbunden sind ((Ward, S. et al., 1975), (Perkins, L. A. et al., 1986)). Eine besondere Eigenschaft der AM-Sensillen ist die spezielle elongierte Form im adulten *C.elegans*. Die vorliegende Dissertation erörtert die Frage, wie sich die AM-Sensillenmorphogenese während der Embryonalentwicklung gestaltet und diskutiert welche morphogenetischen und molekularen Faktoren die AM Entwicklung hierbei initiieren und regulieren.

Nach aktuellem Kenntnisstand erfolgt die neuronale Morphogenese häufig durch aktiv-neuronal gesteuerte Elongation, beispielsweise reguliert durch einen Wachstumskegel, welcher in Reaktion auf positive oder negative Wachstumssignale die neuronale Elongation manövriert ((Tessier-Lavigne, M. and Goodman, C. S., 1996), (Huber, A. B. et al., 2003)). Auch der kürzlich beschriebene Vorgang der retrograden Verlängerung beschreibt die aktive Migration von neuralen Zellkörpern in Verbindung mit der Verknüpfung zugehöriger Dendritenden am anterioren Bereich des Kopfes (Heiman, M. G. and Shaham, S., 2009). Im Kontrast zu solchen aktiv gesteuerten neuronalen Elongationsprozessen können Neuronen auch passiv elongiert werden. Dies erfolgt durch die Verknüpfung der Neuronen mit nicht-neuronalen Geweben, welche Migrationsbewegungen durchlaufen, wodurch Zug-/Spannungskräfte entstehen, welche schließlich die Elongation der Neuronen ermöglichen.

Dieser passive Modus der neuralen Elongation wurde als Schleppen („towing") definiert und erfolgt z.B. während der Entwicklung des Seitenlinienorgans in *Danio rerio* ((Metcalfe, 1985), (Gilmour, D. et al., 2004)) oder vermutlich während der Entwicklung von Kopulations-Spiculae in männlichen *C. elegans* (Jiang, L. I. and Sternberg, P. W., 1999).

Die Epidermis ist von großer Wichtigkeit für die embryonale Morphogenese von *C. elegans*. Denn einerseits ermöglicht die Epidermis die Veränderung der gesamten embryonalen Gestalt von einem bohnenförmigen Stadium („lima-bean stage") zu einer stärker elongierten, wurmförmigen Gestalt („comma to 1.5-fold stages") (Chisholm, A. D. and Hardin, J., 2005). Darüber hinaus führen epidermale Migrationsbewegungen zur Umschließung der dorsalen („dorsal intercalation") und ventralen Bereiche („ventral enclosure") des Embryos und zur Umhüllung des Kopfbereiches („head enclosure") ((Chisholm, A. D. and Hardin, J., 2005), (Altun, Z. F. and Hall, D. H., 2009A)).

Die vorliegende Dissertation untersucht, inwiefern epidermale Migrationsbewegungen im Kopfbereich zur Morphogenese der AM-Sensillen beitragen, da die AM-Sensillen in die Epidermis eingebettet sind. Außerdem werden Erkenntnisse zur Morphogenese der inneren labialen Sensillen (IL), der äußeren labialen Sensillen (OL) und der cephalischen Sensillen (CEP) dargelegt, welche ebenfalls um den Mund des adulten *C. elegans* angeordnet sind (Altun, Z. F. and Hall, D. H., 2010). Darüber hinaus werden Erkenntnisse zur Entwicklung des Pharynx analysiert und weitere Aspekte der embryonalen Kopfentwicklung von *C. elegans* erörtert.

Für die Untersuchung der embryonalen Morphogenese der AM-Sensillen und anderer Sensillen der Kopfregion (IL, OL, CEP), wurden mikroskopische Langzeitaufnahmen aus verschiedenen Perspektiven mithilfe eines hochauflösenden Mikroskops nach dem Nipkow-Scheiben-Prinzip zwischen „lima-bean" und „1.5-fold" Stadien durchgeführt. Hierfür wurden diverse Marker zur Visualisierung der AM-Neuronen (*Pmir-124*), der Epidermis (VAB-10), der Sensillenporen und weiterer Gewebe mit apikalem Lumen (PAR-6), den Zellmembranen (*Ppie-1::PH(PLCd1)*), Komponenten des Zytoskeletts, welche intrazytoplasmatische Kräfte erzeugen (nicht-Muskel Myosin, NMY-2/MLC-4) und Zellen des Pharynx (PHA-1) verwendet. Hierbei ermöglichte insbesondere die Verwendung des spezifischen Markers für die AM-Neuronen *mjIs27 [mir-124p::GFP + lin-15(+)]* und *mjEx142 [mir-124p::mCherry]* (Clark, A. M. et al., 2010) die präzise Analyse der Entwicklung der AM-Sensillen. Zudem wurde *rpn-6.1* RNA-Interferenz mittels Mikroinjektionstechniken realisiert und Embryonen der F1 Generation nachfolgend durch Langzeitmikroskopie untersucht. Eine weitere verwendete Technik ist die UV-Laser-Ablation, welche entweder direkt an der Stelle je einer AM-Pore oder in direkter Nähe zu je einer AM-Pore an epidermalem Gewebe einseitig angewendet wurde. Zudem wurden Messungen der Migrationsbewegungen der AM-Poren, der Länge der AM-Neuronen und Zellstammbaumverfolgung aller AM-Zellen und bestimmter epidermaler Zellen vorgenommen (in Anlehnung an (Sulston, J. E. et al., 1983)).

Die vorliegende Arbeit bringt die Erkenntnis zutage, dass die gleichzeitige Migrationsbewegung der Epidermis, der AM-Pore und der AM-Dendritenden entscheidend für die korrekte Morphogenese der AM-Sensillen während der „lima-bean" bis „1.5-fold" Embryonalstadien ist (**Figure 3.2, Figure 3.3, Figure 3.4, Figure 3.5**). Diese Schlussfolgerung beruht auf den folgenden in dieser Arbeit gewonnenen Ergebnissen: Epidermale Kopfumschließung erfolgt gleichzeitig mit der Migration der AM-Pore und der AM-Dendritenden. Hierbei erfolgt die Migration der AM-Pore gemeinsam mit der migrierenden anterioren Epidermisgrenze (**Figure 3.2**) sowie an der Spitze der AM-Dendriten (**Figure 3.4**). Zudem werden zur gleichen Zeit AM-Dendriten elongiert, während die zugehörigen neuralen Zellkörper stationär positioniert verbleiben. Hinzu kommt, dass UV-Ablation einer Pore die Elongation der AM-Dendriten auf dieser Kopfseite stark beeinträchtigt (**Figure 3.4B, D, Figure 3.5**). Einseitige UV-Ablation der Epidermis im Bereich der Pore zieht die Ablösung der Pore von der Epidermis und das Arretieren dieser Pore (Teile der Pore) nach sich (**Figure 3.2C, D**). Folglich ist die kontinuierliche interzelluläre Verknüpfung zwischen der Epidermis, der AM-Pore und den AM-Dendritenden ein entscheidender Faktor für die erfolgreiche Elongation der AM-Dendriten. Von besonderer Bedeutung ist die Erkenntnis, dass die neuronalen Zellkörper der AM-Neuronen stationär an posterioren Positionen verbleiben und nicht nach anterior migrieren, im Gegensatz zu allen anderen AM-Zellen (AMo, AMsh) und epidermalen Zellen (**Figure 3.1B, Figure 3.4A, C**). Nach RPN-6.1 Depletion weisen die untersuchten Embryonen AM-Sensillen- (**Figure 3.6, Figure 3.7**) und intestinale Phänotypen (**Figure 3.8**) verschiedenen Grades auf. Hierzu zählen die veränderte Morphogenese der AM-Pore (langgezogen, außeinander gerissen, Verlust, **Figure 3.6**), raumzeitlich unpräzise Verknüpfung zwischen AM-Pore und AM-Dendritenden (**Figure 3.6B**, Mitte unten) sowie die fehlende Verbindung zwischen Mundöffnung und Pharynx (**Figure 3.8**). Das Auftreten stark langgezogener und außeinander gerissener AM-Poren legt die Vermutung nahe, dass AM-Poren während der Migration zum zukünftigen Mund starken Zugkräften unterliegen. Hinzu kommt, dass die AM-Poren (in Teilen) von der migrierenden Epidermis dissoziieren und arretieren, nachdem RPN-6.1 moderat depletiert wurde (**Figure 3.7**). Des Weiteren ist die Erkenntnis essenziell, dass, sobald die Migration der AM-Pore beeinträchtigt wird, zugleich die Elongation der AM-Dendriten fehlerhaft ist. Bemerkenswerterweise erfolgt die Migration weiterer Poren von im Kopf befindlichen Sensillen (IL/OL/CEP) unbeeinträchtigt der RPN-6.1 Depletion (**Figure 3.6B**, unten) obwohl gleichzeitig die Morphogenese der AM-Sensillen fehlerhaft ist.

Neben der Untersuchung der AM-Morphogenese analysiert die vorliegende Arbeit Teilaspekte der Morphogenese der IL, OL und CEP Sensillen und der Pharynxentwicklung in "lima-bean" bis "1,5-fold" Embryonalstadien (**Figure 3.1A, Figure 3.2, Figure 3.4, Figure 3.9A**). Die Ergebnisse zeigen kollektive juxtaorale Migration der Poren dieser Kopfsensillen anterior der epidermalen Kante im deutlichen Abstand zu den migrierenden AM-Poren (**Figure 3.9A**).

Gleichzeitig mit dieser kollektiven Migration sind Veränderungen der Zellform zur Trichterform in den am meisten anterior gelegenen Zellen sichtbar (**Figure 3.9B, Figure 3.10B, Figure 3.11**). Zudem treten Faktoren, die intrazelluläre Zugkräfte und apikale Polarität erzeugen, *de novo* auf (NMY-2/MLC-4; PAR-6/PAR-3, **Figure 3.10, Figure 3.11**). Nach RPN-6.1 Depletion ist in einigen Fällen diese Zellformänderung beeinträchtigt (**Figure 3.9C**).

Die vorliegende Arbeit schlussfolgert anhand der oben aufgeführten Ergebnisse, dass die Kopfumschließung die primäre Triebkraft für die AM-Dendritenelongation darstellt, da die Epidermis durch Adhäsionsverbindungen in physischer Verbindung zu allen Zellen der AM-Sensillen steht (Hyp:AMso:AMsh:Dendritenden) ((Ward, S. et al., 1975), (Perkins, L. A. et al., 1986)). Auch kürzlich veröffentlichte Studien ordnen Sensillen als Teil der Epidermis ein und vermuten Gemeinsamkeiten bei der Morphogenese (Low, I. I. et al., 2019). Darüber hinaus wird der in vorliegender Arbeit dokumentierte Vorgang der Kopfumschließung durch aktuelle Ergebnisse zur Entwicklung der anterioren Kopfregion bekräftigt (Grimbert, S. et al., 2020). Eindeutig ist die neuronale Elongation der AM-Sensillen dem morphogenetischen Mechanismus Schleppen von Dendriten ("dendrite towing") zuzuordnen, welcher auf der Definition durch (Gilmour, D. et al., 2004) basiert (**Abbildung 0-1A**). Diese Kategorisierung erfolgt in vorliegender Arbeit, da die AM-Dendritenelongation durch die physisch (durch CeAJ) gekoppelte Migration der AM-Pore erfolgt, welche in der Epidermis eingebettet ist und deren Migration durch die Kopfumschließung initiiert wird. Von besonderer Bedeutung ist hierbei, dass die AM-Neuronen Zellkörper stationär an posteriorer Position verbleiben, während alle durch CeAJ verknüpften AM-Zellen nach anterior migrieren. Durch die Translokation der Epidermis mitsamt der AM-Pore, welche mit der Epidermis und den AM-Dendritenden verknüpft ist, entsteht eine Zugkraft, welche schließlich zur Elongation der AM-Dendriten führt. Nennenswert ist, dass andere Studien die Morphogenese von Sensillen durch retrograde Verlängerung beschreiben. Hierbei wurde erläutert, dass die Dendritenden am anterioren Ende des Kopfes verknüpft werden, sich die neuralen Zellkörper nach posterior bewegen und hierdurch die Dendriten elongieren (Heiman, M. G. and Shaham, S., 2009). Im Gegensatz zu dieser Annahme schlussfolgern aktuelle Studien derselben Arbeitsgruppe, dass Migrationsbewegungen der Epidermis die frühe Elongation der AM-Dendriten initiieren (Fan, L. et al., 2019). Diese Erkenntnis stimmt mit den Ergebnissen der vorliegenden Arbeit überein. Die AM-Dendriten-Elongation ist folglich in dieser Dissertation als Schleppen von Dendriten kategorisiert.

Des Weiteren kommt die vorliegende Dissertation zu dem Ergebnis, dass apikale Konstriktion zur Migration der Poren von IL-, OL- und CEP-Sensillen maßgeblich beiträgt (**Abbildung 0-1B**). Diese Schlussfolgerung beruht auf den Erkenntnissen, dass Trichterform in anterior positionierten Zellen gemeinsam mit dem Auftreten von apikaler Polarität (PAR-6) und unter Anreicherung von Komponenten zur Erzeugung intrazellulärer Zugkräfte (NMY-2, MLC-4) sichtbar ist. Zur selben Zeit ist die Migration der Sensillenporen zu erkennen.

Die beobachteten trichterförmigen Zellen treten ebenfalls während der Gastrulation von *Xenopus laevis* ((Hardin, J. and Keller, R., 1988), (Lee, J. Y. and Harland, R. M., 2007)) und während der Neuralrohr-Entwicklung in Mammalia auf (Moore, D. C. P. et al., 1987). Des Weiteren sind apikale Polaritätsfaktoren für die Entstehung der apikal-basalen Zellpolarität von Bedeutung (Von Stetina, S. and Mango, S. E., 2015). Zudem werden nicht-Muskel Myosin-Komponenten zur apikalen Konstriktion benötigt (Sawyer, J. M. et al., 2010). Es wird demnach in vorliegender Arbeit geschlussfolgert, dass apikale Konstriktion zur Trichterform in anterioren Zellen führt und hiermit zur kollektiven Migration der IL, OL und CEP Sensillen-Poren beiträgt und hierfür eher nicht Rosetten ursächlich sind (Fan, L. et al., 2019). Zudem wurde kollektive *de novo* apikale Konstriktion in den sogenannten Arkaden-Zellen des Pharynx festgestellt ((Mango, 2007), (Altun, Z. F. and Hall, D. H., 2009B)). Diese Arkaden-Zellen nehmen nachfolgend eine Trichterform an und verbinden vermutlich Mundöffnung und Pharynx. Es wird folglich die Hypothese aufgestellt, dass apikale Konstriktion auch zur frühen Entwicklung des Pharynx beiträgt.

Des Weiteren kommt diese Arbeit zu dem Schluss, dass durch Dosis-abhängige Depletion von RPN-6.1, welcher als der Haupt-Aktivator des 26S-Proteasoms beschrieben wurde (Pathare, G. R. et al., 2012), die Morphogenese der AM-Sensillen (verursacht durch die Umschließung des Kopfbereiches) von der Migration der IL, OL und CEP-Sensillen-Poren (begünstigt durch apikale Konstriktion) separiert werden kann. Denn die Migration der IL/OL/CEP-Sensillen erfolgt ungehindert, trotz RPN-6.1 Depletion. Darüber hinaus wird vermutet, dass RPN-6.1 eine wichtige Rolle für die korrekte Morphogenese der AM-Poren spielt und zur präzisen raumzeitlichen Koordination der Verknüpfung von AM-Pore und AM-Dendritenden beiträgt. Auch scheint RPN-6.1 für die Zell-Zell-Verknüpfung zwischen Mund und Pharynx von Bedeutung zu sein.

Neben der AM-Morphogenese (durch epidermal initiiertes Schleppen der Dendrite) und der Translokation der IL-, OL- und CEP-Sensillenporen (Einfluss von apikaler Konstriktion), erfolgen vielerlei weitere Migrationsbewegungen während der embryonalen Kopfentwicklung. Mitunter findet die Entwicklung der Pharynx-Zyste zum elongierten Pharynx statt (Portereiko, M. F. and Mango, S. E., 2001) und der Nervenring entsteht (Altun, 2017). Es wird in vorliegender Arbeit vermutet, dass diese unterschiedlichen Migrationsbewegungen während der Kopfentwicklung möglicherweise eine leichte posteriore Verschiebung der AM-Neuronen Zellkörper nach sich ziehen könnten, nachdem die Elongation der AM-Dendriten durch Schleppen von Dendriten erfolgte.

Schlussendlich lässt sich zusammenfassen, dass die vorliegende Arbeit zwei separate morphogenetische Vorgänge während der embryonalen Kopfentwicklung aufdeckt: Einerseits die epidermale Umschließung der Kopfregion, welche die Morphogenese der AM-Sensillen durch "dendrite towing" ermöglicht. Andererseits die kollektive *de novo* apikale Konstriktion, welche die Migration der IL-, OL- und CEP-Sensillenporen sowie die frühe Pharynxentwicklung begünstigt. Diese morphogenetischen Aspekte können durch graduelle Aktivierung des UPS separiert werden und tragen maßgeblich zur embryonalen Kopfentwicklung von *C. elegans* bei.
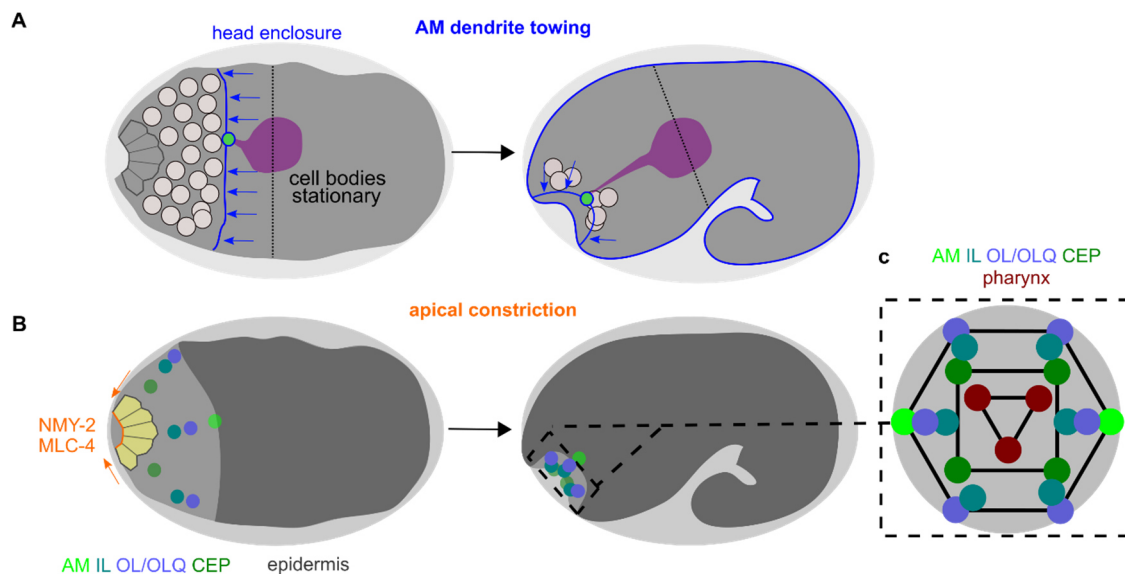
Abbildung 0-1: AM Morphogenese durch epidermale Umschließung des Kopfes und Einfluss von apikaler Konstriktion auf die Morphogenese von Sensillen im Kopfbereich von *C. elegans*

Schema zur Illustration der morphogenetischen Einflüsse von der Umschließung des Kopfes durch Epidermis und dem Einfluss von apikaler Konstriktion auf die Morphogenese von Sensillen im Kopf von *C. elegans* Embryonen. **A:** Epidermale Bedeckung des Kopfbereiches führt zu „dendrite towing" und hierdurch die Morphogenese der Amphidsensillen (AM). **B:** Apikale Konstriktion führt zur Migration von Zellen der inneren Labialen (IL), äußeren Labialen (OL) und cephalen (CEP) Sensillen. **C:** Symmetrische Verteilung der Sensillen-Enden und des Pharynx aus anteriorer Ansicht. Bearbeitet nach (Kunz, P. et al., 2021).

1. Introduction

1.1. *C. elegans* embryonic development – A brief summary

The nematode *Caenorhabditis elegans* (*C. elegans*) is an ideal model system for the investigation of neurodevelopmental aspects during embryogenesis regarding anatomical, cell biological and molecular processes (reviewed in (Altun, Z. F. and Hall, D. H., 2009)). Using *C. elegans* as a model system has multiple advantages: simple and fast propagation, long-term storage through freezing and a compact genome. However, for this study mainly the following two characteristics are highly beneficial: Firstly, the stereotypical development of *C. elegans* can be easily observed in great detail due to its transparent body through live imaging. Secondly, high numbers of progeny after genetic crosses or injection of double-stranded RNA (dsRNA) enable the rapid analysis of genetic manipulations. Also, culturing methods, the complete cell lineage, the worm's neuronal anatomy and life cycle are described in great detail ((Brenner S. , 1973), (Byerly, L. et al., 1976), (Sulston, J. E. et al., 1983), (White, J. G. et al., 1986), (Wood W. B., 1988a), (Lewis, J. A. and Fleming, J. T., 1995)). Thus, thorough investigation of sensory organ morphogenesis is highly tractable in *C. elegans* embryos.

During the *C. elegans* life cycle, the embryonic stages are followed by four larval stages (L1-L4) and eventually the development into the adult animal (reviewed in (Altun, Z. F. and Hall, D. H., 2009)). The embryonic development of *C. elegans* is subdivided into phases of proliferation and morphogenesis ((Sulston, J. E. et al., 1983), (reviewed in (Hall, D.H. et al., 2017) **Figure 1.1**). Throughout the embryonic proliferation phase (0 to ~330/350 min after fertilization at 20-22°C) approx. 550 cells emerge through 9 to 10 rounds of cell divisions ((Wood W. B., 1988b), (reviewed in (Hall, D.H. et al., 2017)). During the early proliferation phase 1 (0 to ~150 min after fertilization), development of the zygote and creation of the embryo's founder cells occurs (reviewed in (Hall, D.H. et al., 2017)). Thereafter, during the proliferation phase 2, the majority of cell divisions and gastrulation until the start of organogenesis/morphogenesis are taking place (~150 to 350 min after fertilization). Throughout the proliferation phase, cells move only short distances, through re-allocation of space by neighboring cell divisions or through polarization of the cell division planes. Explicit migration of cells occurs during gastrulation (~150 to 330 min after fertilization). Hereby, two endodermal founder cells, Ea and Ep, are internalized on the ventral side of the embryo (~150 min after fertilization), thereafter P4 and MS cells move inside (~200 to 250 min after fertilization), followed by C and D cells and pharynx progenitors (AB cells). After these migration events, ventral cleft closure occurs (~270 to 330 min after fertilization). After gastrulation (~330 min after fertilization) and beginning with lima-bean stage (~360 min after fertilization), the embryonic organogenesis/morphogenesis takes place (330-360 min to 720-840 min after fertilization) (reviewed in (Hall, D.H. et al., 2017) **Figure 1.1**).

Throughout embryonic morphogenesis, most cells acquire their final specific structures, become arranged in tissue subgroups, organs get fully differentiated and the embryo elongates threefold (reviewed in (Hall, D.H. et al., 2017)). During final tissue differentiation, cell proliferation has mainly ceased and many migration events occur. During the embryo's development, its form changes from bean-like to worm-like shape through elongation (**Figure 1.1**). Early elongation begins after epidermal enclosure (~400 min after fertilization). After the lima-bean stage (~360 min after fertilization), the embryo is categorized as comma stage (~430 min after fertilization), 1.5-fold stage (~460 min after fertilization), 2-fold stage (~490 min after fertilization) and 3-fold stage (~550 min after fertilization) according to its elongated form. Of major importance for this study hereby are the lima-bean, comma and 1.5-fold stages (reviewed in (Hall, D.H. et al., 2017)).
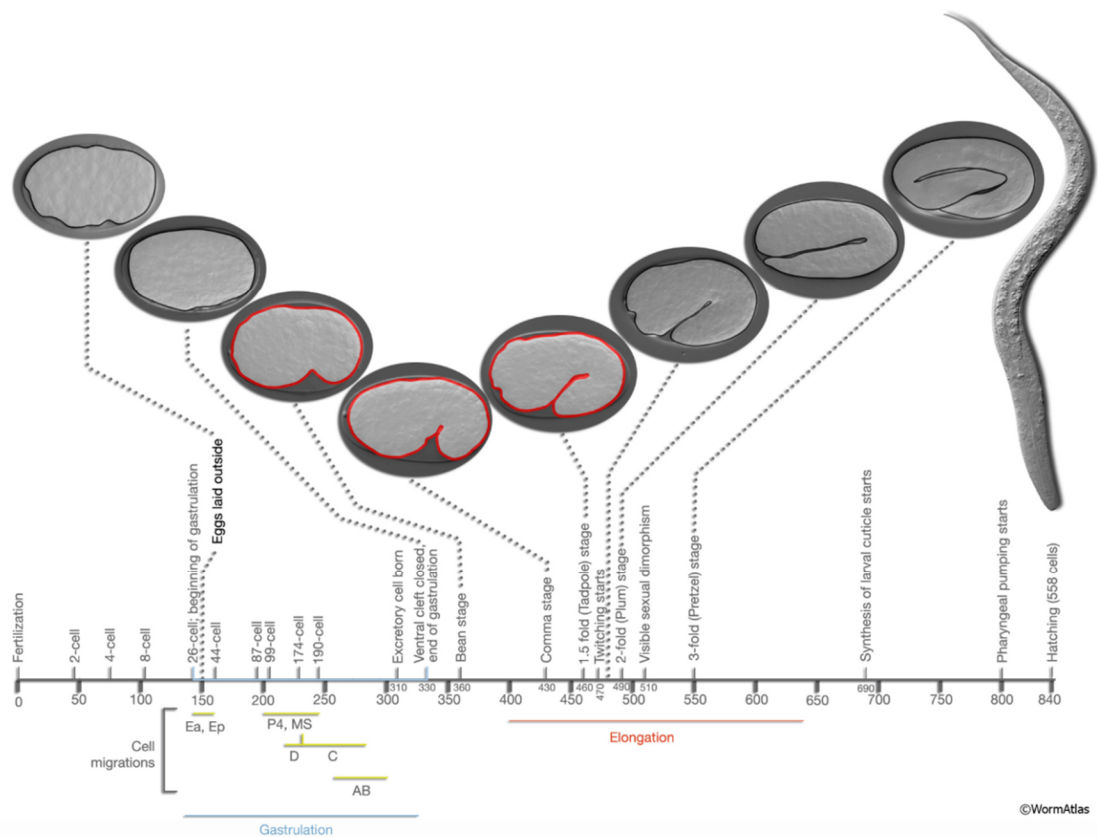
Figure 1.1: Schematic illustration of *C.elegans* embryonic developmental stages
Timeline shows approx. time (min) post fertilization. Gastrulation (blue) occurs between ~150 to 330 min, whereby cell migrations start at 150 min. Elongation (red) is taking place between 400 to 640 min. Organogenesis/Morphogenesis occurs at 330-360 min to 720-840 min. During elongation, the developing embryo gets categorized into comma stage (430 min), 1.5-fold stage (460 min), 2-fold stage (490 min) and 3-fold stage (550 min). Embryos at lima-bean stage, comma stage and 1.5-fold stage highlighted (red) as pivotal stages for this study. (Modified from (Hall, D.H. et al., 2017)).

1.2. Epithelial cells and epidermal morphogenesis in *C. elegans*

The morphogenesis of the *C. elegans* one-layered epidermis (also called hypodermis) fundamentally influences the shape of the developing embryo (reviewed in (Chisholm, A. D. and Hardin, J., 2005)). During its morphogenesis, the epidermis undergoes diverse migration events and interacts with underlying tissues like neuroblasts. The epidermis is categorized into epidermal cells (hyp cells) and specialized epithelial cells (reviewed in (Altun, Z. F. and Hall, D. H., 2009A)). Cellular junctions are positioned at apical borders interlinking neighboring cells and separating each cell into an apical and basolateral section. The basal lamina covers basal surfaces of epithelia and the cuticle, which is secreted only after completion of embryogenesis, is positioned at the apical part. Epidermal cells include the main hyp7 precursors, anterior epidermal precursor cells at the head region (hyp1 to hyp5) and epidermal precursor cells of the tail region (hyp8 to hyp11) (reviewed in (Chisholm, A. D. and Hsiao, T. I., 2012) **Figure 1.2A**). At the 1.5-fold embryonic stage, ventral hyp7 precursors, hyp6 precursors and the pocket (P1-P12) cells are present.

Besides epidermal cells, also specialized epithelial cells are present (Altun, Z. F. and Hall, D. H., 2009A). They are subdivided into interfacial epithelial cells, seam cells, and atypical epithelial cells. Firstly, seam cells (H0-H2, V1-V6 and T, **Figure 1.2A**) are forming a lateral line of cells on each side of the embryo (reviewed in (Altun, Z. F. and Hall, D. H., 2009D)). These cells are suggested to facilitate embryonic elongation of the epidermis. Within the adult worm, seam cells develop into cuticular specifications (lateral alae). Secondly, socket and sheath neuronal support cells (**Figure 1.3.**), arcade cells and epithelial cells of the buccal cavity (**Figure 1.4**) are important examples for interfacial epithelial cells (reviewed in (Altun, Z. F. and Hall, D. H., 2009B)). Interfacial epithelial cells are mostly located at epidermal openings and connect epidermal cells to different neighboring tissues. Interestingly, atypical XXX cells translocate anteriorly during embryonic stages (reviewed in (Altun, Z. F. and Hall, D. H., 2009C)) and are thus of interest for this study. The post-embryonic epidermal sheet is characterized by widespread syncytial character, which is established through fusion events of epidermal cell precursors (reviewed in (Chisholm, A. D. and Hsiao, T. I., 2012)).

a. Epidermal migration and elongation

For the establishment of the correct epidermal sheet architecture in the embryo, three major migration events need to occur (**Figure 1.2**): Those are dorsal intercalation (**B**), ventral enclosure (**C**) and head enclosure (**D**) (reviewed in (Altun, Z. F. and Hall, D. H., 2009A), (Chisholm, A. D. and Hardin, J., 2005)). Moreover, the final state of the embryonic epidermis is created through elongation procedures and the fusion of epidermal and seam cells establishing syncytial sheets.

The first migration event of epidermal morphogenesis is termed dorsal intercalation (~290-340 min after first cleavage or ~330-380 min after fertilization, 20°C) (reviewed in (Altun, Z. F. and Hall, D. H., 2009A) **Figure 1.2B**). After formation of six rows of epidermal (hyp) cells within the main posterior-dorsal epidermal cell cluster, the two innermost cell rows translocate, intercalate and thus create one row of hyp cells ((Podbilewicz, B and White, J. G., 1994), (Chisholm, A. D. and Hardin, J., 2005)). Flanking the inner row, the seam cells are created, while the outer rows build ventral epidermal and pocket (P) cells (reviewed in (Altun, Z. F. and Hall, D. H., 2009A)). Subsequent to dorsal intercalation, ventral enclosure (~310-360 min after first cleavage/~350-400 min after fertilization) occurs, whereby epidermal and pocket cells envelop the uncovered ventral fraction of the embryo through ventral elongation to the midline (reviewed in (Altun, Z. F. and Hall, D. H., 2009A) **Figure 1.2C**). This event is taking place in three phases. Firstly, ventral epidermal pioneering cells move ventrally, reach the midline and form parts of the hyp6 syncytium. Further ventrally located hyp cells form parts of the ventral hyp7 syncytium. Secondly, more posterior ventral cells (P cells) establish the ventral pocket. Thirdly, the ventral pocket closes. Of major importance for this study is the following process termed head enclosure (reviewed in (Chisholm, A. D. and Hardin, J., 2005) **Figure 1.2D**). Hereby, the anterior most epidermal cells are encasing the prospective head region of the embryo eventually forming the most anterior syncytia hyp1-5. It is not fully clarified yet how the procedure of covering the prospective head by hyp cells occurs. Moreover, the anterior-posterior elongation process (~ 350-600 min after first cleavage / ~390-640 min after fertilization) enables the transformation from bean- to elongated embryonic shape (3-fold stage) (reviewed in (Altun, Z. F. and Hall, D. H., 2009A) **Figure 1.2D**). Between comma and 2-fold stage, actin and tubulin filament bundles are formed in all epidermal cells circumferentially, with actin filaments being linked to adherens junctions and actin filament shortening occurring within seam cells ((Priess, J. R. and Hirsh, D. I., 1968), (Costa, M. et al., 1997), reviewed in (Altun, Z. F. and Hall, D. H., 2009A)). Seam cells are presumed to facilitate epidermal elongation and, due to the interconnection of cells by adherens junctions, the contraction force is suggested to be transferred to the whole epidermis (reviewed in (Ding, M. et al., 2004)). Hence, for epidermal elongation to occur, epidermal integrity is vital (reviewed in (Altun, Z. F. and Hall, D. H., 2009A)).

A Epidermal cell types
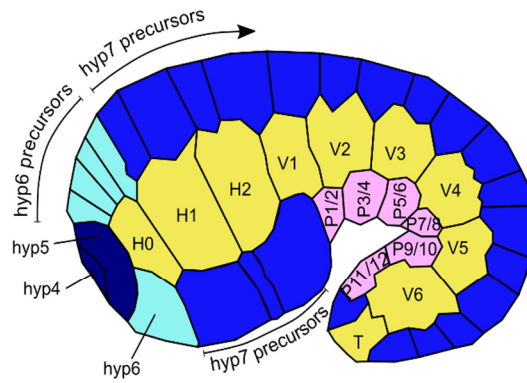
B Dorsal intercalation
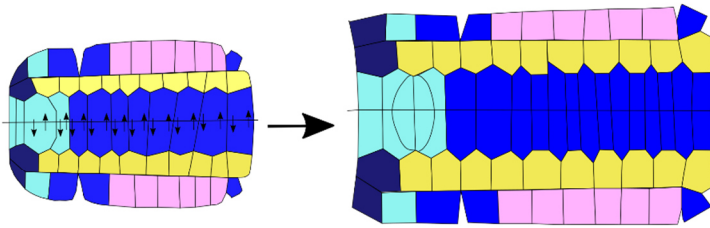
C Ventral enclosure
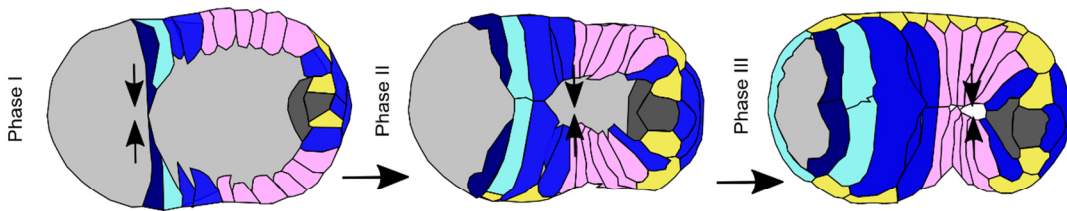
D Head enclosure and early elongation
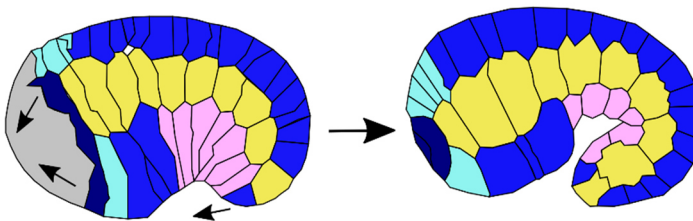
Figure 1.2: Epidermal migration and elongation events during embryogenesis

Schematic illustration of epidermal migration events and elongation events during lima-bean to 1.5-fold embryonic stages. Hyp7 (blue), hyp6 (light blue), hyp5 and hyp4 (dark blue) precursor cells; Seam cells (H0-H2, V1-V6, T, yellow), Pocket cells (P1-12, pink). Anterior left and posterior right. A and D lateral view, B dorsal view, C ventral view. **A**: Epidermal and specialized epithelial cells at 1,5-fold stage. **B**: During dorsal intercalation neighboring cells of middle rows intercalate. **C**: Epidermal enclosure of ventral section of the embryo. Phase I: Elongation of leading cells, phase II: elongation of posterior cells, phase III: sealing of the pocket. **D**: Enclosure of the head and elongation between lima bean and 1,5-fold stage. (Modified from (Lehmann, 2018), based on (Altun, Z. F. and Hall, D. H., 2009A), (Chisholm, A. D. and Hardin, J., 2005), (Chisholm, A. D. and Hsiao, T. I., 2012)).

b. Interfacial epithelial cells: socket and sheath cells

Socket and sheath cells are specific interfacial epithelial cells of circular shape, which are positioned at openings to the environment, interconnecting the epidermis with other tissues (reviewed in (Altun, Z. F. and Hall, D. H., 2009B)). The interfacial epithelial socket and sheath cells function as neuronal support cells within sensilla organs (reviewed in (Altun, Z. F. and Hall, D. H., 2010)) encasing ciliated endings of *C. elegans* sense organs (**Figure 1.3**). The main sense organs in the *C. elegans* head (**1.6**) are the amphid (AM), cephalic (CEP), outer labial (OL) and inner labial (IL) sensilla. Each sensillum contains dendrite(s) from bipolar sensory neuron(s) and a channel enveloping the dendritic tips, which is created by a sheath cell and socket cell(s) (reviewed in (Altun, Z. F. and Hall, D. H., 2010), (Mizeracka, K. and Heiman, M. G., 2015) **Figure 1.3**). The sheath and socket cells elongate towards the anterior most part of the head conjoint with neuronal dendrites (reviewed in (Mizeracka, K. and Heiman, M. G., 2015)). There, the dendrite tips get encased most distally by a ring-like structure (pore), created by the socket cell and more proximally, by a goblet-like structure (pouch) which is formed from the sheath cell. Importantly, the dendrite(s) get connected to the sheath cell through apical junctions, the sheath cell is connected to the socket cell(s) through adherens junctions and socket cell(s) and epidermis are interconnected by adherens junctions. Together, sheath and socket cell build a channel, through which the dendrite tips get in contact with stimuli from the environment. Sheath and socket cells are reported to have glia-like functions in *C. elegans*, for instance assisting neuron guidance (Yoshimura, S. et al., 2008) or facilitating correct sensory organ function (Bacaj, T. et al., 2008).
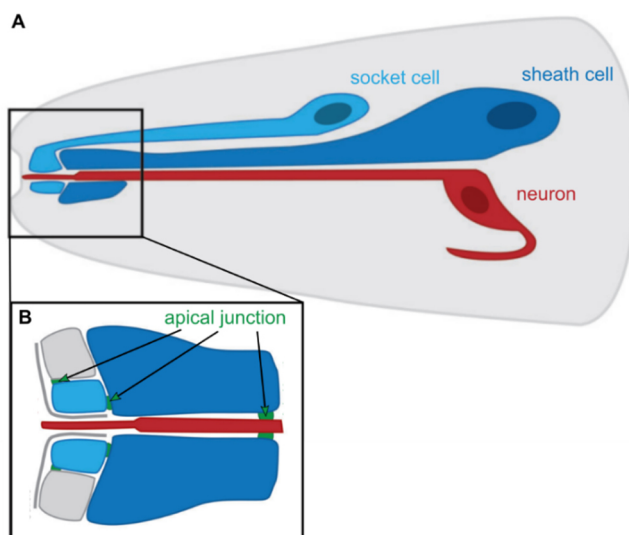
Figure 1.3: Generalized structure of *C.elegans* head sensilla

Schematic depiction of general structure of sensilla within the *C. elegans* head. **A**: Neuron (red), sheath cell (dark blue) and socket cell (light blue) send processes to the anterior most part of the head. There the dendrite tip is enwrapped by the sheath and socket cells. **B**: Apical junctions (green) interconnect the dendritic tips with the sheath-socket-cell channel and the epidermis. Modified from (Mizeracka, K. and Heiman, M. G., 2015).

c. Interfacial and atypical epithelial cells: arcade and XXX cells

Besides socket and sheath cells, also arcade cells and the cells of the pharyngeal epithelium that create the buccal cavity are assigned to interfacial epithelial cells (reviewed in (Altun, Z. F. and Hall, D. H., 2009B)). Adjacent to the mouth region, at the extreme anterior part of the *C. elegans*, hyp1, hyp2 and hyp3 cell rings are covering the adult head. Hyp1 cells and pharynx cells are interconnected through arcade cells (Mango, 2007), which are creating the buccal cavity together with the pharyngeal epithelial cells (reviewed in (Altun, Z. F. and Hall, D. H., 2009B)). Thus, arcade cells connect foregut and gut to the outer space (**Figure 1.4**). Within the adult worm, syncytial anterior and posterior arcade rings are formed through fusion of the projections from three anterior arcade cells (arc ant DL, arc ant DR, arc ant V) and six posterior arcade cells (arc post D, arc post DL, arc post DR, arc post V, arc post VL and arc post VR) ((Wright, K. A. and Thomson, J. N., 1981) **Figure 1.4A**). During embryonic development, arcade cells migrate posteriorly to the anterior part of the pharynx while being connected to their anterior ring. This migration event creates elongated cytoplasmic projections from the arcade cell bodies to each associated cytoplasmic ring. Through adherens junctions, these two syncytial arcade rings are linked and interconnect pharyngeal and epidermal cells (reviewed in (Altun, Z. F. and Hall, D. H., 2009B)).

The alimentary system of *C. elegans* is subdivided into stomodeum, intestine and (posterior to anterior) proctodeum (rectum, anus) (reviewed in (Altun, Z. F. and Hall, D. H., 2009B)). Hereby, the stomodeum contains mouth region (flanked by the lips), buccal cavity and pharynx and is established from ectodermal and mesodermal cells. From late comma embryonic stage on, pharynx morphogenesis starts. At first, a pharyngeal cyst establishes (~330 min after first cleavage/~370 min after fertilization), which is already attached to the intestine but not yet connected to the buccal cavity. At that time, arcade and epidermal cells are positioned between the anterior most part of the embryo's head and the pharyngeal cyst. Subsequently, pharyngeal extension is taking place, whereby not only the pharyngeal ball-shaped cyst but also the anteriorly positioned cells acquire tubular shape and epithelial character, forming an interconnected epithelial buccal cavity and alimentary system ((Portereiko, M. F. and Mango, S. E., 2001), (Mango, 2007) **Figure 1.4B**). Specifically, pharyngeal cells with apicobasal polarity get rearranged in dorsoventral direction, lined up besides the arcade cells (reviewed in (Altun, Z. F. and Hall, D. H., 2009B) **Figure 1.4B**, left and middle panel). Next, arcade cells establish an incessant epithelial sheet by connecting the anterior pharynx to both the buccal cavity and the epidermis by adherens junctions. Hereby, the arcade cells switch their mesenchymal into epithelial character. Afterwards, the cells within the interconnected sheet of pharyngeal epithelium and buccal cavity contract apically (**Figure 1.4B**, right panel). Hence, the pharynx moves anteriorly and the epidermis and buccal cavity posteriorly (Portereiko, M. F. and Mango, S. E., 2001). Thereby, a pharyngeal tube is formed, which, at later stages, differentiates into the mature luminal two-bulbed organ (reviewed in (Altun, Z. F. and Hall, D. H., 2009B)).

Besides interfacial cells, also atypical epithelial cells appertain to the epithelial system (Altun, Z. F. and Hall, D. H., 2009C). This class contains the XXX cells and the tail spike cells. Interestingly, XXXL/R cells arise dorsally next to prospective hyp5 cells (260 min after first cleavage/300 min after fertilization) and migrate anteriorly during embryogenesis, thus being positioned on the ventral side of the embryonic head next to hyp4 cells ((Sulston, J. E. et al., 1983), reviewed in (Altun, Z. F. and Hall, D. H., 2009C) **Figure 1.4C**). XXXL/R cells have roles within the anterior epidermis at first, but in adult worms they are often positioned close to the pharynx, changing their epidermal to neuron-like characteristics ((Sulston, J. E. et al., 1983), (White, 1988)). Moreover, the tail spike scaffold cells are part of the atypical epithelial category (reviewed in (Altun, Z. F. and Hall, D. H., 2009C)). These cells build a syncytium during embryogenesis which creates a cuticular spike at the adult worm's tail.
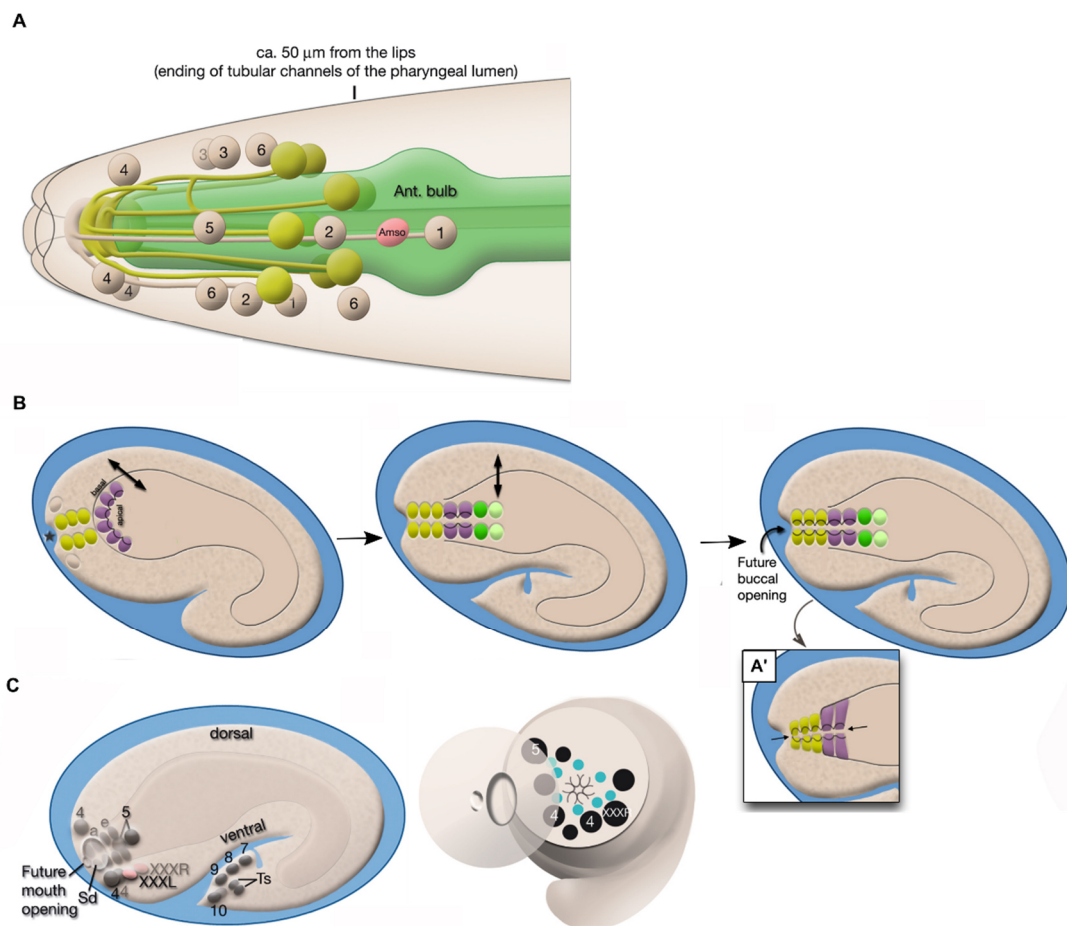
Figure 1.4: arcade cells, morphogenesis of the buccal cavity and migration of XXX cells

Schematic illustration of arcade cell morphology in the adult worm, embryonal pharyngeal extension and positioning of XXX atypical cells. **A:** Morphology of anterior and posterior arcade cells (lime green), epidermal cells (beige, numbers) and left amphid socket (red) in the adult worm head. **B:** Stages of embryonal pharyngeal extension. Arcade cells (yellow), pharyngeal epithelial cells (purple), pharyngeal muscle cells (green), anterior sensory deprivation (*) are shown. Epithelialization & apico-basal orientation (black curved lines). Left & middle panel: pharyngeal cells get rearranged in dorso-ventral direction aligned with arcade cells. Middle panel: arcade cells interconnect anterior pharynx to buccal cavity and epidermis. Right panel: interconnected pharyngeal cells and buccal cavity contract apically. Pharynx moves anteriorly and epidermis/buccal cavity posterior; the pharyngeal tube is created. **C:** XXXL/R position in late embryogenesis. Epidermal cells (numbers) indicated. Left panel: anterior-posterior view; right panel: head-on view.(A,B,C left): Anterior to the left, posterior to the right. (Modified from (Altun, Z. F. and Hall, D. H., 2009B), (Altun, Z. F. and Hall, D. H., 2009C))

1.3. Apicobasal cell polarity in *C. elegans*

In *C. elegans*, the apical PAR proteins (abnormal embryonic PARtitioning of cytoplasm) PAR-6, PAR-3 and the kinase PKC-3 are of major importance for polarity establishment in the early embryo ((Kemphues, K. et al., 1988), (Tabuse, Y. et al., 1998), (Nance, J. et al., 2003), (Nance, J. and Zallen, J. A., 2011)). These factors have been shown to be conserved and to play important roles for epithelial polarity in other organisms (reviewed in (Chen, J. and Zhang, M., 2013), (Von Stetina, S. and Mango, S. E., 2015) **Figure 1.5**). In addition, *C. elegans* apical junctions (CeAJ) contain components like DLG-1 (Discs Large), AJM-1 and HMR-1 (E-cadherin) (reviewed in (Labouesse, 2006)) and they set the boundary in epithelial cells between the apical and the basolateral membrane domains (reviewed in (Nelson, W. J. et al., 2013), (Von Stetina, S. and Mango, S. E., 2015)). The apicobasal positioning of PAR-6, PAR-3, ERM-1 (ezrin/radixin/moesin), HMR-1 (E-cadherin), DLG-1, PAT-3 (β-integrin) and laminins (LAM-1, LAM-3) is well conserved ((Macara, 2004), (Hohenester, E. and Yurchenco, P. D., 2013), (Labouesse, 2006) **Figure 1.5**). The question of how these factors are establishing apicobasal polarity was recently discussed (Klompstra, D. et al., 2015). The authors proposed a model which suggests that HMR-1 recruits the RhoGAP protein PAC-1 to the basolateral domain. Specifically, JAC-1 (p120-catenin) itself binds to HMR-1 (E-cadherin) and interacts with PICC-1 (a linker protein) that can couple PAC-1 to the cadherin-catenin complex at basolateral surfaces. Basal positioning of PAC-1 inhibits the GTPase CDC-42 locally, whereby apical PAR-proteins get excluded basally (Anderson, D. C. et al., 2008). In the apical domain, active CDC-42 helps localizing apical PAR-proteins and lead to non-muscle myosin activation. Besides JAC-1-mediated recruitment of PAC-1, also HMP-1 (α-catenin) seems to have a role in basal PAC-1 localization (Klompstra, D. et al., 2015). Interestingly, within *C. elegans* endodermal precursor cells (Ea, Ep), MRCK-1 (myosin light-chain kinase) is suggested to activate apically positioned non-muscle myosin (Marston, D. J. et al., 2016).
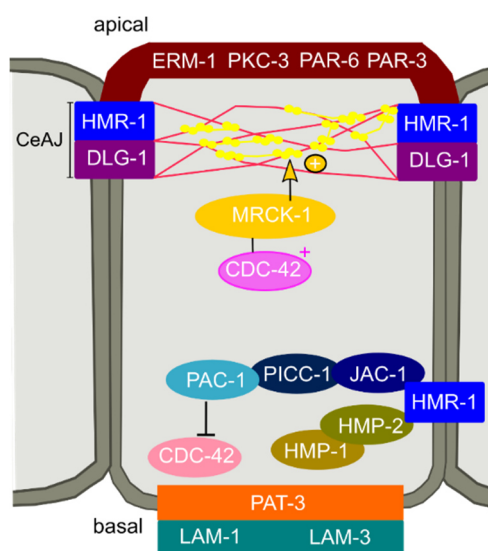

Figure 1.5: Apicobasal polarity in *C.elegans* epithelial cells

Schematic depicting factors reported to be involved in apicobasal polarity establishment. Yellow lines with circles = myosin; red lines = actin. CeAJ = *C. elegans* apical junction. Based on (Von Stetina, S. and Mango, S. E., 2015), (Klompstra, D. et al., 2015), (Marston, D. J. et al., 2016).

1.4. Apical constriction: A major driving force for tissue morphogenesis

The term apical constriction describes the shrinkage of apical cell surfaces driven by apical actomyosin contraction (reviewed in (Martin, A. C. and Goldstein, B., 2014), (Sawyer, J. M. et al., 2010)). Apical constriction is of major importance for multiple events of embryonic development like gastrulation in *C. elegans* ((Lee, J.-Y. and Goldstein, B., 2003), (Pohl, C. et al., 2012)), neurulation in vertebrates (Bush, K. T. et al., 1990) and wound healing in *Xenopus laevis* (Davidson, L. A. et al., 2002b), to only name a few. Fundamental precondition for the occurrence of apical constriction-driven processes is the establishment of apicobasal polarity within each epithelial cell (**Figure 1.5**). Thus apical actin and non-muscle myosin II (NMM II, hereafter referred to as myosin) meshwork contraction within the cell creates intracellular force which is driving apical constriction ((reviewed in (Sawyer, J. M. et al., 2010), (Martin, A. C. and Goldstein, B., 2014) **Figure 1.5, Figure 1.7**). NMM II molecules contain two heavy chains (NMY-2 in *C. elegans*), two regulatory light chains (MLC-4 in *C. elegans*) and two essential light chains (reviewed in (Vicente-Manzanares, M. et al., 2009) **Figure 1.6A**). In addition, two head regions are present in NMM II, which bind actin and constitute the ATPase. They are connected to the light chains via their neck regions. Phosphorylation of the regulatory light chains activates NMM II molecules. Hereby, NMM II molecules associate in bipolar filaments and crosslink actin filaments through their head regions, thus enabling cytoskeletal contraction. Importantly, interconnection of neighboring cells through adherens junctions enables force transmission and thereby tissue bending (reviewed in (Sawyer, J. M. et al., 2010), (Martin, A. C. and Goldstein, B., 2014)).
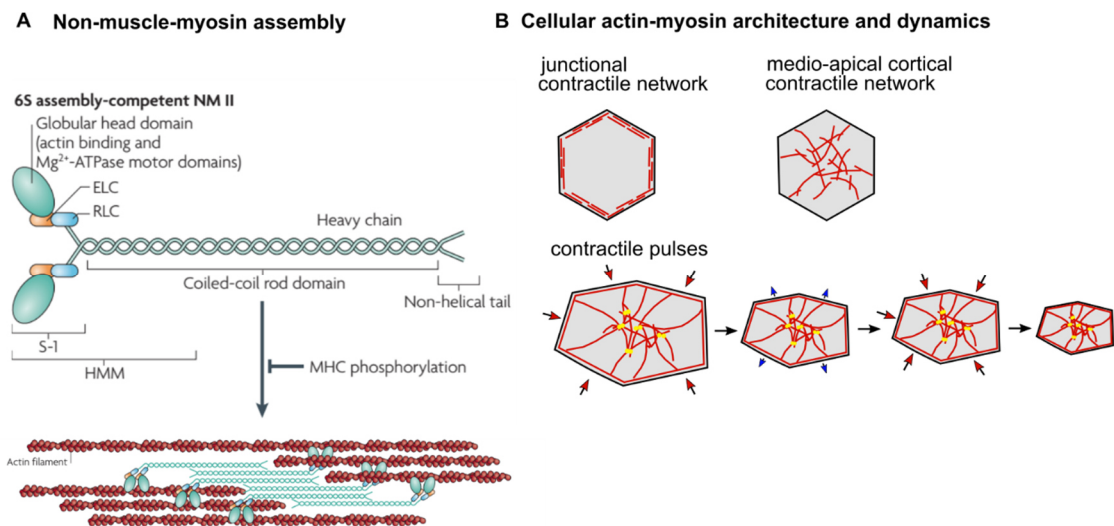
Figure 1.6: Non-muscle-myosin components, actin-myosin assembly and dynamics during contraction
Schematic illustration exhibiting NMM II filament assembly, modes of myosin and actin network positioning and dynamics. **A**: Assembly of NMM II into bipolar filaments creating actomyosin fibers. **B**: Varying arrangement of actin (red) myosin (yellow) meshworks and pulsed apical constriction mode. Modified from (Vicente-Manzanares, M. et al., 2009), (Martin, A. C. and Goldstein, B., 2014).

Actomyosin assemblies and dynamics of force generation are differing in developmental contexts and species (reviewed in (Sawyer, J. M. et al., 2010), (Martin, A. C. and Goldstein, B., 2014) **Figure 1.6B, Figure 1.7**). Within the cell, actomyosin bundles can be arranged as circumferential junctional belts ((Owaribe, K. and Masuda, H.;, 1982) **Figure 1.6B**) or as medio-apical cortical contractile network (reviewed in (Martin, A. C. and Goldstein, B., 2014)). The actin cortex (reviewed in (Lecuit, T. et al., 2011), (Salbreux, G. et al., 2012)) can create cortical tension, thereby initiate a cortical flow which is then driving traction forces ((Aratyn-Schaus, Y. et al., 2011), (Kapustina, M. et al., 2013), reviewed in (Martin, A. C. and Goldstein, B., 2014)). In addition, apical constriction can either occur as consistent actomyosin contractions or as contractile pulses ((Martin, 2009) **Figure 1.6B**).

Moreover, apical constriction-facilitating morphogenetic events can be very divergent, depending on the developmental event and a certain species (reviewed in (Sawyer, J. M. et al., 2010) **Figure 1.7**). Firstly, shape changes of apically constricting cells into bottle- or wedge-shape appear during *Xenopus* wound healing and gastrulation ((Davidson, L. A. et al., 2002b), (Hardin, J. and Keller, R., 1988) **Figure 1.7A, B**) or throughout mammalian neural tube formation ((Moore, D. C. P. et al., 1987) **Figure 1.7D**). During *Xenopus* gastrulation bottle cells appear at the position of tissue invagination ((Hardin, J. and Keller, R., 1988) **Figure 1.7A**). Within these cells apical F-actin and myosin fibers enrich before apical constriction, indicating their role for creation of their bottle shape (Lee, J. Y. and Harland, R. M., 2007). Furthermore, wedge-shape also occurs in hinge point cells during mammalian primary neurulation ((Moore, D. C. P. et al., 1987) **Figure 1.7D**). Hereby, induction of apical constriction in hinge point cells is presumably caused by contractile microfilament meshworks (Baker, P. C. and Schroeder, T.E., 1967) and areas of apical constriction concur with bending tissue parts during neural tube enclosure (Bush, K. T. et al., 1990). Besides gastrulation and neurulation, apical constriction is presumed to aid in wound healing ((Davidson, L. A. et al., 2002b) **Figure 1.7 B**). Thereby, wounds within the outer layer of embryonic *Xenopus laevis* animal cap ectoderm are suggested to get reduced in size through constriction of cells positioned deeper in this ectodermal sheet.

In addition to apical constriction creating bottle- or wedge-shaped cells, apical constriction during *C. elegans* gastrulation and *Drosophila* dorsal enclosure is occurring differently (reviewed in (Sawyer, J. M. et al., 2010), (Martin, A. C. and Goldstein, B., 2014) **Figure 1.7C, E**). During gastrulation of *C. elegans* only individual cells or small cell groups are internalized (reviewed in (Sawyer, J. M. et al., 2010) **Figure 1.7C**). Hereby, a specific morphogenetic module which was termed apical constriction primarily (Lee, J.-Y. and Goldstein, B., 2003), contributes to gastrulation through contractile actomyosin flow and adhesion to adjacent cells (Roh-Johnson, M. et al., 2012). Importantly, during internalization, just the covering cells undergo shape changes but not the internalizing cells ((Pohl, C. et al., 2012) **Figure 1.7C**). Apical constriction during dorsal enclosure of *Drosophila* occurs in a ratchet fashion, whereby pulses (phases of actomyosin network contraction and stabilization) are repeated to constrict the cell apex incrementally ((Martin, A. C. et al., 2009) **Figure 1.6B, Figure 1.7E**).

To sum up, apical constriction is a major force driving diverse morphogenetic events in multiple developmental contexts. Establishment of apicobasal polarity is a fundamental process underlying apical constriction. Asymmetric actomyosin contraction drives the shrinkage of apical cell surfaces. The manifestation of apical constriction occurs according to its specific cytoskeletal arrangement within the cell (junctional networks/cortical networks), temporally distinct (continuous/pulsed) and relative to the developmental context of the vertebrate or invertebrate species.

A Gastrulatoion of _X. laevis_

B Wound healing in _X. laevis_

C Gastrulation in _C. elegans_

D Neural tube formation in mammalia

neural plate

hinge points

notochord

E Dorsal enclosure of _Drosophila_ embryos

Amnioserosa cells

dorsal

Actin-myosin cable

ventral
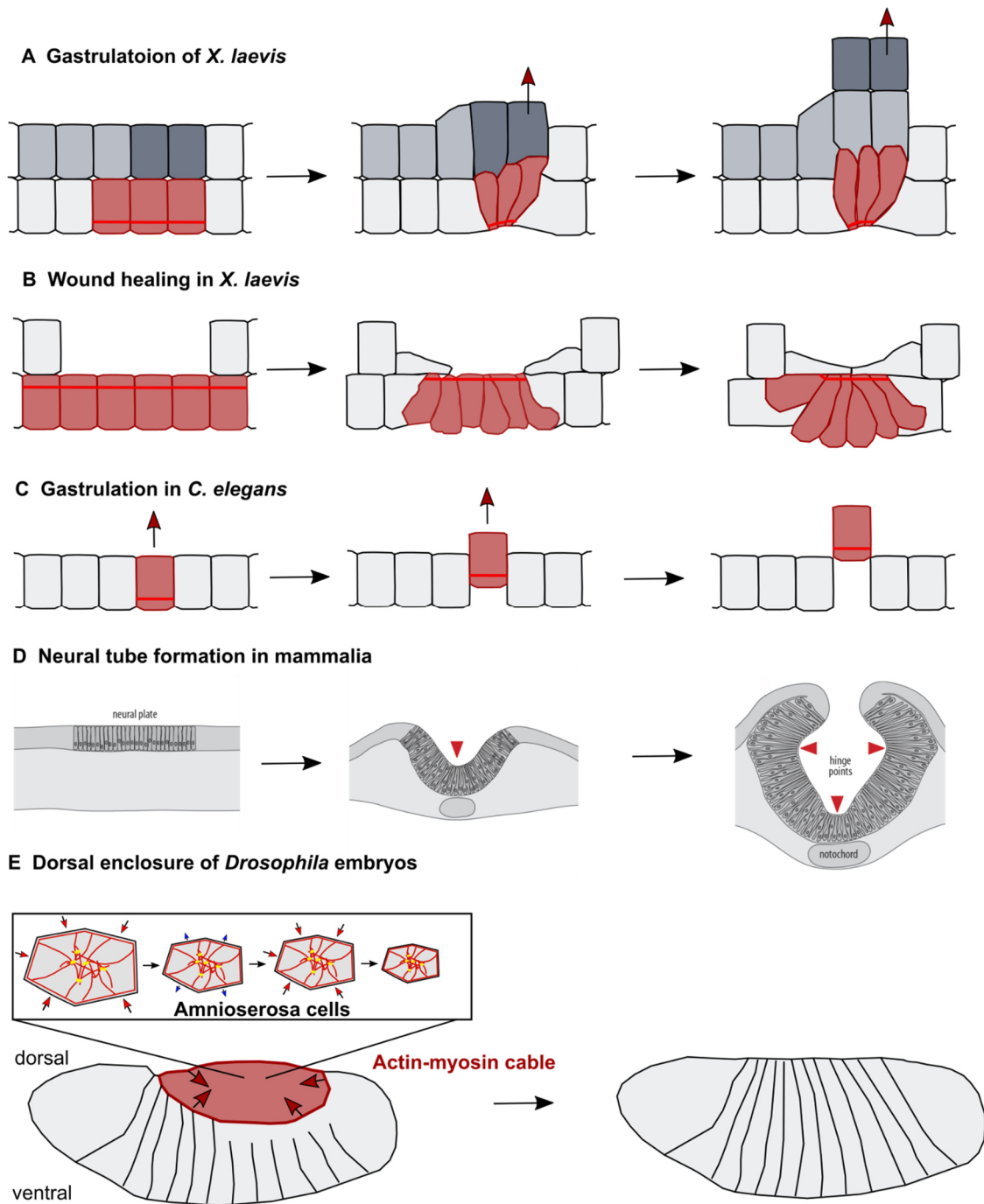
Figure 1.7: Multiple incidences of apical constriction driving morphogenetic events in diverse species

Schematic illustration showing diverse events of apical constriction in different species. Red cells = constricting cells; red lines = actin-myosin networks; red area = dorsal part of embryo containing amnioserosa cells; A, C: apical-side at bottom; B: apical-side up. **A, B, D**: Apical constriction exhibiting bottle- or wedged shaped cells. **C, E**: apical constriction events without bottle-shaped cells. **C**: Internalization of endodermal precursor cells during _C. elegans_ gastrulation. **E**: Pulsed apical constriction in amnioserosal cells and actin-myosin-cable force driving dorsal enclosure of _Drosophila_ embryo. Modified from (Sawyer, J. M. et al., 2010), (Martin, A. C. and Goldstein, B., 2014). http://www.mun.ca/biology/desmid/brian/BIOL3530/DEVO_08/ch08f34.jpg; 21.04.21

1.5. Neuronal polarity and neurite elongation

Specialization of neurons into dendrites and axons is crucial for efficient signal transmission in neural systems (reviewed in (Ou, C.-Y. and Shen, K., 2010)). Proper neural polarization and neural migration are key aspects of neural development (reviewed in (Namba, T. et al., 2015)). For instance, the neuro-developmental disease lissencephaly is caused by impaired neural migration and in those patients also mutations in genes which normally function in neural polarity establishment were found. Many neuronal polarity factors are well conserved from vertebrates to invertebrates (reviewed in (Ou, C.-Y. and Shen, K., 2010) **Figure 1.8, Figure 1.9**). Since neural polarization, neural migration and elongation can get easily examined *in vivo* by microscopy in *C. elegans*, our study investigates amphid (AM) neuronal development during *C. elegans* embryogenesis.

a. Establishment and maintenance of neural polarity

Formation of morphologically and functionally differing axons and dendrites requires diverse external cues in *C.elegans* neural development (Ou, C.-Y. and Shen, K., 2010). For anterior-posterior (a/p) polarity establishment, WNT signaling factors are acting as vital extrinsic cues, for instance facilitating a/p polarity in PLM and ALM neurons ((Hilliard, M. A. and Bargmann, C. L., 2006), (Prasad, B. C. and Clark, S. G., 2006)). WNT components also function as guidance factors for neuronal outgrowth (Pan, C. et al., 2006) and cell fate determination (reviewed in (Ou, C.-Y. and Shen, K., 2010)). Ventral polarity of the HSN neuron in *C. elegans* gets facilitated by UNC-6/netrin (UNCoordinated) signaling, (Adler, C. E. et al., 2006) **Figure 1.8**). The UNC-6 signaling cascade functions through the UNC-6 receptor UNC-40/DCC and the asymmetrically localized downstream factors, adaptor protein MIG-10/lamellipodin and actin regulator UNC-34/Ena ((Adler, C. E. et al., 2006), reviewed in (Ou, C.-Y. and Shen, K., 2010)). In addition to its role for HSN neuron polarity, both ventral UNC-6 and dorsal SLT-1/slit gradients steer AVM and PVM neuron outgrowth to the ventral side ((Hao, J. C. et al., 2001), (Quinn, C. C. et al., 2006)).
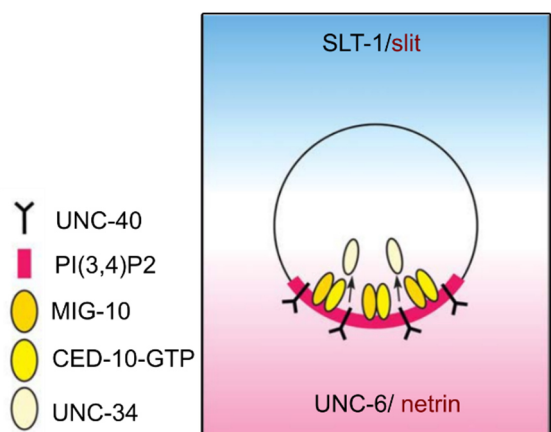

Figure 1.8: External cues inducing neural polarity in *C.elegans*

Schematic illustration depicting factors for initiation of neural polarity establishment in *C. elegans*. Ventral UNC-6/netrin and dorsal SLT-1/slit gradients establish dorso-ventral neuronal polarity. Modified from (Ou, C.-Y. and Shen, K., 2010).

In the developing cortex, neural polarity is organized by extracellular cues like TGF-β (transforming growth factor- β), neurotrophins (BDNF, NT3), Wnt5A, Semaphorin 3A, IGF1 (insulin-like growth factor 1) and cell adhesion molecules (Tag1 and N-cadherin) (reviewed in (Takano, T. et al., 2019) **Figure 1.9**). *In vitro*, aPAR-complex (aPKC, Par3, Par6) components are activated by Wnt5A which facilitates axon identity (Zhang, X. et al., 2007). Also, the TGF-β receptor (TGF-βR) was found to activate Par6 and thereby to initiate axonal fate *in vivo* (Yi, J.J. et al., 2010).

In addition, positive and negative feedback signals which control neural polarity have been studied in tissue culture models (reviewed in (Takano, T. et al., 2019) **Figure 1.9**). It could be shown that positive feedback signals are controlling axon identity and outgrowth, whereby negative feedback signals avert axonal fate and thereby allow dendrite identity establishment. A major positive feedback loop is the PI3-kinase/Cdc42/Par complex/RacGFP/Rac1 signaling pathway. Neurotrophins (e.g. BDNF) control axonal identity through Ras mediated activation of PI3-kinase (phosphoinositide 3-kinase) ((Shi, S. et al., 2003), (Ménager, C. et al., 2004), (Yoshimura, T. et al., 2006)). Thereby, Cdc42 is activated by PI3-kinase, which is interacting with the PAR-complex (Par3/Par6/aPKC), leading to continued PI3-kinase activation ((Ménager, C. et al., 2004), (Nishimura, T. et al., 2005), reviewed in (Takano, T. et al., 2019)). The PAR complex and other factors like Shootin1 or CRMP-2 are enriched within the arising axon as a consequence of positive feedback pathways and affect multiple events like actin dynamics, microtubule stabilization, intracellular trafficking and thereby facilitate axon specification and elongation (reviewed in (Takano, T. et al., 2019)). Altogether, positive signaling cascades determine axonal fate within the main neurite by operating on cytoskeletal dynamics.

Negative feedback signaling cascades guarantee the formation of exclusively one axon per neuron and the establishment of several dendrites (reviewed in (Takano, T. et al., 2019)). One negative feedback signaling pathway involves neurotrophin (NT-3) initiated long-range Ca^{2+} signal which is activating CaMKI (calmodulin-dependent protein kinase I) which further activates RhoA and Rho-kinase ((Takano, T. et al., 2017) **Figure 1.9**). The latter factors are important negative signaling factors influencing actin dynamics in neurogenesis ((Da Silva, J.S. et al., 2003) (Conde, C. et al., 2010)). Thus, RhoA/Rho-kinase mediated negative feedback signaling ensues dendrite identity in minor axons by preventing the formation of multiple axons (reviewed in (Takano, T. et al., 2019)). To summarize, negative signaling cues act in coordination with positive feedback signals to determine axonal fate within the main neurite, which is resulting in correct neuronal polarity.
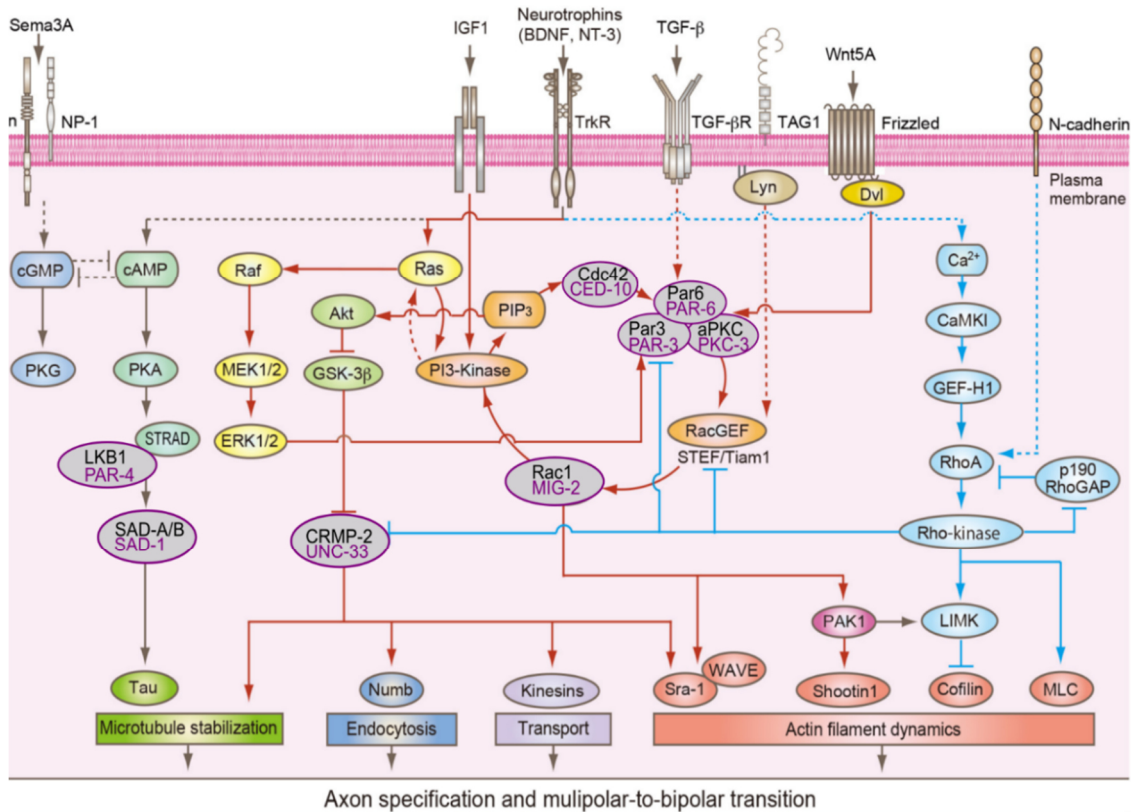
Figure 1.9: Intracellular positive and negative signaling cascades functioning in neural polarity

Schematic showing factors of intracellular positive or negative feedback signaling cascades contributing to neural polarity. Positive feedback loops (red arrows); Negative feedback loops (blue arrows). Homolog factors in *C. elegans* (purple). Positive feedback signaling leads to axon identity while negative feedback signaling cascades promote dendrite faith preventing establishment of multiple axons. Modified from (Takano, T. et al., 2019), (Ou, C.-Y. and Shen, K., 2010).
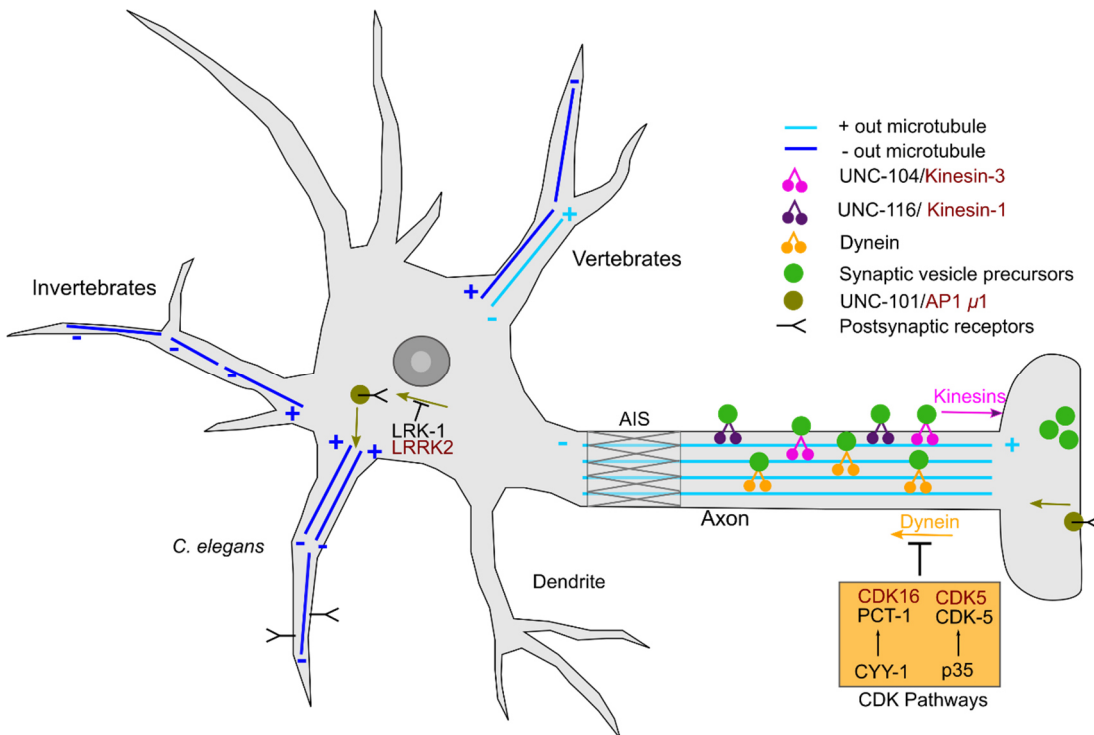
Figure 1.10 : Microtubule arrangement and cytoskeletal trafficking in dendrites and axon
Schematic illustration showing microtubule positioning, intracellular trafficking and factors contributing to neural polarity in *C. elegans*, invertebrates and vertebrates. Modified based on (Ou, C.-Y. and Shen, K., 2010), (Kelliher, M.T. et al., 2019), (Rolls, M. M. and Jegla, T. J., 2015).

Additionally, microtubule arrangements differ in axons and dendrites (reviewed in (Rolls, M. M. and Jegla, T. J., 2015), (Kelliher, M.T. et al., 2019) **Figure 1.10**). The axons of vertebrates contain microtubules all polarized with plus-ends pointing away from the cell center (Baas, P. W. and Lin, S., 2011), dendrites however contain microtubules of mixed polarity ((Baas, P. W. et al., 1988), (Baas, P. W. and Lin, S., 2011). During axonal trafficking, components are transported anterogradely (in plus-end direction) by kinesins and retrogradely by the dynein motor protein complex and associated linker proteins (reviewed in (Hirokawa, N. et al., 2010), (Kelliher, M.T. et al., 2019)). The AIS (axon initial segment) functions as the site of action potential initiation (reviewed in (Bender, K.J. and Tussel, L.O., 2012)) and its components function as diffusion barrier (reviewed in (Rolls, M. M. and Jegla, T. J., 2015)). The AIS contains high concentrations of voltage-gated Na^+-channels and a specialized cytoskeletal organization, where the AIS sub-membrane cytoskeletal structure functions in maintaining plasma membrane polarity within the neuron (Szu-Yu Ho, T. and Rasband, M.N., 2011). This specialized sub-membrane skeleton comprises Ankyrin G (AnkG), a linker protein bridging transmembrane proteins and β-IV-spectrin, which functions in binding actin (reviewed in (Rolls, M. M. and Jegla, T. J., 2015)). These factors form a dense meshwork underneath the axon membrane, whereby a diffusion barrier at the boundary between axonal and neuronal plasma membrane is getting formed. Thus, polarized microtubules and the AIS seem to be important for polarity in vertebrate neurons.

How important are cytoskeletal components for neuronal polarity in invertebrates? The morphology of most *C. elegans* neurons is more simple then in vertebrate neurons, since neurites are mainly unbranched and uni- or bi-polar ((White, J. G. et al., 1986) **Figure 1.10**). Interestingly, in spite of the simpler anatomy of *C. elegans* neurons, axon or dendrite identity was found to be distinguishable in DB class motor neurons, showing axonal microtubules with distal plus-ends and dendrite microtubules with distal minus-ends (Goodwin, P.R. et al., 2012). Directed neuronal trafficking and selective sorting seem to have an important influence on the maintenance of neural polarity in *C. elegans* neurons (reviewed in (Ou, C.-Y. and Shen, K., 2010) **Figure 1.10**). Many of these factors are evolutionarily conserved in mammals. For instance, within *C. elegans* axons the transport of synaptic vesicle precursors is mainly conducted by kinesins like UNC-104/KIF1. Additionally, it is suggested that CDK pathways might reverse polarized trafficking of cargo. UNC-101, an AP-1 adaptor complex subunit, is suggested to be required for correct trafficking of the odorant receptor ODR-10 to olfactory cilia of a chemosensory neuron (Dwyer, N. D. et al., 2001). Interestingly, LRK-1 (homologs PARK8/LRRK2) is suggested to facilitate polarized sorting of synaptic vesicle proteins in head sensory neurons (Sakaguchi-Nakashima, A. et al., 2007). This is highly remarkable, since dominant mutations in LRK-1 homologue LRRK2 are implicated in Parkinson's disease (reviewed in (Ou, C.-Y. and Shen, K., 2010)).

b. Neuronal elongation

In the following section, several distinct mechanisms for elongation of dendrite and axon processes are summarized. Throughout this study, active neuron-driven extension gets distinguished from passive dendrite elongation, which relies on dynamics from other tissues (**Figure 1.12**).

A major procedure facilitating neuronal elongation is active, growth cone-mediated extension ((Tessier-Lavigne, M. and Goodman, C. S., 1996), reviewed in (Huber, A. B. et al., 2003) **Figure 1.11, Figure 1.12A**). The axonal growth cone is positioned at the axonal leading edge, sensing and responding to attractive or repulsive guidance signals, which are transferred to the cytoskeleton, thereby steering neural outgrowth or retraction (reviewed in (Huber, A. B. et al., 2003)). These guidance factors include secreted or contact-mediated molecules acting as long- or short-range cues for the axonal growth cone. Actin is enriched within the peripheral filopodia and lamellipodia regions of the growth cone, whereby in the center region, microtubules and organelles are enriched ((Forscher, P. and Smith, S.J., 1988), reviewed in (Tahirovic, S. and Bradke, F., 2009)). Advancement or retraction of a growth cone is controlled by actin de-polymerization and F-actin retrograde flow, thus attractive guidance signals inhibit retrograde actin flow but enhance actin polymerization and vice versa (reviewed in (Huber, A. B. et al., 2003)). Additionally, the neural centrosome is implicated in axon extension *in situ*, which is especially well studied during formation of multi-layered neuronal networks like the cortex ((Lefcort, F. and Bentley, D., 1989), reviewed in (Solecki, D. J. et al., 2006) **Figure 1.12B**). Moreover, a process termed retrograde extension has been put forward as an additional active neural extension process in *C. elegans* ((Heiman, M. G. and Shaham, S., 2009) **Figure 1.12C**). Retrograde extension implies that "the presumptive dendritic tip remains stationary while the cell body migrates away..." (Heiman, M. G. and Shaham, S., 2009). Importantly, during retrograde extension, anchoring molecules mediate a stable attachment of a dendritic tip to a target tissue, which is followed by active movement of the neural cell body during dendrite elongation, thus, the dendrite is stretched by the movement of the neuronal cell body.
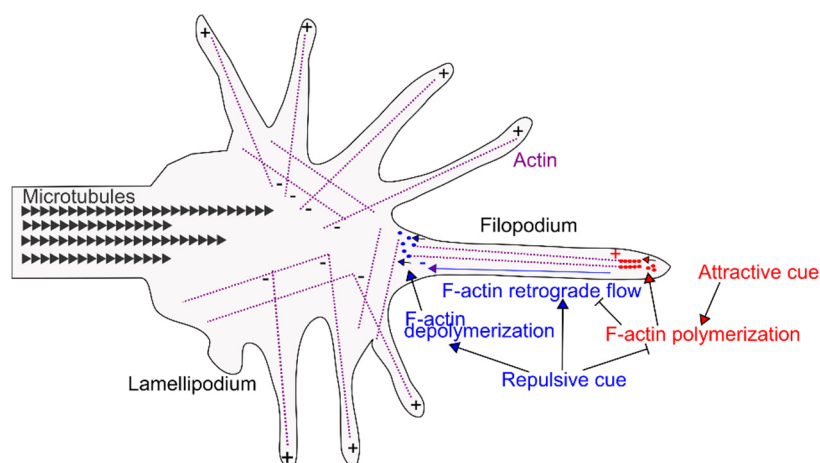

Figure 1.11: The axonal growth cone mediates axonal growth
Schematic illustrating the growth cone mediated elongation or retraction of axonal outgrowth in response to attractive or repulsive environmental cues. Modified based on (Huber, A. B. et al., 2003), (Tahirovic, S. and Bradke, F., 2009).

Furthermore, towing has been demonstrated to constitute a passive neuronal elongation mechanism in distinct invertebrate and vertebrate sensory systems ((Gilmour, D. et al., 2004), (Jiang, L. I. and Sternberg, P. W., 1999) **Figure 1.12D**). During towing, migration of target cells leads to the extension of associated neuronal cells (Gilmour, D. et al., 2004). Throughout the development of the *Zebrafish* lateral line organ, active migration of the lateral line primordium (LLP) coordinates the elongation of associated sensory axons *in vivo* (Gilmour, D. et al., 2004). The lateral line system functions in detection of movement within the water through sensory organs called neuromasts (reviewed in (Ghysen, A. and Dambly-Chaudière, C., 2004)). Those neuromasts are distributed on the surface of the head region (ALL, anterior lateral line system) or at the body and tail region (PLL, posterior lateral line system) and contain mechanosensory hair cells, sensory neurons and support cells. During post-embryonic PLL development, new primordia are build and distributed over the body and tail region and dorso-ventral migration of neuromasts contributes to the variability of adult PLL patterns ((Ledent, 2002), (Sapède, D. et al., 2002)). Also, *C. elegans* spicule morphogenesis involves neuronal elongation events that bear some resemblance to towing (Jiang, L. I. and Sternberg, P. W., 1999). The pair of spicules are an important anatomical structure in *C. elegans'* males for anchoring the male tail to the vulva and to aid in sperm transfer. A spicule contains two neurons (SPD, SPV), four socket cells and two sheath cells (Sulston, J. E. et al., 1980). The SPD and SPV ciliated endings extend through a pore and may get in contact to external signals. Between mid-L4 to L4 stages strong spicule elongation occurs, which especially requires the socket cells (Jiang, L. I. and Sternberg, P. W., 1999). This study suggest that towing could drive spicule morphogenesis, because for both spicule morphogenesis and lateral line morphogenesis, target cell migration drives elongation (**Figure 1.12D**).

To sum up, active growth cone-mediated extension facilitates elongation of neurons through motile growth cones approaching chemo-attractants or avoiding chemo-repulsive molecules. During cerebellar morphogenesis and retrograde extension, active neuron-driven events are facilitating neurite extension. Otherwise, towing describes a mechanism, whereby neurites are elongated passively, driven by the migration of attached target cells.
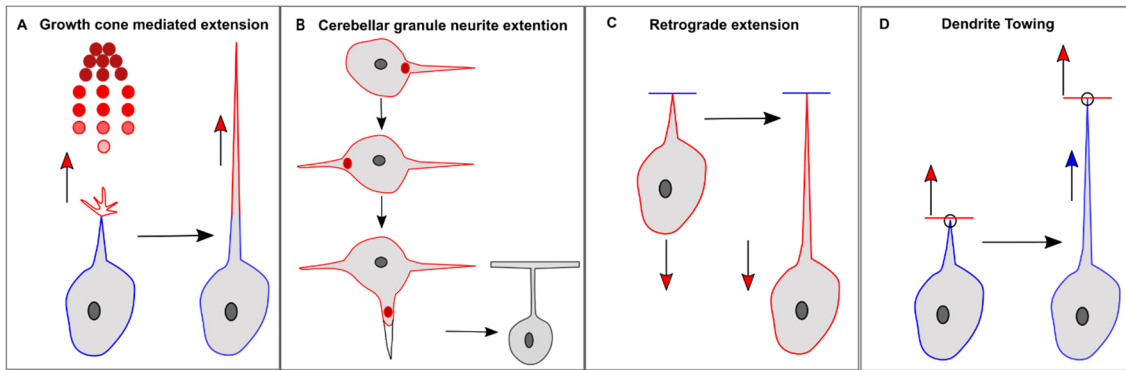
Figure 1.12: Diverse modes of neurite elongation
Active events (red). Passive events (blue). **A**: "Growth cone mediated extension" of axons guided by attractive cues. **B**: Centrosome initiated outgrowth during cerebellar granule neuron development. **C**: Active posterior migration of cell bodies with dendrite tips attached anteriorly facilitates dendrite extension termed "retrograde extension". **D**: Passive elongation of dendrites through migration of attached target cells, coined "dendrite towing" in this study. Based on (Huber, A. B. et al., 2003), (Solecki, D. J. et al., 2006), (Heiman, M. G. and Shaham, S., 2009), (Gilmour, D. et al., 2004).

1.6. *C. elegans* sensory organs with a focus on head sensilla

Sensation of nutrition, detection of peril or location of mating partners, are fundamental requirements for the survival of animal populations. For sensation of environmental stimuli, *C. elegans* utilizes epithelial sensory organs termed sensilla, which contain dendrite tips of sensory neurons and interfacial socket and sheath cell(s) (reviewed in (Altun, Z. F. and Hall, D. H., 2010), (Doroquez, D. B. et al., 2014)). The major adult *C. elegans* sensilla are located in the head region (**Figure 1.13A, B**), including amphids (AM L/R), cephalic sensilla (CEP L/R) and outer-/inner labial sensilla (OL/IL L/R) ((Ward, S. et al., 1975), (Ware, R.W. et al., 1975), (Perkins, L. A. et al., 1986), reviewed in (Altun, Z. F. and Hall, D. H., 2010) **Figure 1.13**). Those head sensilla are subdivided into the distal sensillar region, or sensillar ending, the proximo-distal dendritic region (containing the neuronal processes) and the most proximal sensillar region with the somata, comprising most cell bodies of the sensory neurons and their neuronal support cells (reviewed in (Altun, Z. F. and Hall, D. H., 2010) **Figure 1.13A**). Most sensillar endings of the head are positioned in two-fold (AM, OLL), four-fold (CEP, OLQ) or six-fold symmetry (IL), terminating at the lips which surround the mouth opening (reviewed in (Altun, Z. F. and Hall, D. H., 2010), (Doroquez, D. B. et al., 2014) **Figure 1.13B**). At the sensillar ending, dendritic tip(s) of sensory neuron(s) are enwrapped by sheath (sh) and socket cells (so), whereby distal parts of dendritic tips get enwrapped by socket cells and sheath cells encase the adjacent proximo-distal part of dendritic tips (reviewed in (Altun, Z. F. and Hall, D. H., 2010)). Unbranched sheath and socket cell processes accompany the dendrite projections throughout the proximo-distal region (reviewed in (Mizeracka, K. and Heiman, M. G., 2015) **Figure 1.13A**). The axons of the head sensilla project into the nerve ring (NR) (reviewed in (Altun, Z. F. and Hall, D. H., 2010)), and especially AM axons project into the NR through a commissure (reviewed in (Altun, Z.F. and Hall, D.H., 2011) **Figure 1.14**).
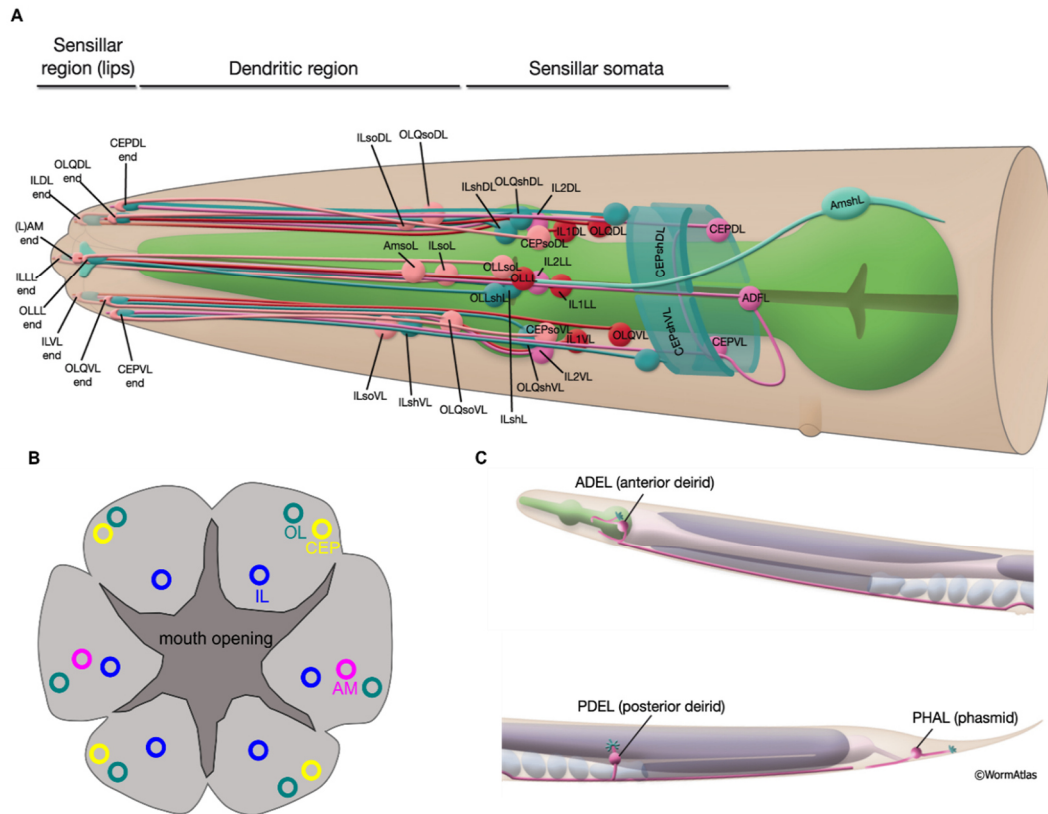
Figure 1.13: Anatomy of main sensilla in the C.elegans head and selected additional sensilla

Schematic illustration of the head sensilla organ anatomy and selected additional sensilla in the adult *C. elegans*. **A**: Main sensilla of the head region. Anterior left, dorsal up. **B**: anterior view sensilla, AM = amphids (magenta), CEP = cephalic sensilla (yellow), OL = outer labial sensilla (light blue), IL = inner labial sensilla (blue). **C**: Additional sensilla of the head, body and tail region. Modified from (Altun, Z. F. and Hall, D. H., 2010), (Mizeracka, K. and Heiman, M. G., 2015).

Importantly, the socket cell is linked to both the neighboring sheath cell and the epidermis via adherens junctions (CeAJ) and, especially in the AM sensilla, ciliated dendrite tips are attached to the sheath cells through CeAJs (reviewed in (Altun, Z. F. and Hall, D. H., 2010). Many sensillar dendritic tips terminate in rigid microtubule-rich ciliated endings, which function as signal receptors. Each cilium can be sub-divided in a bulb-like peri-ciliary membrane compartment (PCMC), a ciliary transition zone (TZ) at the cilia basis, a middle part (axoneme: nine outer doublet MT) and a distal part (axoneme: nine outer singlet MTs) (reviewed in (Doroquez, D. B. et al., 2014)). Interestingly, the morphology of *C. elegans* ciliated endings is very diverse ((Ward, S. et al., 1975), (Ware, R.W. et al., 1975), (Perkins, L. A. et al., 1986) (Doroquez, D. B. et al., 2014)). In addition to the main head sensilla, the anterior deirid sensilla (ADE L/R; located close to the posterior pharynx region) and the posterior deirid sensilla (PDE L/R; located close to vulva and anus) are present (reviewed in (Altun, Z. F. and Hall, D. H., 2010) **Figure 1.13C**, only neurons shown). Most posteriorly, at the tail region, the phasmid sensilla (PHA L/R) are localized.

a. The amphid sensilla (AM)

The amphids (AM) are positioned in the head of *C. elegans* and throughout nematodes they are described as the main chemosensory sensilla (reviewed in (Altun, Z. F. and Hall, D. H., 2010)). This study unveils how their special elongated shape is established during embryogenesis and which morphogenetic events facilitate AM development. The AM are located as a bilateral pair of sensilla (AM L/R), both contain 12 ciliated sensory neurons each, which are encased by one socket (AMso) and one sheath (AMsh) cell ((Ward, S. et al., 1975), (Ware, R.W. et al., 1975), (Perkins, L. A. et al., 1986), reviewed in (Altun, Z. F. and Hall, D. H., 2010) **Figure 1.14**). The cell bodies of the bipolar AM neurons are positioned posterior to the nerve ring and project unbranched dendrites to the tip of the head, where the sensillar endings are located (reviewed in (Altun, Z. F. and Hall, D. H., 2010) **Figure 1.14A**). Also, the AML and AMR axons project into the nerve ring (NR) and the ventral nervous system (VNC) via the amphid commissures on the left and right side of the head (reviewed in (Altun, Z.F. and Hall, D.H., 2011) **Figure 1.14C**). The AMso enwraps the most distal part of the ciliated dendrite tips creating a pore and the AMsh encases the ciliated endings directly posterior to the AMso, thus building a pouch-like structure (reviewed in (Altun, Z. F. and Hall, D. H., 2010) **Figure 1.14B**). Pore and pouch-like structure together form the AM channel, enabling the AM sensory dendrite endings to get in contact with the environment. Eight ciliated AM dendrites penetrate the AMsh cell, project through the AMsh pocket and extend through the AMso pore (ASE, ASG, ASH, ASI, ASJ, ASK, ADF, ADL, **Figure 1.14B, Table 1.1**). Several ciliated dendrite endings project throughout the AMsh pocket but re-enter and terminate within the AMsh (AWA, AWB, AWC). In addition, one dendritic ending is located completely inserted in the AMsh without entering the AM channel (AFD). The AM neurons mainly function in chemosensation, thermosensation and mechanosensation ((Bargmann, C.I. and Mori, I., 1997), (Driscoll, M. and Kaplan, J., 1997), (Bargmann, 2006) **Table 1.1**). The AM dendritic tips exhibit ciliated endings with multiple shapes: One or two rod-like cilia shape (ASE, ASG, ASH, ASI, ASJ, ASK, ADF, ADL), wing-like shape (AWA, AWB, AWC) or even finger-like shape with numerous microvilli (AFD) ((Ward, S. et al., 1975), (Ware, R.W. et al., 1975), (Perkins, L. A. et al., 1986), (Doroquez, D. B. et al., 2014) **Figure 1.14B, B'**). The cilia of ADF, ADL and AWB dendrites branch at the transition zone (TZ), whereby AWA and AWC cilia branch distal to the TZ and AFD cilia are branching proximal to the TZ (Doroquez, D. B. et al., 2014). Interestingly, the morphology of wing-like expansions at the two AWB ciliary branches adapts to external stimuli (Mukhopadhyay, S. et al., 2008). The AFD cilium shows completely different morphology, because it's shape is unbranched, originates from an enlarged dendrite and it comprises microvilli without microtubules (Doroquez, D. B. et al., 2014).

AM dendrites are collectively projecting within a lateral nerve bundle on each side of the head, accompanied by AMsh and AMso extensions (reviewed in (Altun, Z. F. and Hall, D. H., 2010) **Figure 1.14A, C''**). Within the nerve fiber, AM dendrites are suggested to be arranged very ordered ((Ward, S. et al., 1975), (Doroquez, D. B. et al., 2014)), but their order is not consistent throughout the length of the whole nerve fiber (Yip, Z. C. and Heiman, M. G., 2018). For instance, the ASE dendrite is located in the center of the bundle throughout the posterior nerve part until a switch point occurs, from which one AFD dendrite is mainly positioned in the center of the bundle throughout the anterior part of the head (Yip, Z. C. and Heiman, M. G., 2018). Most constant positioning of the dendrites within the bundle is present at anterior parts close to the tip of the head. But correct positioning of ciliated endings seems to be not necessary for the arrangement of dendrites within the AM bundle. The order of dendrites persists from early stages throughout larval development. Moreover, the cell adherens molecule (CAM) SAX-7 seems to determine establishment and maintenance of correct dendrite order within the AM nerve-bundle (Yip, Z. C. and Heiman, M. G., 2018).

Recently, several factors were reported to be involved in AM sensilla development. Thereby, DAF-6 (Patched-like) and CHE-14 (Dispatched-like) were suggested to contribute to AM lumen formation ((Perens, E.A. and Shaham, S., 2005) **Figure 1.15**). CHE-14 was described as functioning in exocytosis (Michaux, G. et al., 2000). The proposed model for AM channel lumen establishment hypothesizes that "DAF-6 may inhibit endocytosis, while CHE-14 may promote exocytosis" (Perens, E.A. and Shaham, S., 2005). In addition, DYF-7 (zona pellucida protein) and DEX-1 (zonadhesin domain containing protein) are suggested to contribute to attaching dendrite tips to the anterior part of the head during the embryonic development of the AM sensilla (Heiman, M. G. and Shaham, S., 2009). Also, epithelial adhesion components are suggested to influence the morphology of sensory dendrite endings ((McLachlan, I.G. and Heiman, M.G., 2013) **Figure 1.15**). Importantly, since the AM sensilla openings contain junctional components interlinking dendrite tips, AMsh, AMso and the epidermis ((Ward, S. et al., 1975), (Perkins, L. A. et al., 1986), (Altun, Z.F. et al., 2009)), the AM sensilla are placed completely embedded within the epidermis (reviewed in (Chisholm, A. D. and Hsiao, T. I., 2012)), thus epidermis and integrated AM sensilla together can be interpreted as a continuous sheet (**Figure 1.15**).
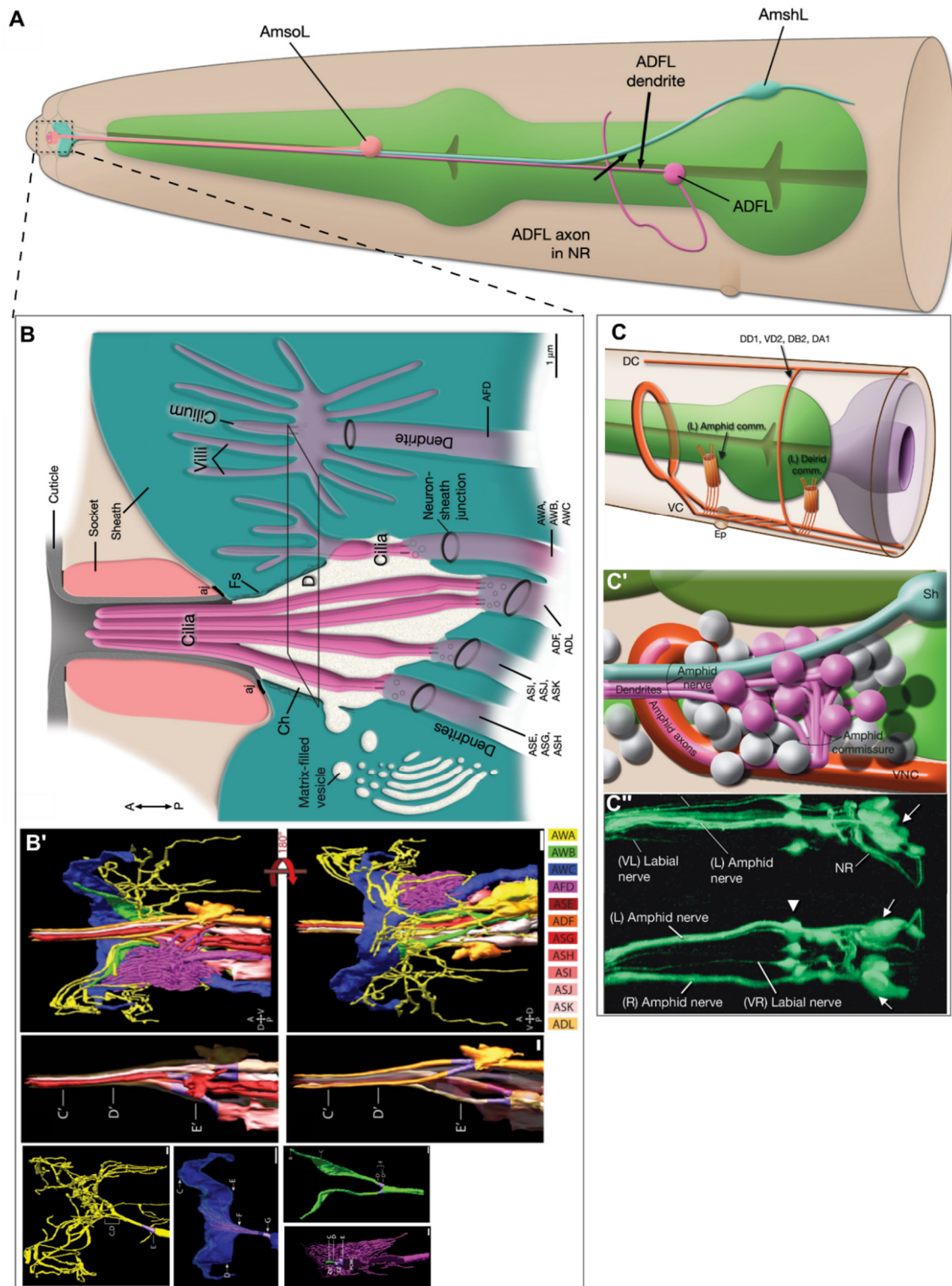
Figure 1.14: Detailed AM anatomy

A: Schematic illustration of anatomy of amphid left sensillum. Exemplary ADFL neuron, left AM socket (AMso) and left AM sheah (AMsh) shown. ADFL axon projects into nerve ring (NR). **B**: Closed-up longitudinally view of amphid sensillar ending anatomy. AMso creates pore and AMsh builds pouch. Pore and pouch = AM channel. Ciliated dendrite endings penetrate pocket and pore and reach environment (ASE, ASG, ASH, ASI, ASJ, ASK, ADF, ADL); get embedded in the AMsh partly (AWA, AWB, AWC) or fully (AFD). Adherens junctions (aj) **B'**: 3D reconstruction of ciliated endings of the AM dendrites. **C-C''**: Schematic illustration and imaging of AM commissures (C, C') and AM/ labial nerve trajectories (C''). Modified from (Altun, Z. F. and Hall, D. H., 2010), (Altun, Z.F. and Hall, D.H., 2011), (Doroquez, D. B. et al., 2014).

Table 1.1: Amphid neuron morphology and functions

Modified from (Altun, Z.F. and Hall, D.H., 2011) (Altun, Z. F. and Hall, D. H., 2010) (Bargmann, 2006) wormatlas.org.

AM Neuron	Function	Morphology	NT	Target	Response
AW AWA/AWB/AWC		AMsh-Pocket-Amsh Amphid wing cells, sheet-like sensory endings			
AWB (R/L)	odorsensory	Amphid wing "B" cells	Ach	AIZ	Chemotaxis
	electrosensory				light
	photosensory (350-470nm)				towards negative pole
AFD (R/L)	thermosensory CO2-sensory	completely embedded in AMsh Finger like ciliated endings	Glu	AIY	Thermotaxis
					Thermonociseption
AS ASE/ASG/ASH/ASI/ASJ/ ASK		Amsh - Pocket - AMso - outside Single ciliated endings axon: projects into VC & NR via amphid commissure diverse synaptic connections in ring neuropil			
ASH (R/L)	polymodal nociceptive		Glu		Nociception
	osmo-, mechano-, electro-,				innate immune response
	photo-, odorsensory				Chemotaxis, social feeding
ASI (R/L)	chemosensory			AIA, AIB, AIY, AIZ	Chemotaxis
	gustatory				dauer entry
	thermosensory				life span
ASK	chemosensory		Glu		dauer entry
					life span
					Chemotaxis
AD ADF/ADL		Amsh - Pocket - AMso - outside dual ciliated endings			
ADF (R/L)	chemosensory	axon: projects into VC & NR via amphid commissure	Ach	RIA, AIZ, AUA, SMB	Chemotaxis (hypoxia)
	gustatory		Ser		dauer entry
	oxygen-sensory				
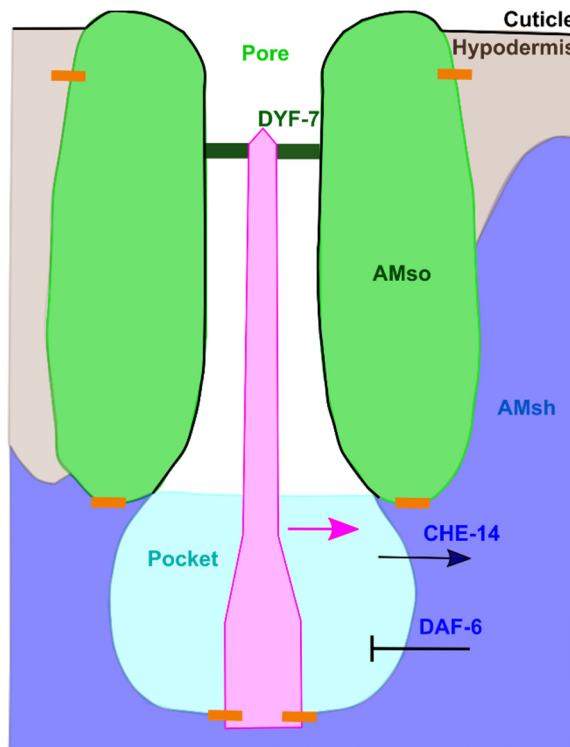
Figure 1.15: The AM sensilla opening, junctional components and described factors

Schematic illustration of the AM sensilla ending highlighting the position of adherens junctions and factors reported to contribute to AM development. AM cells adherens junctions (orange). AMso = amphid socket cell, AMsh = amphid sheath cell. Modified based on (Altun, Z. F. and Hall, D. H., 2010), (Heiman, M. G. and Shaham, S., 2009), (Perens, E.A. and Shaham, S., 2005).

b. The cephalic (CEP) and labial sensilla (IL/OL)

The *C. elegans* head does not only contain the two-fold lateral AM sensilla, but also four-fold symmetric cephalic (CEP) and six-fold symmetric inner labial/outer labial sensilla (IL/OL) (reviewed in (Altun, Z. F. and Hall, D. H., 2010) **Figure 1.16**). Every CEP sensillar ending comprises one sheath and one socket cell (CEPsh/CEPso) which ensheath one ciliated dendrite (CEPVL, CEPVR, CEPDL, CEPDR). All CEP neurons are dopaminergic and suggested to function in mechanosensation ((Sulston, J. et al., 1975), (Sawin, E.R. et al., 2000)). Thereby, the axon of every CEP neuron projects into the nerve ring (NR) and the dendritic tip terminates in a ciliated ending within the cuticle of the lips ((White, J. G. et al., 1986) **Figure 1.16A, D, F**). Interestingly, each CEPsh cell manifests lamellar invaginations and bipolar morphology (reviewed in (Altun, Z. F. and Hall, D. H., 2010), (Mizeracka, K. and Heiman, M. G., 2015)). Thus, every CEPsh cell projects one anterior process accompanying the dendrite tracks, which is eventually encasing one CEP ciliated neuronal tip (reviewed in (Altun, Z. F. and Hall, D. H., 2010)). Thereby a channel created by CEPsh ending and CEPso ending enwraps one CEP dendrite tip **(Figure 1.16D)**. The cilium within each CEP sensillar ending extends through the CEP channel and terminates embedded within the cuticle. Also, the CEP cilia structure exhibits a widened shape. As a special feature within CEP, each posterior AMsh process encases parts of the NR. Also, the NR morphogenesis is proposed to get facilitated through CEPsh cells (Wadsworth, W. G. et al., 1996). Importantly, adherens junctions interconnect the dendrite tips with the CEPsh, the CEPsh and the CEPso and the CEPso itself with the epidermis (reviewed in (Altun, Z. F. and Hall, D. H., 2010)).

Inner labial sensilla (IL) localize with six-fold symmetry in the adult *C. elegans* head (ILDL/R, ILLL/R, ILVL/R (reviewed in (Altun, Z. F. and Hall, D. H., 2010) **Figure 1.16C**). Within each of the IL sensilla endings, one socket cell (ILso) and one sheath cell (ILsh) enwrap two ciliated dendrite tips (IL1, IL2, **Figure 1.16E**). Thereby the IL1 ciliated dendrite tip ends within an electron-dense disc ((Ward, S. et al., 1975), (Perkins, L. A. et al., 1986)) and the ciliated ending of IL2 passes through the ILsh, ILso and the cuticle, hereby getting in contact with the environment (reviewed in (Altun, Z. F. and Hall, D. H., 2010) **Figure 1.16F**). IL2 neurons are suggested to function in chemosensation (Perkins, L. A. et al., 1986) while IL1 neurons sense mechanical stimuli (Driscoll, M. and Kaplan, J., 1997). IL1 and IL2 dendrite trajectories extend anteriorly to the IL sensilla endings through six nerve bundles and their axons project posteriorly into the NR (reviewed in (Altun, Z. F. and Hall, D. H., 2010)). Interestingly, adherens junctions interconnect all compartments of the IL sensillum with each other and the epidermis such as within the CEP or AM sensilla establishing a continuous sensilla-epidermis compartment.

Furthermore, six outer labial sensilla (OL) are positioned posterior to the IL sensilla (reviewed in (Altun, Z. F. and Hall, D. H., 2010) **Figure 1.16B**). Every OL sensillar ending inherits one sheath cell (OLsh), one socket cell (OLso) and one ciliated dendrite ending (OLL or OLQ) ((Ward, S. et al., 1975), (Ware, R.W. et al., 1975), (Perkins, L. A. et al., 1986) **Figure 1.16D**). Two OLL neurons extend one dendritic tip to each of the two lateral OL sensilla and four OLQ neurons project one dendritic ending to every of the two ventral or dorsal outer labial quadrant sensilla (OLQ, **Figure 1.16B**). All OL neurons are suggested to function in mechanosensation ((Perkins, L. A. et al., 1986), (Driscoll, M. and Kaplan, J., 1997)). Within each OL sensilla, one ciliated dendrite penetrates the channel formed by OLsh and OLso terminating within the cuticle (reviewed in (Altun, Z. F. and Hall, D. H., 2010) **Figure 1.16D, F**). Also, OLsh cells exhibit lamellae structures. As described for the AM, CEP and IL, also the OL sensilla are embedded and interconnected to the cuticle through adherens junctions.
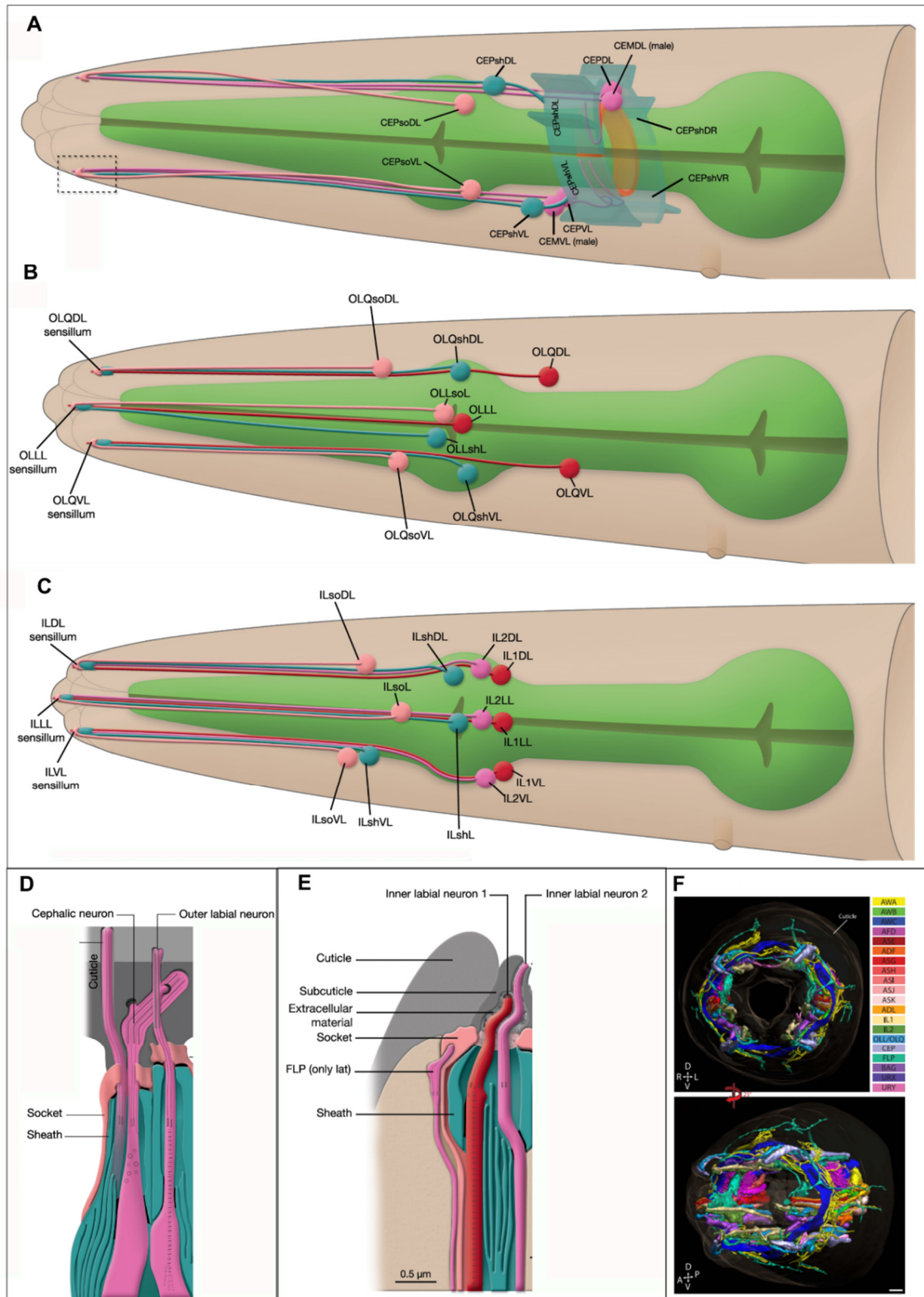
Figure 1.16: Anatomy of cephalic (CEP), inner labial (IL) and outer labial (OL) sensilla in the adult *C.elegans*
Schematic illustration of CEP, IL and OL sensilla organs. **A**: Left side cephalic (CEP) sensillum **B**: Left outer labial (OL) sensillum. **C**: left inner labial sensillum. **D**: Sensillar ending of CEP & OL. **E**: IL sensillar ending morphology. **F**: 3D reconstruction exhibiting positioning of head dendrites. Modified from (Altun, Z. F. and Hall, D. H., 2010), (Doroquez, D. B. et al., 2014).

c. *C. elegans* sensory neurons – brief overview

Within the mature hermaphrodite *C. elegans* worm 302 neurons with monopolar or bipolar structures and mainly unbranched neurites are present ((White, J. G. et al., 1986), reviewed in (Altun, Z.F. and Hall, D.H., 2011)). The neurons are either generated during embryonic stages (proliferation phase) or at larval stages (late-L1, L2) ((Sulston, J.E. and Horvitz, H.R., 1977), (Sulston, J. E. et al., 1983)) and most neurons and all neuronal support cells arise from the AB lineage ((Sulston, J. E. et al., 1983), (Altun, Z.F. and Hall, D.H., 2011)). The *C. elegans* neurons are categorized into sensory neurons, motor neurons, interneurons, polymodal neurons (multiple functions) and neurons with unknown function (reviewed in (Altun, Z.F. and Hall, D.H., 2011)). Most sensory neurons act in chemosensation and many function in thermo- or mechanosensation (**Table 1.2**), they often contain ciliated endings and mostly occur assembled within sensilla or as solitary sensory neurons (reviewed in (Bargmann, 2006), (Bergamasco, C. and Bazzicalupo, P., 2006), (Altun, Z.F. and Hall, D.H., 2011)).

Table 1.2: Sensory neuron categories and associated neurons in *C.elegans*
Modified from (Altun, Z.F. and Hall, D.H., 2011).

Chemosensors (Taste)
Cilia exposed to outside
Amphids
  ADF (2, head) 5,9
  ASE (2, head) 6,7,9
  ASG (2, head) 5,9, 21
  ASH (2, head) 1,7, 8, 10, 13, 19, 22
  ASI (2, head) 5, 9, 20, 21
  ASJ (2, head) 5, 9, 21
  ASK (2, head) 6, 9, 19, 20, 21
  ADL (2, head) 10, 22

Inner labials
  IL2 (6, head)

Phasmids 8
  PHA (2, tail)
  PHB (2, tail)

Odorsensors (Smell)
Cilia embedded in sheath
Amphids
  AWA (2, head) 11, 21
  AWB (2, head) 10
  AWC (2, head) 11, 20, 21
Cilia exposed to outside
Amphids
  ASH (2, head) 1,7, 8,10,13, 19, 22

Oxygen sensors
Cilia or cell body in psuedocoelomic cavity 22
  AQR (1, head)
  PQR (1, tail)
  URX (2, head)
Unexposed ciliated endings in the lips
  BAG (2, head) 3

Nociceptors (Pain)
Amphids
  ASH (2, head) 1,7, 8,10,13, 19, 22

Osmoceptors
Amphids
  ASH (2, head) 1,7, 8,10,13, 19, 22
(Also AFD, FLP, PHC and PVD neurons as thermonociceptive) 24

Thermosensors
Cilia embedded in sheath
Amphids
  AFD (2, head) 23
  AWC (2, head) 23
Extensively branched (thermonociceptive)
  FLP (2, head) 24
  PVD (2, body) 24
Tail tip (thermonociceptive)
  PHC (2, tail) 24

Mechanosensors
Microtubule-filled dendrites (MT cells)
Bodywall 12
  ALM (2, body)
  AVM (1, body)
  PLM (2, tail)
  PVM (1, body)
Unexposed cilia ending in cuticle
Inner labials
  IL1 (6, head) 3,13
Cephalic
  CEP (4, head) 4
Outer labials
  OLQ (4, head) 3,13
  OLL (2, head) 3,17
Anterior and Posterior deirids
  ADE (2, head) 4
  PDE (2, body) 4
Cilia exposed to outside
Amphids
  ASH (2, head) 1,7, 8,10,13, 19, 22
Extensively branched
  FLP (2, head) 13, 23
  PVD (2, body)

Possible sensory neurons with unknown modality
Unexposed endings (no cilia)
  AUA (2, head)
  URY (4, head)
  URA (4, head)
  URB (2, head)

Proprioceptors 18
Putative stretch-sensitive processes
Somatic-bodywall
  FLP (2, head) 13
  PVD (2, body) 14
  DVA (1, tail)
  PVC (2, tail) 14
  ALN (2, tail) 16, 22
  PLN (2, tail) 16, 22
  VA 15
  VB 15
  DA 15
  DB 15
Head
  SMB (4, head) 15
  SMD (4, head) 15
  SAA (4, head) 15
Tail tip 16
  AVG (1, head)
  PDB (1, tail)
  PHC (2, tail) 3
  PVR (1, tail)
  ALN (2, tail)
  PLN (2, tail)
  PLM (2, tail)
Pharynx 2
  I1 (2, head)
  I2 (2, head)
  I3 (1, head)
  I5 (1, head)
  I6 (1, head)
  MC (1, head)
  M3 (2, head)
  NSM (1, head)

©WormAtlas

Firstly, chemosensation/gustatory sensation of water-soluble chemicals and odor sensation/olfactory sensation of volatile chemicals are conducted by 32 sensory neurons ((Mori, 1999), reviewed in (Bargmann, 2006), (Altun, Z.F. and Hall, D.H., 2011) **Table 1.1, Table 1.2**). Most of these neurons belong to the AM sensilla (**Table 1.1**), some are within the IL sensilla (IL2) or are part of the phasmid sensilla (**Table 1.2**) (reviewed in (Altun, Z.F. and Hall, D.H., 2011)). Repellant or attractive cues are mostly sensed by different AM neurons, but also some neurons are able to detect both ((Bargmann, C.I and Horvitz, H.R., 1991), (Troemel, E.R. et al., 1997)). Chemosensation of water-soluble chemicals is suggested to be mainly executed by ASE, getting assisted by the ADF, ASE, ASG, ASI, ASJ and ASK neurons (reviewed in (Altun, Z.F. and Hall, D.H., 2011) **Table 1.1**). Volatile chemicals are detected and discriminated by AWA, AWB and AWC neurons ((Wes, P.D. and Bargmann, C.I., 2001), reviewed in (Altun, Z.F. and Hall, D.H., 2011)), whereby "the two AWC neurons display molecular and functional asymmetry" (reviewed in (Alqadah, A. et al., 2016)).

Secondly, mechanosensation includes the sensation of gentle/light touch, harsh touch and texture (**Figure 1.17, Table 1.2, Table 1.1**) through different categories of touch receptors (reviewed in (Altun, Z.F. and Hall, D.H., 2011)). Thereby, ciliated mechanoreceptors, neurons comprising thick microtubules (MT cells) and neurons without stereotypic cytoskeletal aspects occur. The worm reacts to all mechanosensory stimuli with avoidance behaviors. Within the head, touch is detected by IL1, OLQ and FLP neurons ((Kaplan, J. M. and Horvitz, H. R., 1993), (Chatzigeorgiou, M. and Schafer, W.R., 2011), reviewed in (Altun, Z.F. and Hall, D.H., 2011) **Figure 1.17A**). Sensation of surface texture within the head is implemented by CEP and ADE (anterior deirid, ADEL/R neurons (Sawin, E.R. et al., 2000) **Figure 1.17B**) aiding in navigation for food sources (reviewed in (Altun, Z.F. and Hall, D.H., 2011)). Throughout the worm's body, gentle touch is detected posteriorly by the two PLM (posterior lateral MT cells, PLMR/PLML) and the unpaired PVM (posterior ventral MT cell) touch receptor neurons (reviewed in (Altun, Z.F. and Hall, D.H., 2011) **Figure 1.17C**). Anteriorly, the two ALM (anterior lateral MT cells, ALMR/L) neurons and the single AVM (anterior ventral MT cell) neuron function in gentle touch sensation. Notably, AVM and PVM are born post-embryonically, whereas ALM and PLM arise during embryonic stages. Gentle body touch modifies egg-laying and pharyngeal pumping. Sensation of harsh body touch mainly is suggested to be sensed by PVD neurons (PVDR/L) (Way, J.C. and Chalfie, M., 1989) **Figure 1.17D**). Detection of surface texture within the body is executed by the PDE neurons (posterior deirids PDEL/R) ((Sawin, E.R. et al., 2000) **Figure 1.17B'**). Moreover, *C. elegans* sensory neurons also function in thermosensation, carbon dioxide/oxygen sensation and detection of damaging external conditions (nociception) (reviewed in (Altun, Z.F. and Hall, D.H., 2011) **Table 1.2**, **Table 1.1**).
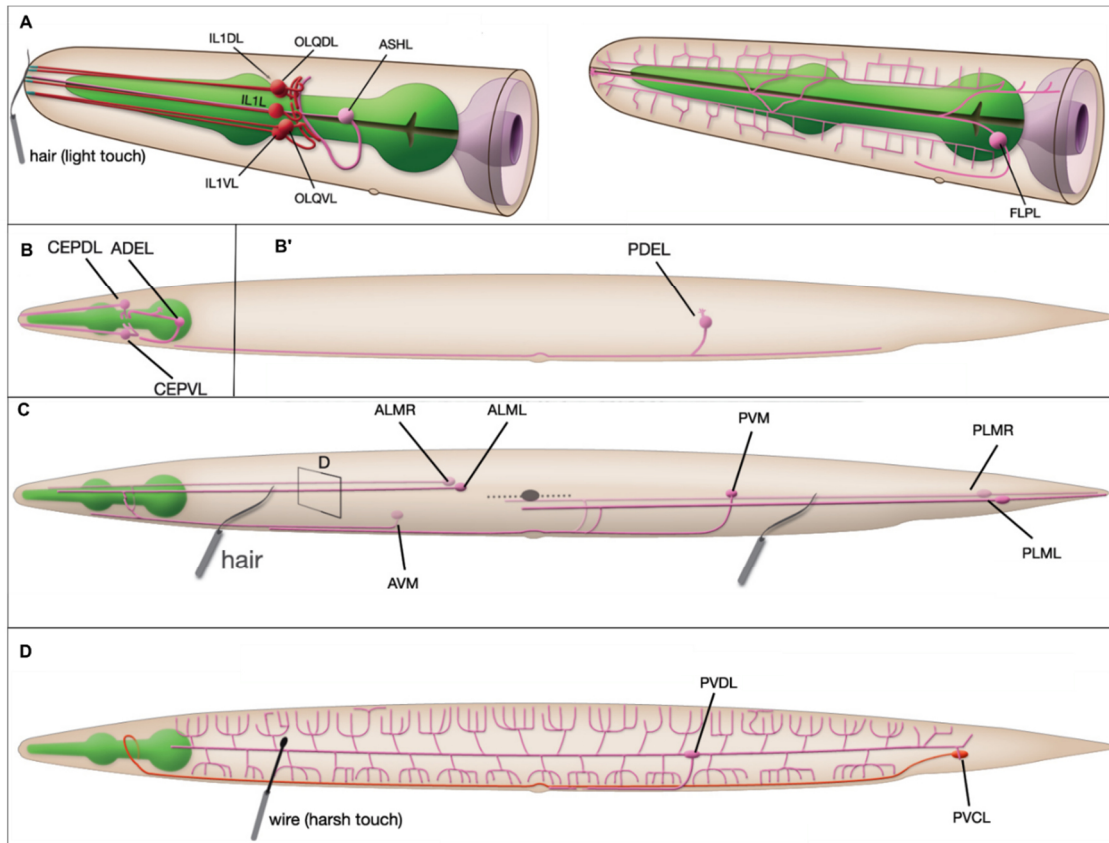
Figure 1.17: Position of selected sensory neurons in the adult *C.elegans*

Schematic illustrating position of selected sensory neurons in C. elegans head and body. **A**: Sensory neurons in the head detecting gentle touch (IL1, OLQ, FLP) and harsh touch (OLQ, FLP, ASH) **B-B'**: Texture sensing neurons within head (B, CEPD, ADE) and the body (B', PDE) **C**: Sensory neurons detecting gentle body touch anteriorly (AVM, ALM) and posteriorly (PVM, PLM) **D**: Harsh touch body detection neurons (PVD, PVC). Neurons shown on left side only (IL, OLQ, ASH, FLP, CEP,ADE,PDE,PVD,PVC). Modified from (Altun, Z.F. and Hall, D.H., 2011).

1.7. The Ubiquitin-Proteasome-System (UPS) - Focus on the nervous system

Protein degradation by the ubiquitin-proteasome system (UPS) is important for the nervous system in multiple aspects (reviewed in (Hegde, A.N. and Upadhya, S.C., 2007), (Hamilton, A. M. and Zito, K., 2013)). For instance, the UPS contributes to synaptic plasticity (Bingol, B. and Schuman, E.M., 2005), axonal pruning ((Kuo,C.T. et al., 2005), (Hoopfer, E.D. et al., 2006)) and intracellular trafficking (reviewed in (Acconcia, F. et al., 2009), (Schwarz, L.A. and Patrick, G.N., 2012)). Importantly, incorrect UPS-mediated degradation of dysfunctional proteins is suggested to be involved in nervous system derived illnesses like Alzheimer's disease (de Vrij, F.M. et al., 2004). Through the UPS, specific or misfolded proteins get first tagged with ubiquitin (Ub) and then decomposed by the proteasome (reviewed in (Hamilton, A. M. and Zito, K., 2013), (Massaly, N. et al., 2015) **Figure 1.18**). Firstly, ubiquitination is mediated by ubiquitin activating enzymes (E1), ubiquitin-conjugating enzymes (E2) and ubiquitin ligases (E3) (reviewed in (Massaly, N. et al., 2015)). Thereby, E1 activates Ub which is transferred to E2, where after E2 together with E3 link Ub to a target protein (**Figure 1.18B**). Through repeated conjugation of Ub and their interconnection via specific Ub lysine residues (K6, K11, K27, K29, K33. K48, K63), different poly-Ub chains are created (reviewed in (Hamilton, A. M. and Zito, K., 2013)). Especially, K-48 linked poly-Ub chains are tagging a target for degradation via the 26S proteasome. However, besides marking proteins for proteasomal degradation, specific ubiquitination can lead to lysosomal degradation, protein trafficking or even protein activation. Additionally, deubiquitinating enzymes (DUBs) act by removing Ub (reviewed in (Massaly, N. et al., 2015)). The 26S proteasome (**Figure 1.18A**) contains two regulatory 19S proteasome complexes (regulatory particles, RP) and the catalytic 20S proteasome (core particle, CP), the latter being responsible for protein degradation (reviewed in (Massaly, N. et al., 2015)). In more detail, the barrel shaped 20S CP comprises two internal ($\beta1$ to $\beta7$) and two external rings ($\alpha1$ to $\alpha7$). The internal rings have catalytic function ($\beta1$, $\beta2$, $\beta5$) and the external rings enable proteins to reach the internal rings. The two 19S RP complexes flank the 20S catalytic core and are designated as proximal lid and distal base (reviewed in (Pathare, G. R. et al., 2012), (Massaly, N. et al., 2015)). The base contributes to protein unfolding and localization to the 20S CP and contains six Rpt (regulatory particle ATPases, Rpt1-Rpt6) and four Rpn proteins (Rpn1, Rpn2, Rpn10, Rpn13). The lid functions in detecting Ub tagged proteins and in Ub removal (**Figure 1.18A**). It consists of nine Rpn protein subunits (regulatory particle non-ATPase, Rpn3, Rpn5-Rpn9, Rpn11, Rpn12), which are subdivided by their proposed structure (Pathare, G. R. et al., 2012). The first subclass (Rpn3, Rpn5, Rpn6, Rpn,7, Rpn9, Rpn12) mainly share eIF3 (PCI module) and COP9/signalosome domains, whereby the second subunits (Rpn8, Rpn11) share MPN (Mpr1, Pad1) domains. Importantly, Rpn6 was reported as essential for *Drosophila* development (Lier, S. and Paululat, A., 2002), for proliferation in *Saccharomyces cerevisiae* (Saito, A. et al., 1997) and to function as UPS activator (Pathare, G. R. et al., 2012).
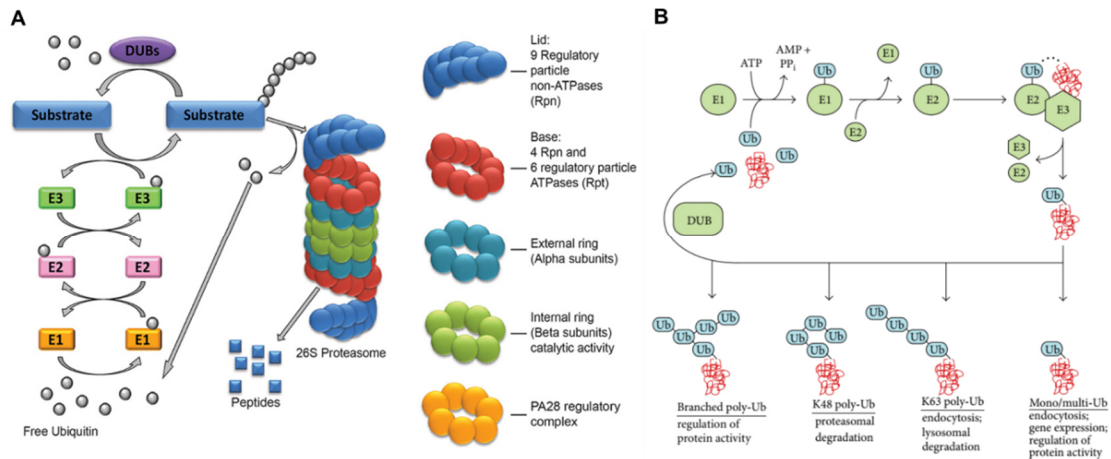
Figure 1.18: The 26S proteasome and the Ubiquitin-Proteasome-System (UPS)

Schematic illustration of ubiquitination/deubiquitination and 26S proteasome components. **A**: 26S proteasome complex. Ubiquitination through E1, E2 and E3 and deubiquitination by DUBs. **B**: Ubiquitination and polyubiquitination can lead to proteasomal degradation, endocytosis, protein activation according to specific added Ub tags. Modified from (Massaly, N. et al., 2015), (Hamilton, A. M. and Zito, K., 2013).

Within the *Drosophila melanogaster* 26S proteasome, Rpn6 (49 kDa, regulatory particle non-ATPase 6; *C. elegans:* RPN-6.1) is positioned at the outward edge of the 19S RP lid, extending to the external rings (α1 to α7) of the catalytic 20S CP linking to the ATPase ((Pathare, G. R. et al., 2012) **Figure 1.19A**). Rpn6's ultrastructure is composed of a PCI module, an α-helical solenoid (**Figure 1.19B**) and a "horseshoe" structured PCI module (**Figure 1.19A**). Rpn6 seems to be in direct contact with the PCI subunit Rpn7, thereby possibly forming a PCI:PCI interaction module. The PCI subunits are proposed to be arranged as Rpn9-Rpn5-Rpn6-Rpn7-Rpn3-Rpn12 in the lid section. Of major importance for this study is the conclusion that "the reported interactions of Rpn6 with the ubiquitin ligase regulatory complex COP9/signalosome probably control its own degradation ((Kwok, S.F. et al., 1999), (Lier, S. and Paululat, A., 2002)), which might in turn regulate the assembly and activation of 26S proteasomes through the availability of monomeric Rpn6" (Pathare, G. R. et al., 2012).

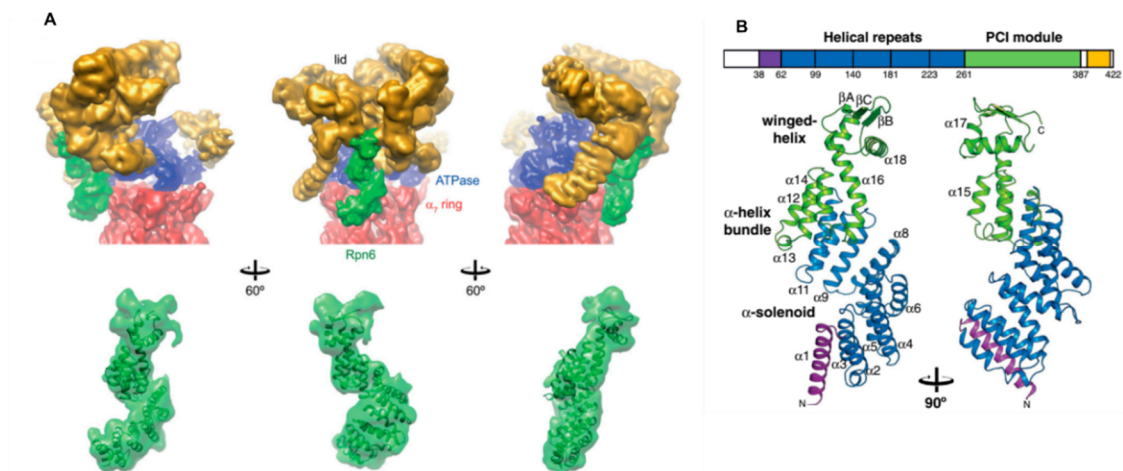**Figure 1.19: Schematic 3D illustration of the proximal half of the proteasome, highlighting Rpn6 protein structure**

A: 26S proteasome and Rpn6 structure showing Rpn6 (green), lid (yellow), α-rings (red) and ATPase (blue). Rpn6 contacts lid, ATPase and α-rings. **B**: Crystal structure of Rpn6. Top: Domains of Rpn6. Bottom: Rpn6 structure ribbon illustration. Modified from (Pathare, G. R. et al., 2012).

Since this study's focus mainly lays on neuronal morphogenesis, the influence of UPS factors for morphological aspects in axons, dendrites and dendritic spines will be briefly described below (reviewed in (Hamilton, A. M. and Zito, K., 2013) **Figure 1.20**). The main factors acting in axon growth and guidance are PHR-family E3-ligases, which were identified for functioning in axonal growth and guidance. The *Drosophila* E3-ligase Highwire and its *C. elegans* (RPM-1) and vertebrate orthologs (Phr1), were documented as important UPS factors in axon guidance or synaptogenesis ((Schaefer, A.M. et al., 2000) (Bloom, A.J. et al., 2007) (Shin, J.E. and DiAntonio, A., 2011)). Besides the PHR-family E3-ligases, the modular Ub-ligase anaphase promoting complex (APC) regulates axon growth through controlling several downstream transcription factors (e.g. SnoN, Id2, Ccd1) (reviewed in (Hamilton, A. M. and Zito, K., 2013)). Interestingly, the E3-ligase Nedd4-1 (Neuronal Precursor Cell Expressed and Developmentally Downregulated Protein) was found to play roles in axonal and dendritic morphogenesis. Also, dendrite morphogenesis and branching are suggested to be influenced by multiple UPS factors (**Figure 1.20**). For instance, the E3-ligases APC^{Cdc20} and Nedd4-1 facilitate dendrite growth and arborization ((Kim, A.H. et al., 2009), (Kawabe, H. et al., 2010)). The E3-ligase Mind bomb-1 (Mib1) is described to play a role for dendrite development in zebrafish and *Drosophila* through regulation of Notch signaling ((Itoh, M. et al., 2003), (Daskalaki, A. et al., 2011)). Additionally, proteasome activity and localization is suggested to regulate outgrowth of dendritic spines ((Hamilton, A.M. et al., 2012), reviewed in (Hamilton, A. M. and Zito, K., 2013)).
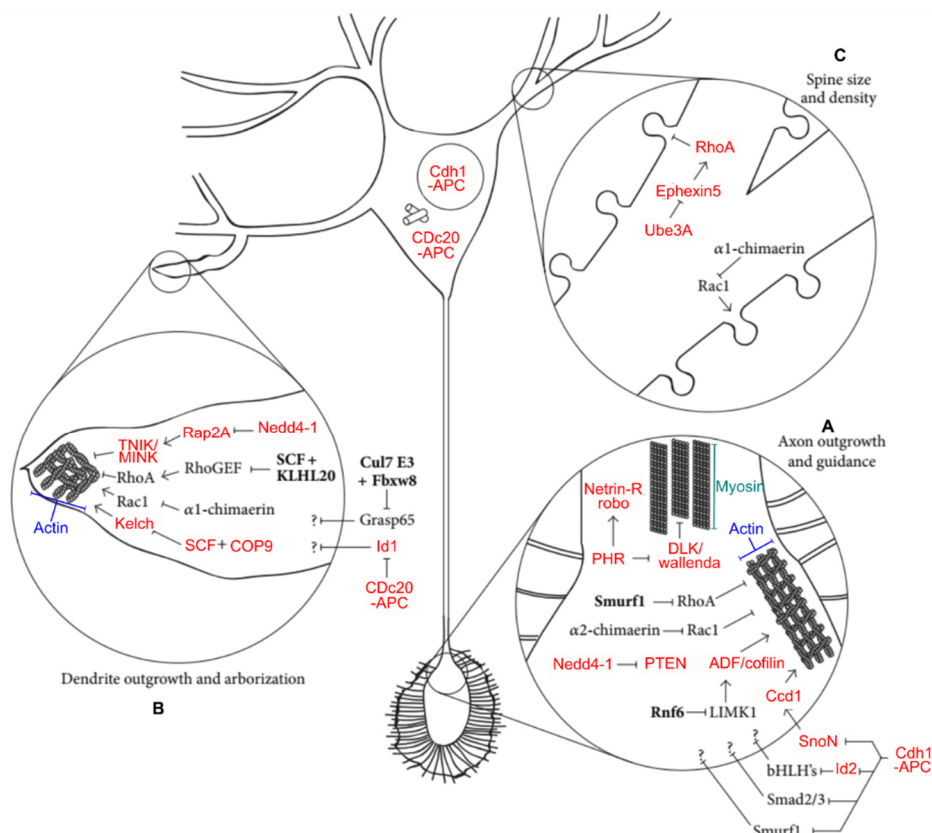

Figure 1.20: UPS factors function in neural development
Schematic overview showing UPS factors controlling neuronal development. **A**: UPS factors facilitate axon growth & guidance. **B**: Dendrite growth & branching controlled by UPS factors. **C**: UPS-regulated dendrite spine outgrowth. Modified from (Hamilton, A. M. and Zito, K., 2013).

2. Materials & Methods

2.1. Materials

a. Laboratory equipment

Table 2.1: Laboratory equipment

Equipment	Type	Source
Balance	Precision Balance PCB CP64	Kern Sartorius
Beaker/ Flasks/ Erlenmeyer Flasks	100 µL, 250 µL, 500 µL, 1000 µL 100 mL, 250 mL, 500 mL, 1000 mL, 2000 mL 250 mL, 500 mL	
Bunsen Burner	gas profi 1 – micro	WLD-TEC
Centrifuge	Heraeus Megafuge 16R Heraeus Pico17 Microcentrifuge Avanti® Centrifuge J-26 XP Microcentrifuge with Micro Tube Rotor and PCR Strip Adapter	Thermo Scientific Thermo Scientific Beckman CoulterTM NeoLab®
Dissection Stereo Microscope	SMZ-168	Motic
Fluorescence Microscope	Leica M165 FC	Leica
Freezer (-80°C) Fridge	HeraFreeze TOP CN 4315 Comfort	Thermo Scientific Liebherr
Gel/Blot Illumination System	ChemiDocTM MP Imaging System	Bio Rad
Gel-Electrophoresis System	Mini Gel II	VWR
Hairpick (eyelash)		
Ice Mashine	AF 80	Scotsman®
Incubator/Shaker Incubator Inoculating Loop	Unimax 1010 HerathermTM Compact Microbiological Incubator Certomat BS-1 Nichrome Innoculation Wire Loops	Heidolph Instruments Thermo Scientific B.Braun Biotech International Fisher Scientific
Laminar Flow	Maxisafe 2020 Class II Biological Safety Cabinet	Thermo Scientific
Laser ablation setup	MLC03A-DPI VS-FRAPcontrol VS-Laser Control system Integrated 355 nm UV laser	Visitron Systems
Magnetic Stirrer	R basic 2	IKA
Metalpick	99,9% platinum wire (0,3 mm) 99,9% platinum wire (0,5 mm)	VWR
Microwave	Smart Inverter Magneton	LG
Micropipette puller	P-97 Flaming/Brown micropipette puller	Sutter Instruments
Microinjection setup	Leica DMIL LED microscope with 40×/0.75 PH2 air objective Hoffman modulation contrast SMX micromanipulator MINJ-1 microinjector with a MINJ-4 needle holder Einhell compressor	Leica Microsystems Sensapex Oy Tritech Research Einhell

Mouth Pipette		Dutta et al., 2015
Objective	HC PL APO 40x/1.30 oil objective HC PL APO 63x/1.4-0.6 oil	Leica Leica
Paintbrush (soft)		
PCR Cycler	Arktik™ Thermocycler	Thermo Scientific
Peristaltic Pump	LA900	Landgraf Laborsysteme
Pipettes	2 μL, 10 μL, 20μL, 200 μL, 1000μL	Eppendorf™
Rotor (with flasks)	FIBER Lite® F10BCI – 6x500y	Beckman
Scalpel		
Shaker	Nutating Mixer KS130 basic	VWR IKA
Spectrophotometer	NanoDrop1000 Spectrophotometer	Thermo Scientific
Thermomixer/shaker	ThermoStat Plus Termomixer comfort GrantBio – PHMT-PSC20	Eppendorf™ Grant
UV Illuminator	UV Transilluminator 312 nm (23 x 30 cm)	Intas Science Imaging
VisiScope spinning disk confocal microscope system (long-term imaging)	Leica DMI6000B inverted microscope Yokogawa CSU X1 scan head Hamamatsu ImagEM EM-CCD Piezo-driven motorized stage Leica HC PL APO 63X/1,4-0,6 oil objective	Visitron Systems Leica Yokogawa Hamamatsu Applied Scientific Instrumentation
Vortex	Vortex genius 3	IKA

b. Reagents & Consumables

Chemicals for this study mainly were obtained from VWR (Darmstadt, Germany), Carl Roth (Karlsruhe, Germany) or SIGAM-Aldrich (now Merck KGaA, Darmstadt, Germany).

Table 2.2: Chemicals

Chemicals	Supplier
Acetic Acid	Carl Roth
Agar	AppliChem
Agarose	Carl Roth/ Sigma Aldrich
Ampicillin	AppliChem
Calcium chloride (diydrate)	Carl Roth
Cholesterol	
Diethylpyrocarbonate (DEPC)	
Dipotassium phosphate	Carl Roth
Disodium phosphate	Carl Roth
Ethanol	Carl Roth
Glycerol	Carl Roth
LB-Medium (premix)	
Magnesium chloride (tetrahydrate)	Carl Roth

Magnesium sulfate	Carl Roth
Mangages chloride (tetrahydrate)	Carl Roth
Monopotassium phosphate	Carl Roth
Nystatin	AppliChem
Peptone	Carl Roth
Potassium chloride	Carl Roth
Sodium acetate	Carl Roth
Sodium chloride	Carl Roth
Sodium hydroxide	Carl Roth
Streptomycin	AppliChem
Tris	Carl Roth
Vaseline	Carl Roth

Table 2.3: Consumables

Consumables	
Borosilicate Capillaries (Kwik-Fil 1B100F-4)	Objective immersion oil
Cellview cell culture dishes with 4 compartments	Pasteur Pipettes (glass)
Cover Slips (20mm x 20 mm); (24 mm x 60 mm)	Parafilm
Cryo Vials (2 mL)	PCR Tubes
Filter Tips (10 µL and 300 µL)	Petri Dishes (3 cm, 6 cm, 10 cm)
Halocarbon oil 700 (Sigma Aldrich)	Pipette Tips (10 µL, 200 µL, 1000 µL)
Ice Bucket	Poly-styrene Microspheres (45 µm, 25µm, 20 µm)
Lense cleaning wipe	Reaction Tubes (15 mL and 50 mL)
Micro-reaction Tube (1.5 mL and 2 mL)	Syringes (50 mL) Syringe Membrane filter (0.45 µm pore size)
Microscopy Glass Slides (24 mm x 60 mm)	48-well plates

c. Buffers, Media & Kits

Table 2.4: Buffers and media

Buffers and Media	
Bleaching Solution (contamination)	1.5 ml 2 N NaOH, 0.5 ml NaClO solution (12% Cl), 3 ml M9 Buffer
DEPC-water	0,1 ml DEPC + 100 ml ddH$_2$O, incubate at 37°C, over night and autoclave
DNA loading dye (6x)	New England Biolabs
LB-Agar	LB-Medium + 1.5% (w/v) agar
LB-Medium	25 g LB-Medium premix (10 g NaCl, 10 g tryptone, 5 g yeast-extract); add to 1 L with ddH2O

M9 Buffer	3 g KH2PO4, 6 g Na2PO4, 5 g NaCl, 1 ml 1 M MgSO4, add to 1 L with ddH2O
NGM-agar	3 g NaCl, 2.5 g peptone, and 20 g agar in 975 mL ddH2O (auto-clave); add 1 ml of 1 M CaCl, 1 mL of 1 M MgSO4, 1 mL of 5 mg/mL cholesterol in EtOH, 25 mL of 1 M Phosphate Buffer
Phosphate Buffer	108.3 g KH2PO4, 35.6 g K2HPO4, add to 1 L with ddH2O
Soft Agar Freezing Solution	0.58 g NaCl, 0.68 g KH2PO4, 34.9 g glycerol (86%), 0.56 mL 1 N NaOH, 0.4 g agarose, add to 100 mL with ddH2O

Table 2.5: Kits and enzymes

Usage	Kit/Enzyme	Supplier
DNA amplification	Taq 2X Master Mix, Phusion poly-merase	NEB; ThermoFisher
PCR purification	NucleoSpin® Gel and PCR Clean-up	Macherey-Nagel
Plasmid DNA preparation	NucleoSpin® Plasmid	Macherey-Nagel
dsRNA transcription	AmpliScribe T7 High Yield Transcription	Epicentre

d. Clones, Vectors and bacterial strains

Table 2.6: Plasmids

Clone	Host	Vector	Marker	Designated use	Source
F57B9.10	HT115(DE3)	pL4440-DEST	AmpR	RPN-6.1 dsRNAi Sequencing primer: for 5'-GTTTTCCCAGTCACGACGTT-3' rev 5'-TGGATAACCGTATTACCGCC-3' T7 primer: 5'-TAATACGACTCACTATAGGG-3'	(Rual, J-F. et al., 2004)

Table 2.7: Bacterial strains

Strain	Designated use	Source
E. coli OP50	Food source for *C. elegans*	CGC

2.2. Molecular biology methods

a. Plasmid DNA extraction

On the first day, clone F57B9.10 from a commercially available RNAi feeding library (Rual, J-F. et al., 2004) was streaked on LB-Ampicillin/Tetracycline plates (1:1000 Amp/Tet, 1.5% Agar (Byerly, L. et al., 1976)) and cultured at 37°C overnight. The next day, a single clone was picked from the plate, inoculated in 5 ml LB-Amp (1:1000 Amp) and grown over night at 37°C. During the third day, the plasmid was extracted by using the Nucleospin® Plasmid/Plasmid (NoLid) protocol for isolation of high-copy plasmid DNA from *E. coli* (Nucleospin® Plasmid Kit, Machery-Nagel). The concentration of the isolated plasmid was measured by using the NanoDrop1000 Spectrophotometer (Thermo Scientific). Afterwards, the isolated plasmid sequence was verified via Sanger sequencing using the primers pL4440-dest-RNAi-FOR (5'-GTTTTCCCAGTCACGACGTT-3') or pL4440-dest-RNAi-REV(5'-TGGATAACCGTATTACCGCC-3').

b. Polymerase chain reaction (PCR)

The amplification of extracted DNA-fragments was performed with Taq Master Mix (NEB) with a standard PCR protocol performed based on the supplier's manual with usage of a T7 primer (5'-TAA-TACGACTCACTATAGGG-3') for forward and reverse amplification. Reaction setup preparation and used conditions are shown below.

Table 2.8: PCR reaction mix

PCR reaction components	
2x PCRBIO Taq Mix Red	25 µl
T7 for (10 µM)	2 µl
Template DNA (50-100 ng)	X µl
Add to 50 µl final Volume with ddH$_2$O	X µl
Total reaction Volume	50 µl

Table 2.9: PCR cycle conditions

Cycles	Temperature	Time	Notes
1	95°C	2 min	Initial denaturation
40	95°C	15 sec	Denaturation
	60°C	15 sec	Annealing
	72°C	20 sec	Extension
1	72°C	5 min	
	4°C	∞	Pause

c. PCR purification

PCR product purification was performed following the protocol for PCR-clean-up given by the supplier of the NucleoSpin®Gel and PCR-clean-up kit (Machery-Nagel). Concentration of purified PCR-product was controlled using the NanoDrop1000 Spectrophotometer (Thermo Scientific).

d. dsRNA Transcription

The purified PCR product was transcribed into dsRNA following the Standart AmpliScribe High Yield Transcription Reaction protocol provided by the supplier of the AmpliScribe™T7 High Yield Transcription Kit (Epicentre). Reaction setup is shown below. The following reagents were added in the order given at room temperature and mixed before adding the AmpliScribe Enzyme Solution. Afterwards the reaction was carefully mixed again and incubated at 37°C for 2 hours. At the end, the dsRNA solution was diluted with DEPC-treated ddH$_2$O and its concentration tested with the NanoDrop1000 Spectrophotometer (Thermo Scientific) until desired concentration was reached (0.2-1.0μg) and the samples were then stored at -20°C.

Table 2.10: dsRNA transcription

dsRNA transcription reaction mix (20μl)	
RNase-Free water	X μl
Linearized template DNA with appropriate promotor	1 μg
10X AmpliScribe T7 Reaction Buffer	2 μl
100 mM ATP	1.5 μl
100 mM CTP	1.5 μl
100 mM GTP	1.5 μl
100 mM UTP	1.5 μl
100 mM DTT	2 μl
RiboGuard RNase Inhibitor	0.5 μl
AmpliScribe T7 Enzyme Solution	2 μl
Total reaction Volume	20 μl

2.3. *C. elegans* handling and methods

a. *C. elegans* strain maintenance and crossing

The *C. elegans* strains of this study were ordered from CGC (Caenorhabditis Genetics Center), previously generated in the Pohl lab or generated by crossing. Maintenance followed standard conditions according to (Brenner S. , 1974). Desired strains were maintained on *E. coli* OP50 seeded Nematode Growth Media (NGM) plates and animals were cultured at 20-25°C. Strain names and genotypes used in this study are listed below. Since the strain SX392 contains an extrachromosomal *mir-124p::mCherry* marker, the presence of the marker had to be checked regularly by fluorescence microscope and only worms containing the marker were propagated.

Before setting up genetic crosses, plates were checked for existence of males and if no males were present they were generated by the following procedure. Around 4 plates containing approximately 10 hermaphrodites of the desired strain were incubated at 30°C for 4 h. After 4-5 days the occurrence of males was checked on those plates. The setting of crosses was performed by placing 10-13 males and 2 to 4 L4 stage hermaphrodites on a 3 cm plate with minimal OP50 *E. coli* lawn storing the plate at 20°C for 36 h. Then, single F0 worms were removed from this plate and placed on separate plates each (F0-plates). 2-3 days later, F1 worms were picked from F0-plates with high numbers of males and animals were checked for being heterozygous for the desired marker. Therefore, each F1 worm was analyzed separately under a florescence microscope in a single drop of M9. Each worm showing the desired was then put onto a separate new plate (F1-plate). Male worms were removed carefully from all plates throughout the crossing procedure (starting from F0-plates). Throughout the next days, the F1-plates were checked for F2 embryos containing both desired markers. Therefore, single F2 embryos were positioned in M9 drops and analyzed with a fluorescence microscope, whereby every embryo containing both markers was put on a separate plate (F2-plate). Throughout the next days, F3 embryos on F2-plates were again checked for containing both markers and this procedure was repeated for F4 embryos. After the F4 embryos were verified to contain both markers, twice a week (later once a week) worms were checked for containing the correct markers and those worms were collected onto fresh plates.

Table 2.11: *C.elegans* strains

Strain	Genotype	Source/Reference
BV24	*(OD70xRW10029); ltIs44 [pie-1p-mCherry::PH(PLC1delta1) + unc-119(+)]; zuIs178 [his-72(1kb 5' UTR)::his-72::SRPVAT::GFP::his-72 (1KB 3' UTR) + 5.7 kb XbaI - HindIII unc-119(+)]; stIs10024 [pie-1::H2B::GFP::pie-1 3' UTR +unc-119(+)].*	Bao lab.
BV34	*(AZ235xOD70); ruIs48[unc-119(+) + pie-1::GFP::tubulin]; ltIs44 [pie-1p mCherry::PH(PLC1delta1) + unc-119(+)] V.*	Bao lab.
BV36	*(JJ1473xOD70); zuIs45[nmy-2::NMY-2::GFP + unc-119(+)]; ltIs44 [pie-1pmCherry::PH(PLC1delta1) + unc-119(+)] V.*	Bao lab.

BV43	(FT17xOD70); xnIs3[par-6:PAR-6::GFP + unc-119(+)]; ltIs44 [pie-1p mCherry::PH (PLC1delta1) + unc-119(+)]V.	Bao lab.
BV113	zbIs2 [pie-1::lifeact-RFP + unc-119(+)]; zuIs45[nmy-2::NMY-2::GFP + unc-119(+)] IV.	Bao lab.
CHP13	(JH2825xKK1216) unc-119(ed3) III; axIs1943 [(pFM050) mCherry::mlc-4 + unc-119(+)]; par-3(it298[par-3::GFP]) III.	(Dutta, P. et al., 2019)
CHP19	(LP162xJH2647); nmy-2(cp13[nmy-2::GFP + LoxP]) I; axIs1928 [mCherry::par-6].	(Dutta, P. et al., 2019)
CHP56	(ML916xBV43) mcIs40 [lin-26p::ABDvab-10::mCherry + myo-2p::GFP]; xnIs3 [par-6:PAR-6::GFP + unc-119(+)]	(Kunz, P. et al., 2021)
CHP71	(ML916xSX621); mcIs40 [lin-26p::ABDvab-10::mCherry + myo-2p::GFP]; lin-15B&lin-15A(n765) X; mjIs27; mjIs27 [mir-124p::GFP + lin-15(+)].	(Kunz, P. et al., 2021)
CHP200	(SX392xKK1248); mjEx142 [mir-124p::mCherry]; par-6(it319[par-6::GFP]) I.	This study.
CHP201	(JH2825xSX621); unc-119(ed3) III; axIs1943 [(pFM050) mCherry::mlc-4 + unc-119(+)]; lin-15B&lin-15A(n765) X; mjIs27 [mir-124p::GFP + lin-15(+)].	This study.
JH2825	unc-119(ed3) III; axIs1943. axIs1943 [(pFM050) mCherry::mlc-4 + unc-119(+)].	CGC
KK1248	par-6(it319[par-6::GFP]) I	CGC
N2		CGC
SM481	pxIs10 [pha-4::GFP::CAAX + (pRF4) rol-6(su1006)].	CGC (Portereiko, M.F. and Mango, S.E., 2001)
SX392	mjEx142 [mir-124p::mCherry].	CGC (Clark, A. M. et al., 2010)
SX621	lin-15B&lin-15A(n765) X; mjIs27. mjIs27 [mir-124p::GFP + lin-15(+)].	CGC (Clark, A. M. et al., 2010)
VH624	rhIs13 V; nre-1(hd20) lin-15B(hd126) X. rhIs13 [unc-119::GFP + dpy-20(+)].	CGC

b. Mounting of embryos

Embryos were mounted as described by (Dutta, P. et al., 2019), thereby either embryos were collected directly from OP50 seeded NGM-plates with an eyelash pick and washed in a drop of M9 buffer or they were dissected from gravid hermaphrodites. Imaging was performed during early lima- bean to 1.5-fold stages. For a head-on view imaging setup, single embryos were mounted inside one chamber of a CELLview cell culture dish. All four chambers were filled with M9 buffer and 1μl diluted 45 μm diameter poly-styrene microspheres was added to the chamber where the desired embryo was added afterwards. Head-on position of embryos was gained by carefully moving the embryo within the M9 solution with the aid of an eyelash pick.

c. Long-term-imaging

Imaging of early lima-bean to 1.5-fold embryos was performed with a VisiScope spinning disk confocal microscope system (Visitron Systems) using a 63X/1,4-0,6 oil objective (Leica) at 20-23°C. Most image series were collected over a 1-3h timespan containing z-stacks with 45 steps at 1.0 μm distance each and 2, 3, 4 or 5 min intervals. Thereby the 488nm laser was used at 4-6% intensity and the 566 nm laser at ~60% intensity with exposure times of ~190 ms for both lasers. Imaging of head-on-view embryos was executed by using 3-4 min intervals (to prevent tilting of embryos).

To gain image series for lineage-tracing, 250 time points of 3 min intervals were collected from 2 or 4-cell embryonic stage on with sampling z distance of 1 μm each with 30 μm total depth. To image and analyze effects of UV laser ablation, we collected a single time point before UV laser ablation and performed imaging after the ablation with 2 min intervals and z stacking at 1 μm each for a total depth of 40-45 μm.

d. UV laser ablation

For UV laser ablation of the AM pores (marked by PAR-6::GFP), a pulsed UV laser was used at the position of one AM pore per embryo, with 5 ms frap time per pixel in a diameter equivalent to the pore diameter. UV laser ablation of the epidermis was performed at a focal epidermal layer (marked by *ABDvab-10:mCherry*) close to the AM pore on one side of the embryo using a larger diameter then for pore ablation and using 10 ms frap time per pixel. Application of the UV laser was executed manually by using 3-8 frap cycles on one side of the embryo's head so the other side was unaffected and considered as control. Only correctly developing embryos with unaffected AM dendrite morphogenesis on the control side were analyzed after UV laser ablation.

e. RNAi via microinjection

Before microinjection of dsRNA was executed based on (Evans, 2006), the desired *C. elegans* strain was cultured until young adult stage (containing a single embryo up to one row of embryos). Additionally, it was assured the worms were clean, well-fed and the respective markers were present. Several days before performing a microinjection, agarose injection pads were prepared by heating an agarose solution (2% agarose in ddH$_2$O), putting a drop of it on a coverslip and flattening the drop with a second coverslip, which was removed after a few minutes. These agarose pads were dried at 37°C overnight. On the day of microinjection, injection needles with closed tips were prepared using a micropipette puller (Flaming/Brown, ramp: 284, heat: 280; pull: 140, velocity: 100, pressure: 500, time: 150). The dsRNA injection-mix was centrifuged (4°C, 10min, 11.000g). The injection needle was filled with 1μl of the dsRNA solution and the needle tip was manually broken open.

Afterwards, a young adult worm was positioned on the injection pad within a drop of halocarbon oil 700. The dsRNA solution was injected inside the ovaries of young adult worms using 50-60 psi pressure and 1-8 injection cycles per worm with the microinjection setup listed above. Test injection was performed using dH$_2$O. After performing a microinjection, every worm was recovered in a drop of M9 on an OP50 seeded NGM plate at 20°C and then grown overnight. F1 embryos of those injected worms were imaged and analyzed from the next morning on throughout the day. Embryos with severe abnormalities like loss of marker signal, vacuoles or extreme developmental defects (e.g. developmental arrest, loss of elongation, ~30% of cases) were excluded from imaging. Remaining 70% of the F1 embryos were analyzed via long-term microscopy. Since penetrance was incomplete, detailed quantification of phenotypes was performed (**Table 3.1**, **Figure 3.8**.).

2.4. Measurements, Lineaging and Data analysis

a. Measuring of sensilla pore translocation, AM dendrite elongation, AM neural cell body positioning & statistical analysis

Quantification of sensilla pore translocation, AM dendrite length and AM neural cell body positioning was executed on maximum intensity z-stack projections of time lapse image series (resolution 7 pixels per µm) with usage of a linear measuring tool in Fiji (ImageJ, (Schindelin, J. et al., 2012)) used every second or fifth time point. Either the distance of translocating sensilla pores or dendrite tips was measured in relation to the arcade cell's apical anterior position (most trackable anterior mouth position). Or the AM dendrite bundle length was measured from the dendrite tips (directly next to AM pore) to the anterior boarder of AM neural cell bodies. Additionally, the positioning of AM cell bodies was analyzed by measuring the distance between the apical anterior front of the arcade cells to the middle of the accumulated cell body mass. Every measurement was normalized to each individual embryo's length or to embryo's width (head-on measurements). Statistical analysis was performed in GraphPad Prism 9 using two-way ANOVA and two-stage linear step-up procedure (Benjamini et al., 2006).

b. Lineage tracing of AM cells, tracking of arcade cell morphogenesis

Both lineage tracing of AM cells (AMsoL, AMshL, ASEL) coherent with tracking of epidermal cells (hyp5 left, XXXL) and analysis of arcade morphogenesis was performed manually. Thereby either nuclei or apical surfaces and cell membranes were tracked by highlighting those structures from 4-cell stage until late embryogenesis (2-fold) within time-lapse z-stacks using Fiji. Also, bottle-shaped cell forms were highlighted via Fiji and tracked throughout lima-bean to 1.5-fold stages.

3. Results

3.1. Collective anterior migration of sensilla pores in the embryo's head

Within the adult *C. elegans* head, 16 sensilla endings (AM, OL, IL, CEP) are positioned around the mouth opening in a specific pattern (Altun, Z. F. and Hall, D. H., 2010). This study investigated which morphogenetic steps during embryogenesis enable this stereotypic positioning. These sensilla are in contact to the environment through pores (created by socket cells), which are containing an apical lumen. Thus, different apical PAR-6 markers (*xnIs3[par-6::PAR-6::GFP]*; *it319[par-6::GFP]*; *asIx1928[par-6::mCherry::PAR-6])* and a PAR-3 marker (*it298[par-3::GFP])* were used to visualize these pores by highlighting their apical lumen (**Figure 3.1A**). In addition to highlighting the apical lumen of the AM, OL, IL, CEP, phasmid and anterior deirid sensilla pores during lima-bean to 1.5 fold stages (posterior deirid sensilla occur at L2 stage (Altun, Z. F. and Hall, D. H., 2010), also apical polarization of the mouth opening, intestine, rectum and excretory pore is visualized by the PAR-6 marker. Interestingly, sheath glial cells are not highlighted by PAR-6 marker so they may not execute apical polarization within their elongated projections. By imaging wt embryos between lima-bean stage and 1.5-fold stage, their morphogenesis during early elongation is recorded. During these stages simultaneous anterior movement of AM, OL, IL and CEP sensilla pores was observed with final symmetrical encircling of the future mouth opening (**Figure 3.1A**). Hereby, the position of the AM pores at 1.5-fold stage is most posterior-lateral to all other head sensory pores. Also, they begin their anterior translocation at the far-most posterior position and in constant distance to the other pores during their anterior movement. In addition, anterior migration of the hyp4 cell (**Figure 3.1A** bottom panels) was observed, suggesting a coherence between sensilla pore migration and epidermal head enclosure.

To gain deeper insight into the translocation events occurring during the morphogenesis of AM sensilla and also other head sensilla, lineage-tracing of one AM socket cell (AMsoL), one sheath cell (AMshL) and ASEL as one exemplary AM neuron cell from early lima-bean until 2-fold stage was performed (**Figure 3.1B**). Additionally, lineage-tracing of the epithelial cells XXXL and hyp5 were executed to explore the coherence of AM morphogenesis and epidermal head enclosure. The results show three sequential events during AM sensilla development: First, all AM cells get focused at an accumulative posterior-lateral position (cell focusing, **Figure 3.1B**, left panels), thereafter AMSoL and AMshL are moving anteriorly together with the epidermal XXXL and hyp5 cells (co-migration, middle panels). Importantly the neural cell body of ASEL is not translocating concomitant with the other AM sensilla cells but stays stationary at the original position. Within the third phase, the AM cells lose the contact and arrange at their final position for 2-fold stage (contact loss, right panels). The epidermal cells (XXXL, hyp5 left) reach the anterior tip of the embryo, AMsoL is getting positioned posterior to the epidermal border, followed by AMshL. Importantly, the ASEL stayed behind at their original posterior-lateral position.

The findings of the study in hands unveil that anterior pore translocation and epithelial cell migration occur concomitantly. AM sensilla cells show complex trajectories with AMsh and AMso cells moving anteriorly together with XXXL and hyp5 cells, while neural cell bodies are staying stationary.
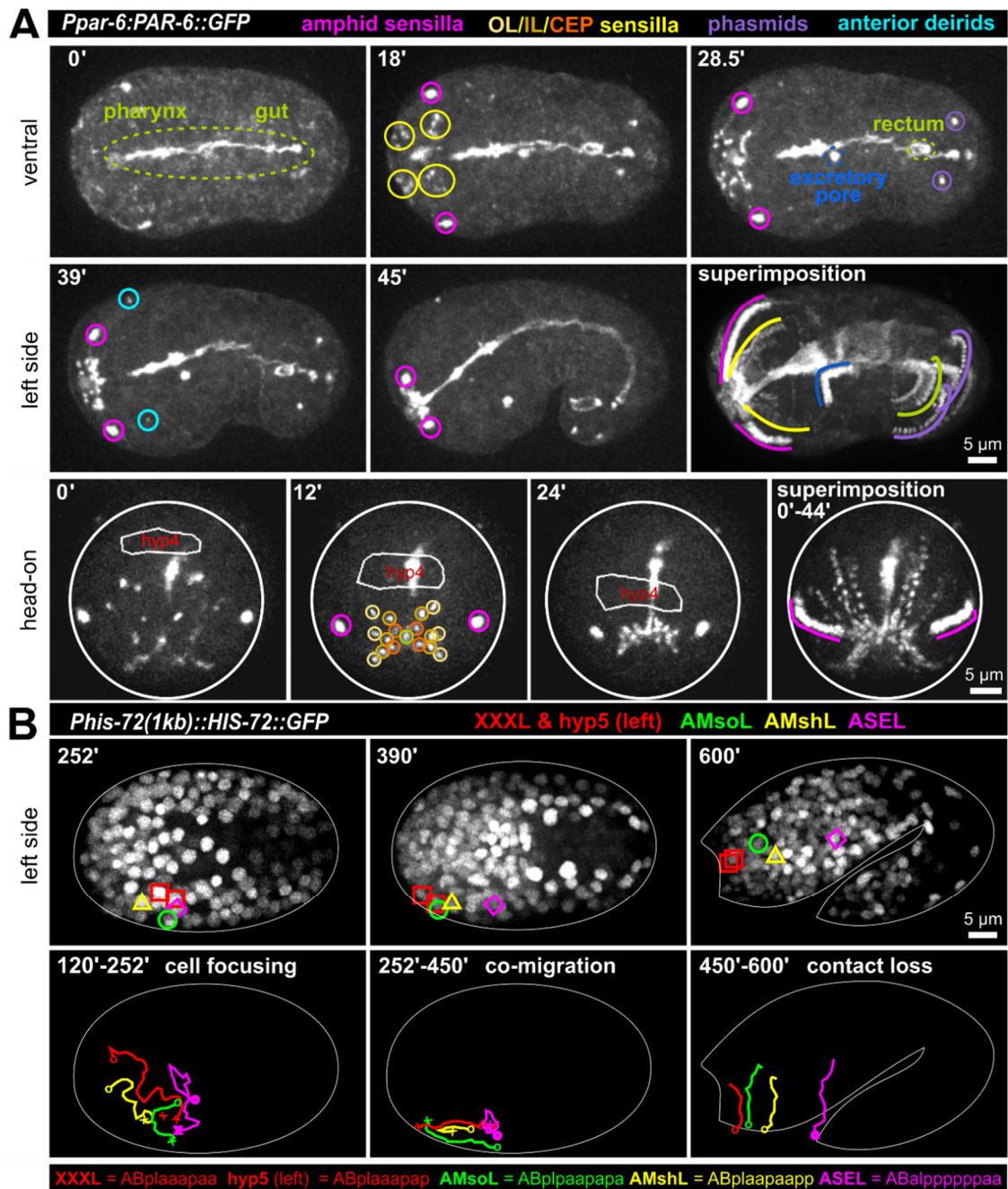

Figure 3.1: Simultaneous polarization and movement of apical pores in *C.elegans* during embryonic elongation

A: Maximum intensity projections of stacks of confocal images from time lapse recordings of ventral (top), left side (middle) and head-on (bottom) views of wt embryos expressing PAR-6::GFP, highlighting the anterior directed movements of the amphid (AM, magenta), outer labial (OL, light yellow), inner labial (IL, yellow), cephalic (CEP, orange), phasmid (purple) and anterior deirid sensilla pores (light blue) during lima bean to 1.5-fold stage. PAR-6::GFP additionally highlights pharynx, gut, rectum (green), and the excretory pore (blue). In the head-on view, the anterior most epidermal cell is traced (hyp4, traced based on a membrane marker which is not shown for clarity). **B**: Maximum intensity projections of stacks of confocal images from time lapse recordings of lateral (left side) view a representative wt embryo expressing GFP-marked histones from lima bean to 2-fold stage. Movement of the XXXL, hyp5 (epidermal cell) (both red), AMsoL (amphid socket left, green), AMshL (amphid sheath left, yellow) and ASEL (amphid neuron cell body, magenta) are lineaged. Images in panel B required time-dependent brightness adjustment due to onset and increased expression of the histone from its zygotic promotor. Modified from (Kunz, P. et al., 2021).

3.2. Epidermal migration and AM sensilla morphogenesis

a. Coupling of AM pore translocation and epidermal migration

Since the data showed simultaneous anterior movement of epidermal cells (hyp4, hyp5, XXX) and concurrent sensilla pore movement, a possible role of coupling between epidermal head enclosure and sensilla pore translocation for correct sensilla morphogenesis was further examined. Therefore the sensilla pores were visualized with a PAR-6 marker and the epidermal migration events were highlighted with a *lin-26* promoter driven VAB-10 marker (**Figure 3.2**). With the beginning of head epiboly (early limabean stage), the AM pores form at the anterior-lateral part of the epidermal leading-edge (**Figure 3.2A**, white arrowheads). During progression of head enclosure, AM pores move anteriorly at the epidermal leading edge, until they reach their final position adjacent to the prospective mouth, with the end of epidermal ensheathing of the head at around 1.5-fold stage (**Figure 3.2B**, white arrowheads). Importantly, just the AM pores are moving together with the epidermal anterior leading edge, while the other sensilla pores are moving anterior of the epidermal leading edge (**Figure 3.2B**, dashed lines). For further elucidation of the possible interconnection between the AM pore and the epidermis, UV laser ablation of the epidermis neighboring the AM pore on one side of the embryo was conducted (**Figure 3.2C, D**). It was observed that the AM pore is detaching from the epidermis and arrests close to the position of epidermal ablation, while the AM pore on the non-ablated side still moved to the anterior tip of the embryo like in wild type (wt) embryos (**Figure 3.2C**, arrowheads). Hence, epidermal migration seems to be not majorly affected by UV laser ablation.

The results lead to the suggestion, that the AM pores are embedded and physically linked to the epidermal sheet. This study infers that the coupling of AM pore and epidermis during anterior epidermal migration is essential for AM pore translocation. Additionally, other sensilla pores seem to get positioned through different events, since those move in front of the epidermal leading edge (**Figure 3.2E**).
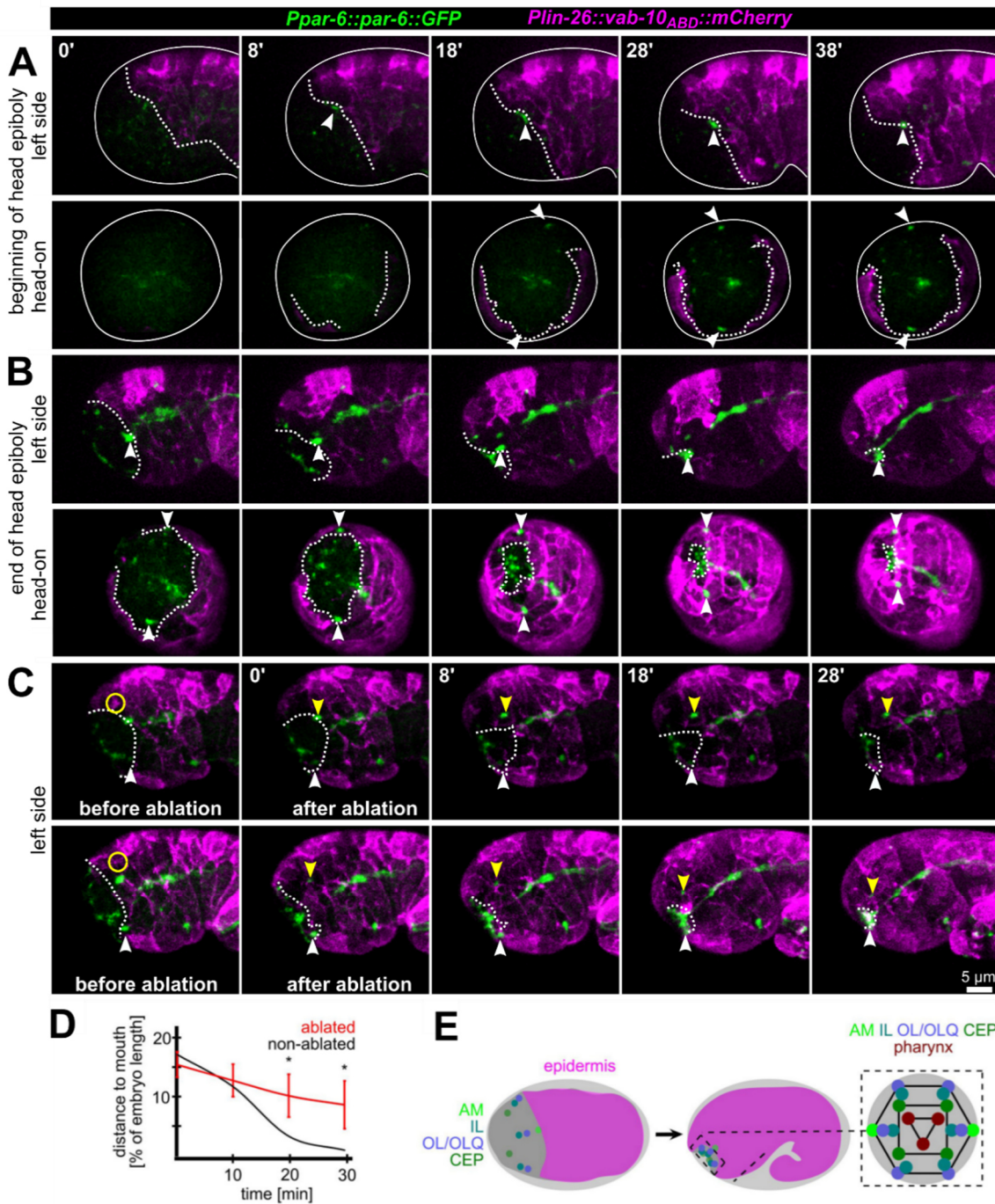
Figure 3.2: Epidermis migration and AM pore translocation
A: Maximum intensity projections of stacks of confocal images from time lapse recordings of ventral (top)and head-on (bottom) views of epidermis movement and movement of AM pores during lima bean stage. **B**: Same as panel (A), however, stage is lima bean to 1.5-fold stage. **C**: Lateral view of embryos before and after UV laser ablation of the epidermis close to the AM pore. White dashed lines highlight the epidermal front. White arrowheads point to the position of the AM pore, and yellow arrowheads mark the position of the pore close to the ablated epidermis. Yellow circle marks the position of the laser ablation. **D**: Quantification of epidermis ablation experiments (n = 4). The relative distance of the ablated (red) and un-ablated (black) AM pores to the mouth was measured. P-values from a multiple unpaired t-test and with two-stage linear step-up procedure (Benjamini et al., 2006) are shown (*≥0.05; **≥0.01). **E**: Left and middle: Schematic depicting the spreading of the epidermis around the head (head enclosure) and the initial and final positions of the sensory organ pores. Note that only the AM pores are located at the anterior epidermal edge. Right: Schematic depicting a juxta-oral cross section that highlights the symmetry of sensory organ pores and the symmetry of the pharynx. Modified from (Kunz, P. et al., 2021).

b. Coupling of AM dendrite elongation and epidermal enclosure

After exploring the importance of coupled epidermis and AM pore translocation, the coherence of head enclosure and AM dendrite morphogenesis was investigated. AM neuronal morphogenesis was monitored trough construction of strains enabling the visualization of many AM neurites (ASE, ASH, ASI, ASK, AWA, AWB, AWC) using a microRNA promotor strain *mjIs27[mir-124p::GFP + lin-15(+)]* (Clark, A. M. et al., 2010) in concert with an epidermal marker (see above) (**Figure 3.3**). Additionally, the *mir-124* reporter highlights a few other ciliated neuronal cells like the inner labial neuron 1 (IL1) and phasmid neurons (PHA, PHB, not shown). The results exhibit the onset of the neuronal reporter expression highlighting the AM neural cells at the time of epidermal ventral enclosure (**Figure 3.3**, top panels). During head enclosure, the epidermal anterior border moves along the AM neuronal cell bodies and, concomitantly, AM dendrite bundles form. Together with progressive anterior migration of the epidermis covering the anterior tip of the embryo, also AM dendrite tips are translocating coherently and dendrite bundles are elongating concomitantly until the end of head epiboly (**Figure 3.3**, middle and bottom panels, white arrowheads). Importantly, during the translocation of AM dendrite tips and the elongation of AM dendrite bundles, the cell bodies stay stationery without noticeable active movement.

We thereby conclude that epidermal migration during head enclosure is coupled to dendrite tip translocation and functions as a precondition for AM dendrite bundle elongation.
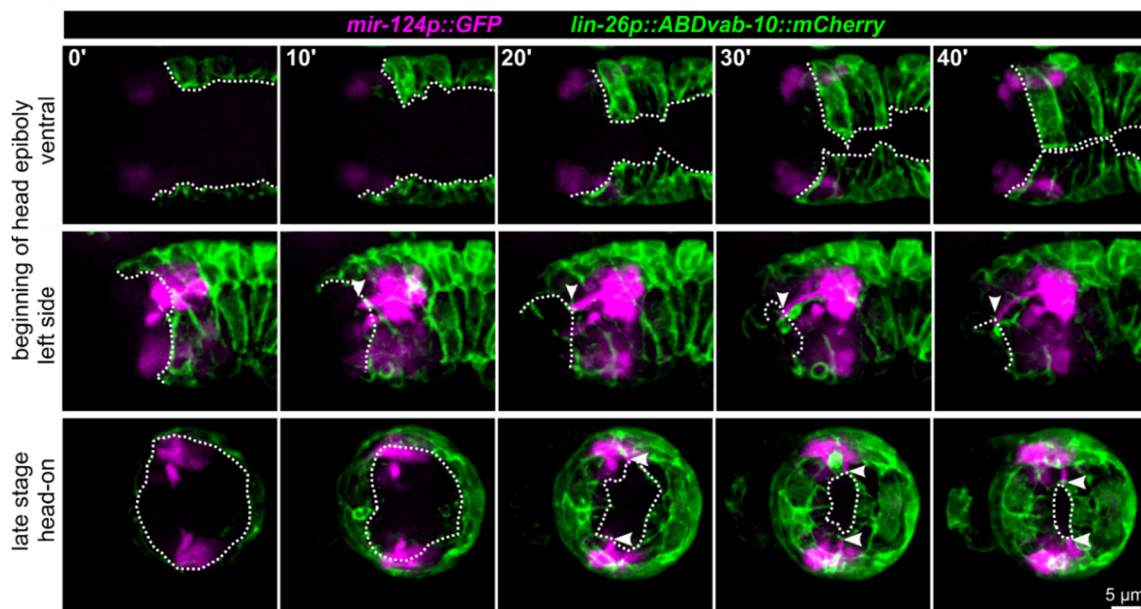

Figure 3.3: Epidermal enclosure and AM dendrite elongation
Maximum intensity projections of stacks of confocal images from time lapse recordings of ventral (top), left side (middle) and head-on (bottom) view of wt embryos from lima-bean to 1.5-fold stage. AM cell bodies and dendrites are highlighted in magenta and the epidermis in green. White arrowheads point to the position of AM dendrite tips at the anterior edge of the epidermis. White dashed lines mark the anterior and ventral edges of the epidermal sheet. Modified from (Kunz, P. et al., 2021).

c. Coupling of AM pore translocation and AM dendrite elongation

Whereas the results unveil that epidermis migration is coupled with both AM pore movement and translocation of AM dendrite tips, the study investigated how these events are coordinated to achieve correct morphogenesis of AM sensilla. For visualization of both AM pore and AM dendrite developmental events, constructed strains using the markers *mjEx142[mir-124p::mCherry]* (Clark, A. M. et al., 2010) and GFP-labelled PAR-6 were used to monitor apical polarization. The results show the explicit coupled translocation of AM pores and dendritic tips towards the anterior-most tip of the embryo between lima-bean and 1.5-fold stage (**Figure 3.4A**, white arrowheads). The measured distance between AM pore and prospective mouth is getting smaller during development, while, at the same time, the length of the dendrites is getting larger (**Figure 3.4C**, left and middle panel). Interestingly, additional head sensilla pores are moving in front of the epidermal leading edge (dashed lines) and ahead of AM pores. These other head sensilla pores also eventually reach their final position next to the prospective mouth, whereby AM pores are positioned more posteriorly. Importantly, the elongation of the AM dendrite bundle is occurring without active movement of the neuronal cell bodies (**Figure 3.4A, C** right panel, also see above). To clarify the importance of the attachment between AM pores and AM dendritic tips, UV laser ablation was performed (**Figure 3.4B, Figure 3.5B**). In these cases, the ablation was executed at the position of one AM pore per embryo (yellow circle) leading to arrest of dendrite tips and hindered dendrite elongation on the ablated side. Despite the strongly impaired AM dendrite elongation, all other sensilla pores moved to the prospective mouth unaffectedly. Remarkably, the development of the treated embryo and the non-ablated AM sensillum was not hindered, since pore migration and dendrite elongation at the non-ablated side of the embryo were not impaired, commissures were formed (blue arrowhead) and also tail elongation occurred normally.

This study concludes that the attachment between AM pore and AM dendrite tip is crucial for dendrite bundle elongation. Moreover, pore movement to the prospective mouth seems to be essential for the passive elongation of the dendrite bundle. Importantly, neuronal cell bodies stay stationary without any active movement. These findings are consistent with the lineage-tracing results (**Figure 3.1B**). All in all, the study infers a coupled morphogenetic mechanism for AM sensilla development including events of epidermis migration and AM pore translocation leading to AM dendrite elongation. AM neural cell bodies are hereby staying stationary.
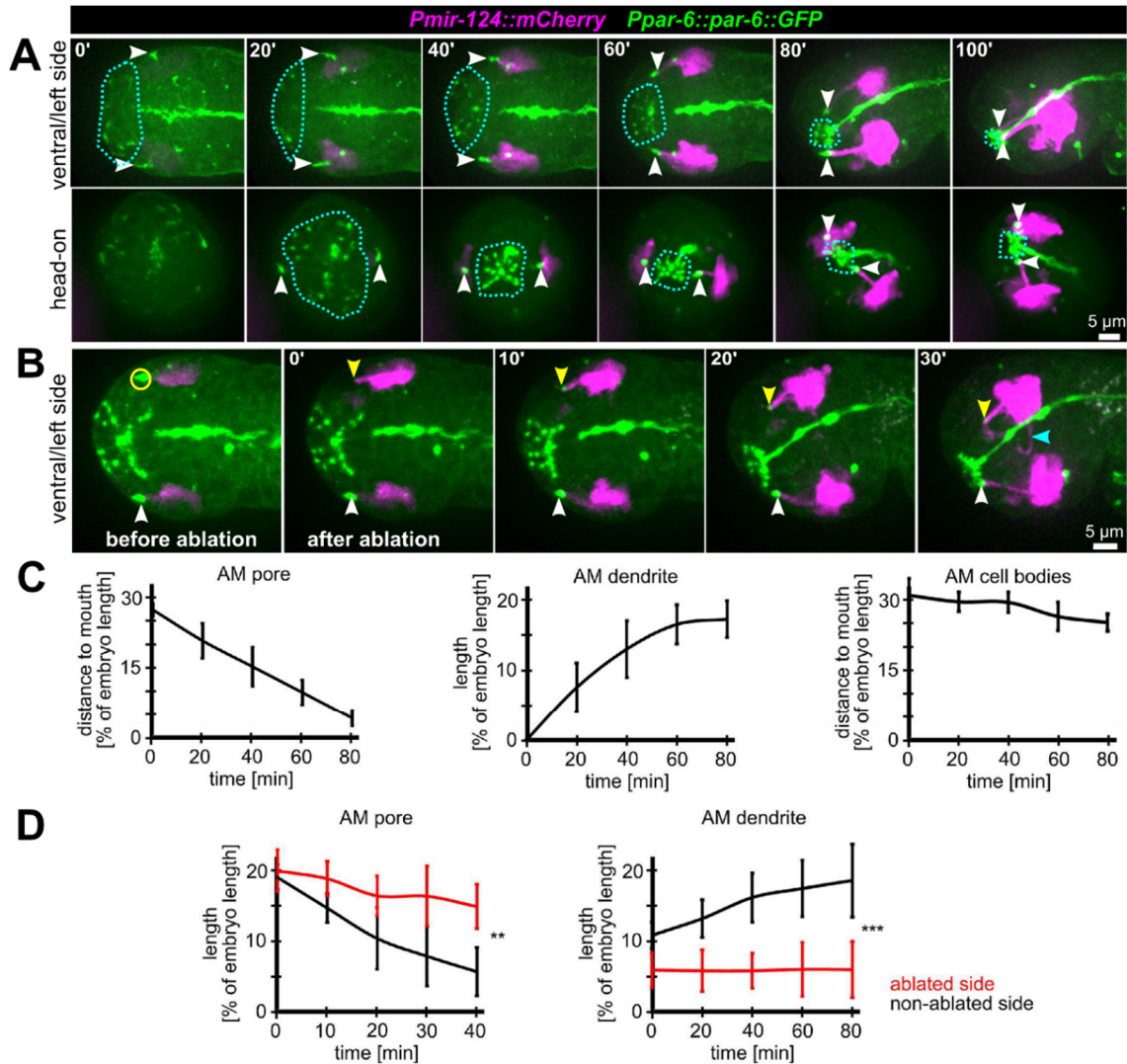
Figure 3.4: Coupling of AM pore translocation to AM dendrite extension

A: Maximum intensity projections of stacks of confocal images from time lapse recordings of ventral/left side (top) and head-on (bottom) view of wt embryos from lima-bean to 1.5-old stage. AM cell bodies and dendrites are marked in magenta, and pores and apical lumen of pharynx and intestine are marked in green. Dashed lines indicate the anterior epidermal edge. White arrowheads mark the AM pores. **B**: Depictions as in (A); ventral/left side view of a representative embryo before and after UV laser-ablation of one of the two AM pores. The ablated area is marked by a yellow circle, the non-ablated AM pore is marked by a white arrowhead, and the ablated AM pore is marked by a yellow arrowhead. **C**: Quantifications of the distance of the AM pore to the mouth (left), AM dendrite elongation (middle) and position of the AM neuron cell bodies relative to the mouth (right) (n = 5). **D**: Quantifications of AM pore movement (left) and AM dendrite length in embryos where one AM pore was UV laser ablated, and the pore or dendrite on the other side was measured as internal control (n = 5; ±SD; two-way ANOVA P; ** ≥ 0.01; *** ≥ 0.001). Modified from (Kunz, P. et al., 2021).
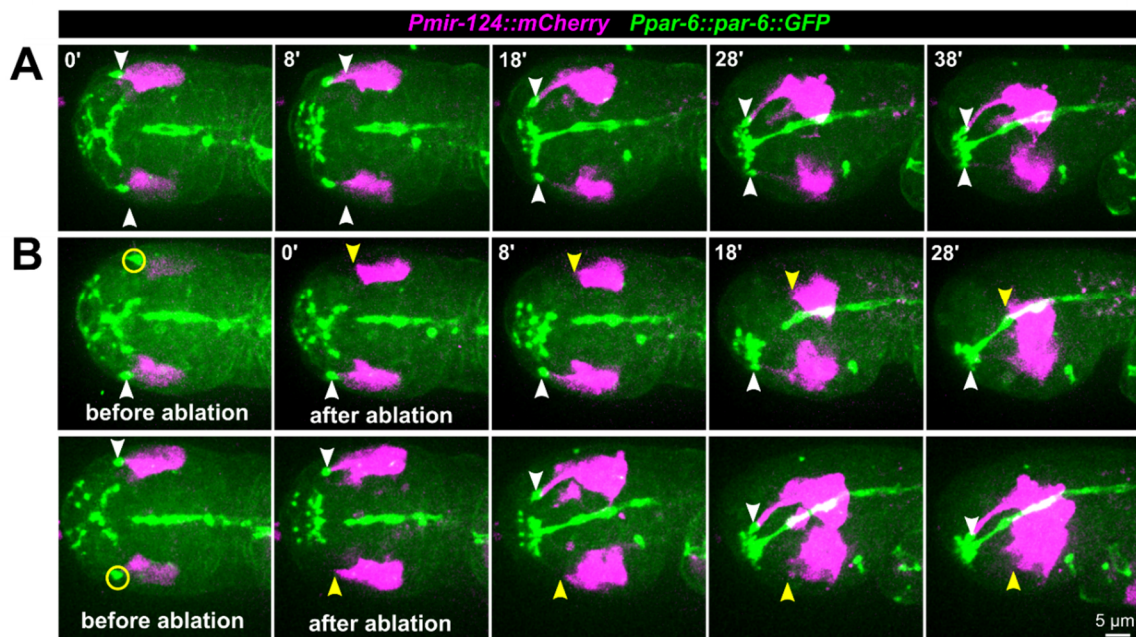
Figure 3.5: Pore ablation results in impaired AM dendrite extension

A: Ventral/left side view of wt embryos from lima bean to 1.5-fold stage. **B**: Same depictions as in (A), embryos before and after UV laser ablation of the left or right amphid pore are shown. White arrowheads point to the migrating wt AM pores. Yellow circle marks position of laser ablation. Yellow arrowheads illustrate the previous position of the pore. In the embryos, apical surfaces including AM pores (green, PAR-6) and AM cell bodies (magenta, *Pmir-124*) are highlighted. All fluorescence images are maximum intensity projections of stacks of confocal images from time lapse recordings. Scale bar = 5 μm.

3.3. The role of RPN-6.1 for AM morphogenesis

a. RPN-6.1 depletion disrupts AM morphogenesis

Several UPS factors influence distinct events of neuronal development (reviewed in (Hamilton, A. M. and Zito, K., 2013). Hence, this study investigated if the proteasome component RPN-6.1, which has been shown to act as an activator of proteasome activity (Pathare, G. R. et al., 2012), might influence AM sensilla development. After depletion of RPN-6.1 by RNA interference, embryos of the next generation showed pleiotropic phenotypes (**Figure 3.6B**, yellow arrowheads). The most obvious phenotypes were incorrect AM dendrite elongation and impaired AM pore translocation. Importantly, although strongly impaired AM dendrite elongation and pore translocation occurred, all other sensilla pores still moved to the anterior most tip of the embryo unaffected (dashed lines). Very detailed examination of AM sensilla phenotypes after RPN-6.1 depletion displayed diverse dosage-dependent effects with frequent asymmetrical differences in strength of these phenotypes, which are described in (**Table 3.1**).

After modest RPN-6.1 depletion, embryos exhibited stretched AM pores, whereby the pore on one side of the embryo could develop normally (**Figure 3.6B**, top panels). Elongation of the AM dendrites occurred like in wt. Moderate RPN-6.1 phenotypes include splitting of pores or stretched pores (**Figure 3.6B**, middle panels). After splitting of the pore, it occurred that the anterior part of the pore moved to the prospective mouth while the posterior part arrests. The arrest of pores (parts of the pores) occurs concomitantly with impaired dendrite elongation. Strong phenotypes after RPN-6.1 depletion exhibited failure in timing of establishment of the pore or partial loss of the pore (**Figure 3.6B**, middle and bottom panels). Hereby, the elongation of the dendrite bundles was either strongly impaired (appearance of only a thin fragile dendrite bundle, (**Figure 3.6B**, bottom panels) or no elongation occurred (**Figure 3.6B**, middle bottom panels). Even with one pore showing strongly impaired pore movement, the other pore can still be found developing normally (bottom panels). Quantification of embryos with moderate and strong phenotypes after RPN-6.1 depletion increased the evidence of concomitant occurrence of arresting pore movement and impaired dendrite elongation through highly significant values (**Figure 3.6C**).

This study also analyzed the interplay of epidermal migration and pore migration after RPN-6.1 depletion (**Figure 3.7**). Here, corresponding to the results shown above, depletion of RPN-6.1 resulted in embryos with graded phenotypes concerning the AM pores: Apparently less affected embryos showed stretched pores (**Figure 3.7**, middle panels) and moderately affected embryos showed split pores whose posterior part arrested (**Figure 3.7**, bottom panels). The migration of the epidermis was unaffected and additional head sensory sensilla migrated anteriorly with the epidermal leading edge like in wildtype embryos. The author of this study suggests that the arrest of the AM pore (or parts of it) is due to disconnection from the epidermal sheet. This is further supported by the fact that the AM pore needs to be embedded and physically attached to the migrating epidermis for efficient migration.

In summary, the observed phenotypes after RPN-6.1 depletion strengthen the proposed mechanism that AM sensilla are formed as a unit with interconnected pores and dendrites. Stretching, splitting and rupture of the pores strongly indicate that AM pore cohesion is of great importance and needs to be maintained throughout AM morphogenesis to withstand pulling force. Also, precise coordination of AM pore to dendrite coupling seems to be important. This study conjectures that AM sensilla are shaped by stretch, because neuronal cell bodies are stationary and constituting an abutment. The embryonic development of AM sensilla seems strongly vulnerable to depletion of the proteasome factor RPN-6.1 by showing stochastic pleiotropic effects. Remarkably, the depletion of RPN-6.1 uncoupled the morphogenesis of the AM sensilla from morphogenesis of other head sensilla. Hence, this study concludes that the morphogenesis of the IL/OL/CEP sensilla has to occur differently.
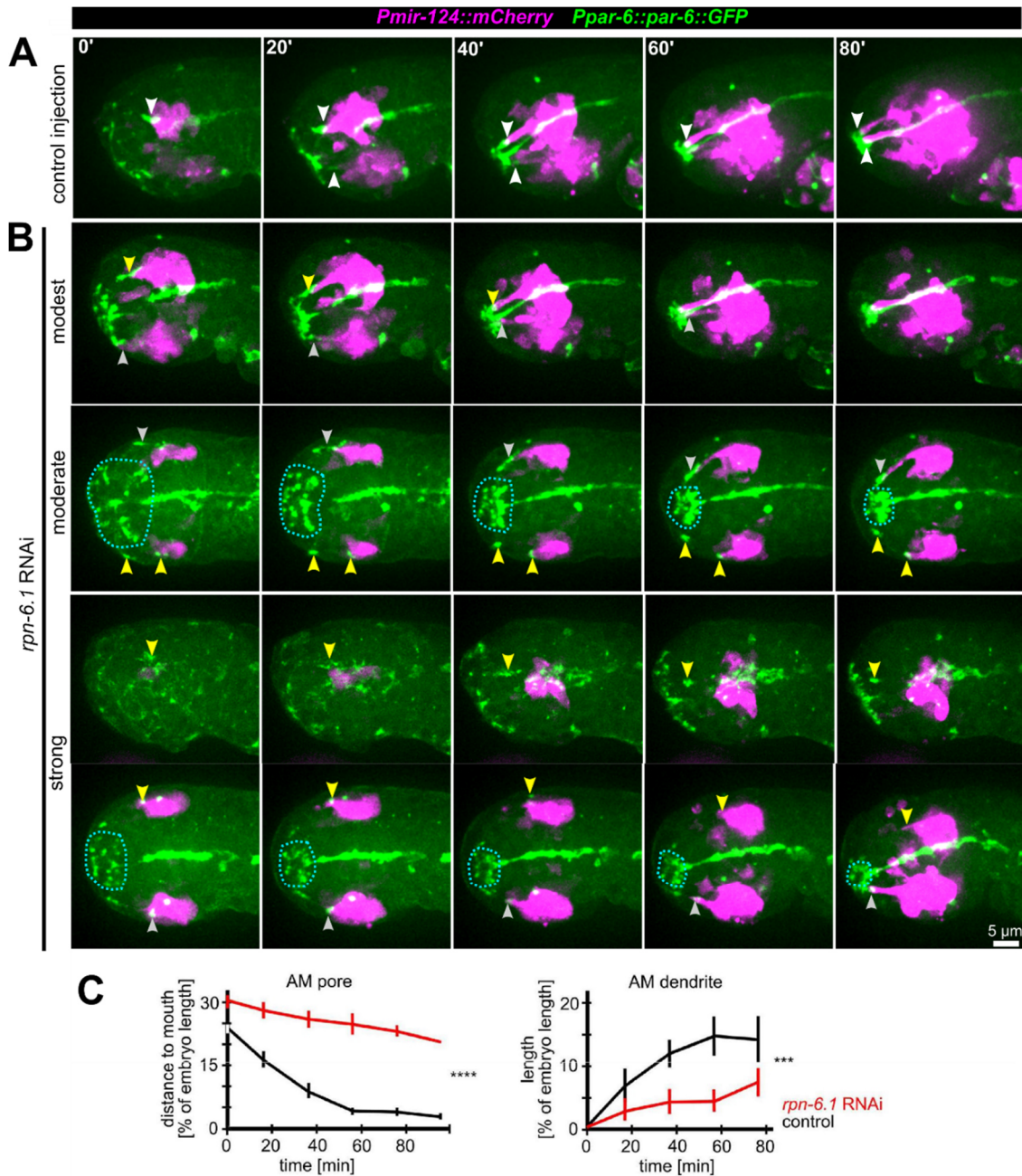
Figure 3.6: RPN-6.1 is required for correct AM pore and dendrite morphogenesis
A: Maximum intensity projections of stacks of confocal images from time lapse recordings of left side views of embryo after control injection illustrating the movement of the sensilla pores (green) correlated with elongation of the AM dendrites (magenta). White arrowheads point to AM pores/dendrite tips. **B**: Depictions as in (A), however, rpn-6.1 RNAi embryos are shown. Injection of dsRNA leads to different levels of penetrance (from top to bottom). Yellow arrowheads highlight impaired AM pore and/or dendrite morphogenesis. **C**: Quantification of the effects of *rpn-6.1* RNAi on AM pore movement (left) and on AM dendrite morphogenesis (right) (n > 5, ±SD; two-way ANOVA P; *** ≥ 0.001; **** ≥ 0.0001). Modified from (Kunz, P. et al., 2021).
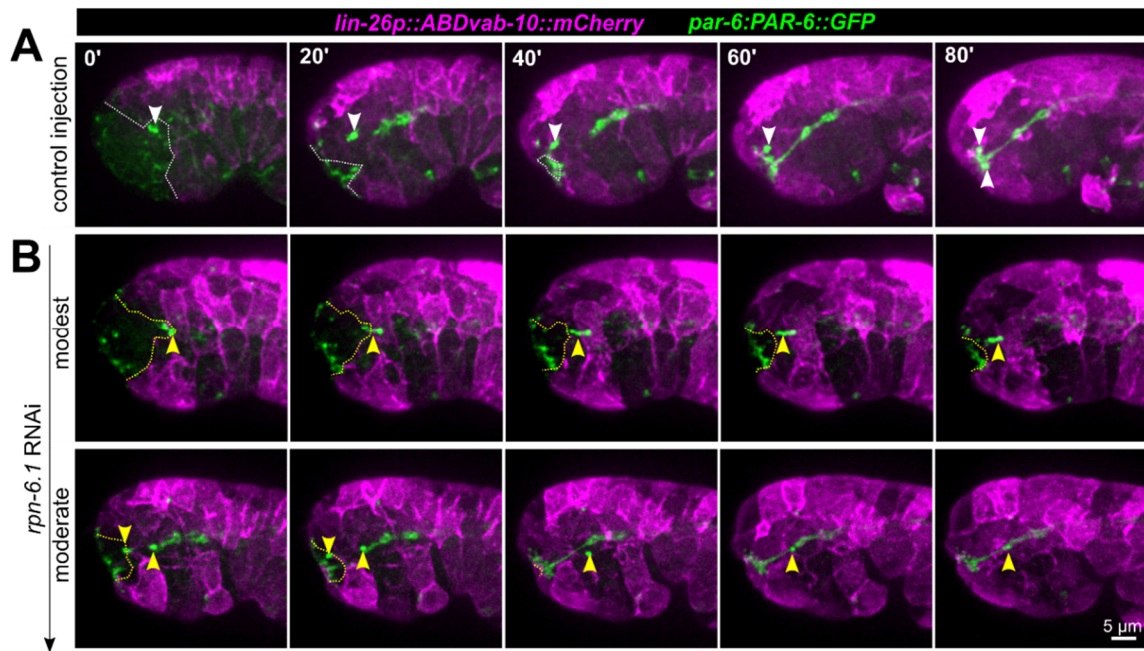
Figure 3.7: Phenotypes of rpn-6.1 RNAi embryos revealed by using polarity and epidermal markers
A: Left side view of embryos of lima-bean to 1.5-fold stage after control injection illustrating the migration of the amphid (AM) sensilla pores and the epidermal sheet. **B**: Left side view of embryos after rpn-6.1 depletion showing impaired pore morphogenesis in increasing severity (from top to bottom). White arrowheads are pointing to the AM pores undergoing wt morphogenesis. White dashed lines mark the anterior margin of the epidermal sheet. Yellow arrowheads highlight impaired amphid pore establishment or migration. Yellow dashed lines mark the margin of the epidermal sheet after rpn-6.1 depletion. All fluorescence images are maximum intensity projections of stacks of confocal images from time lapse recordings highlighting apical surfaces including sensory organ pores (green, PAR-6) and epidermis (magenta, VAB-10). Scale bar = 5 μm. Modified from (Kunz, P. et al., 2021)

b. RPN-6.1 is required for proper lumen formation of the alimentary system

Regarding the findings of incorrect connection between AM dendrite tips and split or torn apart AM pores after RPN-6.1 depletion, the question arose if also cell-cell-contact formation within polarizing intestinal tissues could be influenced by RPN-6.1. Therefore, embryos were analyzed after *rpn-6.1* RNAi focusing on the intestine, pharyngeal cells (both via PAR-6::GFP) and the AM sensilla (*pmir-124::mCherry*) (**Figure 3.8**). The results showed gaps between the prospective mouth and the pharynx (**Figure 3.8B**, top panels, asterisks) and discontinuities within the through-gut, for instance, a disrupted apical intestinal surface, frayed lumen (**Figure 3.8B**, middle panels), or both concomitantly (**Figure 3.8B**, bottom panels). Also, a failure in connection of the gut to the rectum was observed (**Figure 3.8**, bottom panels).

These findings lead to the conclusion that RPN-6.1 seems to be important for cell-cell-contact formation during through gut formation, especially for connecting the pharynx to the prospective mouth opening. Also, RPN-6.1 seems to play a role for apical lumen establishment within the intestine. Thus study suggests that AM sensilla morphogenesis is the most vulnerable morphogenetic event after RPN-6.1 depletion, whereas intestinal phenotypes occur less frequently (**Figure 3.8C**).
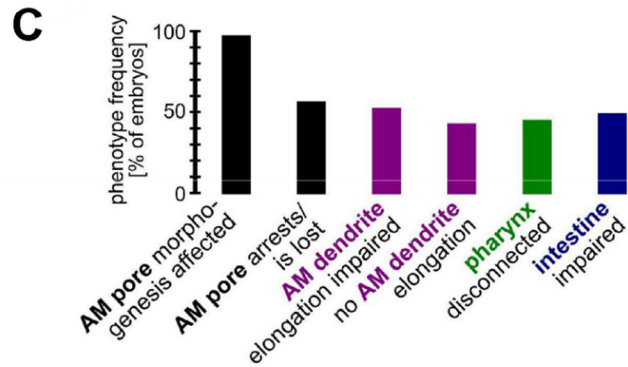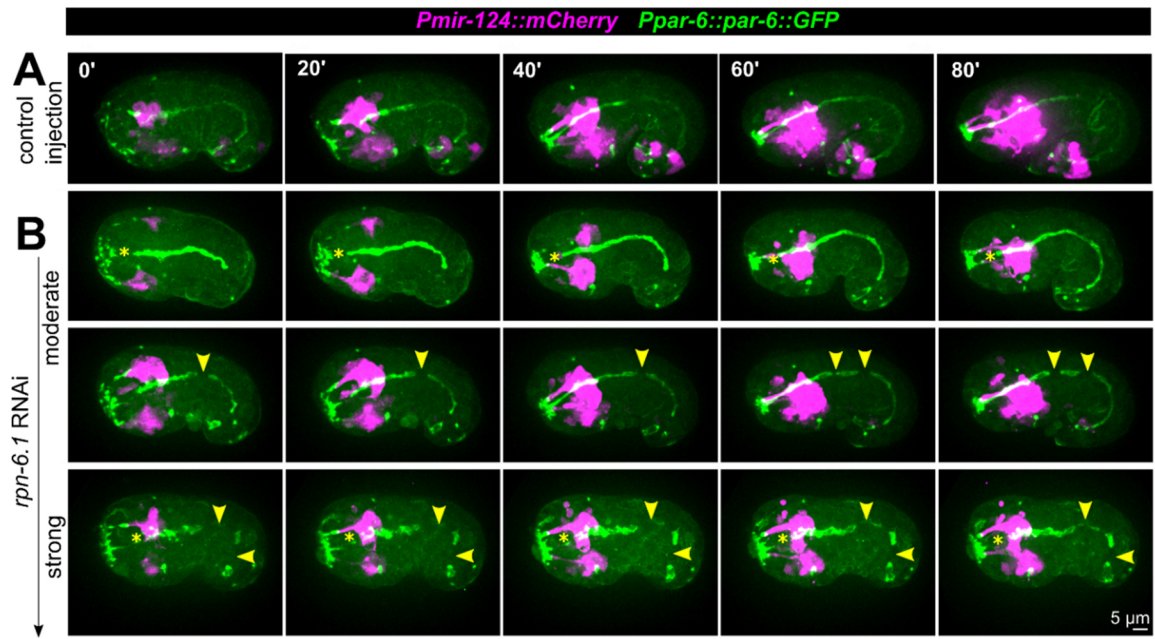
Figure 3.8: RPN-6.1 is required for the morphogenesis of organs with apical lumen
A: Maximum intensity projections of stacks of confocal images from time lapse recordings of left side view of embryo after control injection; apically polarized surfaces (sensory organ pores, excretory pore, pharynx, intestine) are shown in green, AM neurons and dendrites in magenta. **B**: Depictions as in (A), however, for *rpn-6.1* RNAi embryos. Yellow arrowheads mark discontinuities of pharynx or intestine. Yellow asterisks highlight loss of connection between mouth opening and pharynx. **C**: Quantification of phenotypes observed in *rpn-6.1* RNAi embryos (n = 29 for AM and n = 22 for all other phenotypes). None of the phenotypes has been observed in control injected embryos (n ≥ 20). Modified from (Kunz, P. et al., 2021).

Table 3.1: Quantification of phenotypes after RPN-6.1 depletion
Modified from (Kunz, P. et al., 2021)

n sensilla = 29 Embryos
n pharynx & intestine = 22 Embryos

Legend:
Color	Meaning
green	pore ok
purple	dendrites ok
light green	pharynx/intestine ok
orange	pore impaired
blue	elongation impaired
olive green	no connection pharynx to mouth
red	pore arrests
magenta	no elongation
medium green	intestine morphogenesis impaired

Embryo	pore left	dendrites left	pore right	dendrites right	pharynx	intestine
270819_sess2_E1	split but find back together, migration	ok	lost	no elongation	ok	interrupted
270819_sess2_E2	split , posteriorerior part arrests	strong impaired elongation	long, partwise split, getting together	ok	ok	ok
270819_sess2_E3	long, migratrion ok	ok	ok	ok	ok	interrupted
270819_sess3_E1	nearly split, migration	ok	split, posterior part arrests	elongation till posterior part split pore, still partly working	no connection	ok
270819_sess3_E2	split, still migration	elongation till posterior part pore	ok	ok	ok	ok
270819_sess3_E4	split, posterior part arrests	most dendrites no elongation . Those attached to poeterior part pore, thin bundle reaches anterior part	lost	no elongation	no connection	no throughgut
270819_sess4_E1	split, posterior part migrates slowly	slow elongation	partwise split/long, gets back together, migration	ok	no connection	no throughgut
270819_sess4_E3	ok	ok	long, migrating ok	ok	no connection	not normal
270819_sess4_E4	partwise split, migrates	ok	ok	ok	no connection	strong interruptions
290819_sess1_E4	arrest	no elongation, messed up	no correct migration	no elongation, messed up	no connection	okish
290819_sess2_E1	partwise split, gets together, migration	ok	slower migration	ok	ok	ok
290819_sess2_E2	loong, part split?	ok	loong, part split?	ok	ok	ok
290819_sess2_E3	split, posterior part arrests	no elongation	split, posterior part arrests	no elongation, messed up		
290819_sess2_E5	loong, partwise split	elongation slower	think ok, not well visible	think ok, not visible well	ok	interrupted
290819_sess3_E1	loong, migration ok	ok	lost	no elongation		
290819_sess3_E3	partly split, migration ok	ok elongation till posterior part, thinner bundle till anterior part, elongation works	not visible well	not visible well	ok	ok
290819_sess3_E4	spatio-temporal failure, split? migration	no elongation.	not visible well	not visible well		
100919_sess1_E2	loong, still migrating	ok	loong, migrating okish	ok	ok	ok
100919_sess1_E3	not properly established	no proper migration, just small bundle migrates	pore split, posterior part arrests	no elongation	no connection	no throughgut
100919_sess1_E4	in between split, migrating fine	ok	split, posterior part stuck, anterior part migration	elongation just till posterior part pore properly, very thin bundle till anterior pat	ok	ok
100919_sess1_E5	part pore stuck	no elongation	no pore?	no elongation	no connection	getting disrupted
100919_sess1_E6	just part pore? Migration	very poor elongation, very thin bundle	pore migrating, or just part pore?	very poor elongation, thin bundle		
100919_sess2_E1	loong, migrating	elongation happening impaired	not visible	not visible		
100919_sess2_E2	pore long, partly falling apart, stil migrating	ok	not visible	not visible	ok	ok
100919_sess2_E3	partwise long, migration	ok	not vsible	not visible		
100919_sess2_E4	migration ok	okish	not vsible	not visible	no connection	no throughgut
100919_sess3_E1	pore split no properl migration	elongation till posterior part pore	split, posterior part arrests	no proper elongation, just small bundle	no connection	no throughgut, but gut tissue dying?
100919_sess3_E3	pore split, tiny part migration	elongation thin bundle?	ok	ok		
100919_sess3_E4	pore very split, some migration	elongation happens impaired	not visible	not visible	ok	ok, shape not proper

3.4. Apical constriction affects pore migration and pharynx development

Since the results show that IL/OL/CEP sensilla pores migrate anteriorly with respect to the epidermal leading edge, separated from AM pores (**Figure 3.1, Figure 3.2, Figure 3.4**), the study investigated which events might facilitate their migration. Therefore PAR-6::GFP marker was used concomitant with visualizing cell membranes (*Ppie-1::PH(PLCδ1)::mCherry*) to examine their migration in more detail (**Figure 3.9A**). The analyses revealed that during the simultaneous movement of the pores, dorsal OLQ socket cells (OLQsoDL/R) showed the longest moving distance with approx. 50% of embryo width, followed by the IL dorsal socket cells (ILsoD, approx. 40%) together with the dorsal CEP pores (CEPD) and hereafter the IL pores (ILsoL/R) with approx. 30% of embryo width as moving distance (**Figure 3.9A**, right bottom panel). AM pores move approx. 50% distance. Importantly, AM pores begin the translocation at the most posterior-lateral position and they continuously translocate in a clearly visible distance to the other pores after finally getting positioned posteriorly to all other pores at 1.5-fold stage. The CEP, OL, and IL pores translocate simultaneously with the AM pores, but altogether anteriorly to the epidermal front, with AM pores following posteriorly at the level of the epidermal leading edge (**Figure 3.9A**, dashed lines). These results lead to the conclusion that the underlying driving event for translocation of the AM pores is different to the event driving the movement of the other head sensilla pores. Importantly, the data reveal the occurrence of bottle-shaped cells at the anterior most part of the embryo's head, which appear concomitantly with the translocation event of the head sensilla pores (**Figure 3.9B**, **Figure 3.10B, Figure 3.11B**, white dashed lines). Next, it was tested if RPN-6.1 could influence these events by depleting it. Consistent with the hypothesis is, that establishment of bottle shape was impaired in several cases (**Figure 3.9C**). We also observed weaker phenotypes with less impairment of bottle shape formation in anterior most cells (not shown).

To further investigate if cytoskeletal forces, which are known to be involved in apical constriction (reviewed in (Sawyer, J. M. et al., 2010)), might contribute to the establishment of the bottle-shape within these cells, analysis of the non-muscle-myosin components NMY-2 (*nmy-2::GFP*) or MLC-4 (*mCherry::mlc-4*), actin (*pie-1::lifeact-RFP*) and tubulin (*pie-1::GFP::tubulin*) was performed. Also, markers for AM pores, PAR-6 (*mCherry::par-6*), or cell membranes (*Ppie-1::PH(PLCδ1)::mCherry*) were used (**Figure 3.10, Figure 3.11B**). Additionally, monitoring of the expression of the apical polarity marker PAR-3 (*par-3::GFP*) was conducted to clarify if the entire apical PAR-complex is present. The results show NMY-2 and MLC-4 foci close to the position of the prospective mouth (**Figure 3.10A, C, D, E**, dashed lines). Moreover, actin is enriched at the anterior most tip of the embryo (**Figure 3.10A**). Additionally, monitoring of both bottle-shaped cells at the anterior tip of the embryo and tubulin bundles moving towards this area was executed (**Figure 3.10B**). Expression of the PAR-complex subunit PAR-3 was visible at the same positions as PAR-6 (**Figure 3.10E**), indicating their *de novo* apical localization.
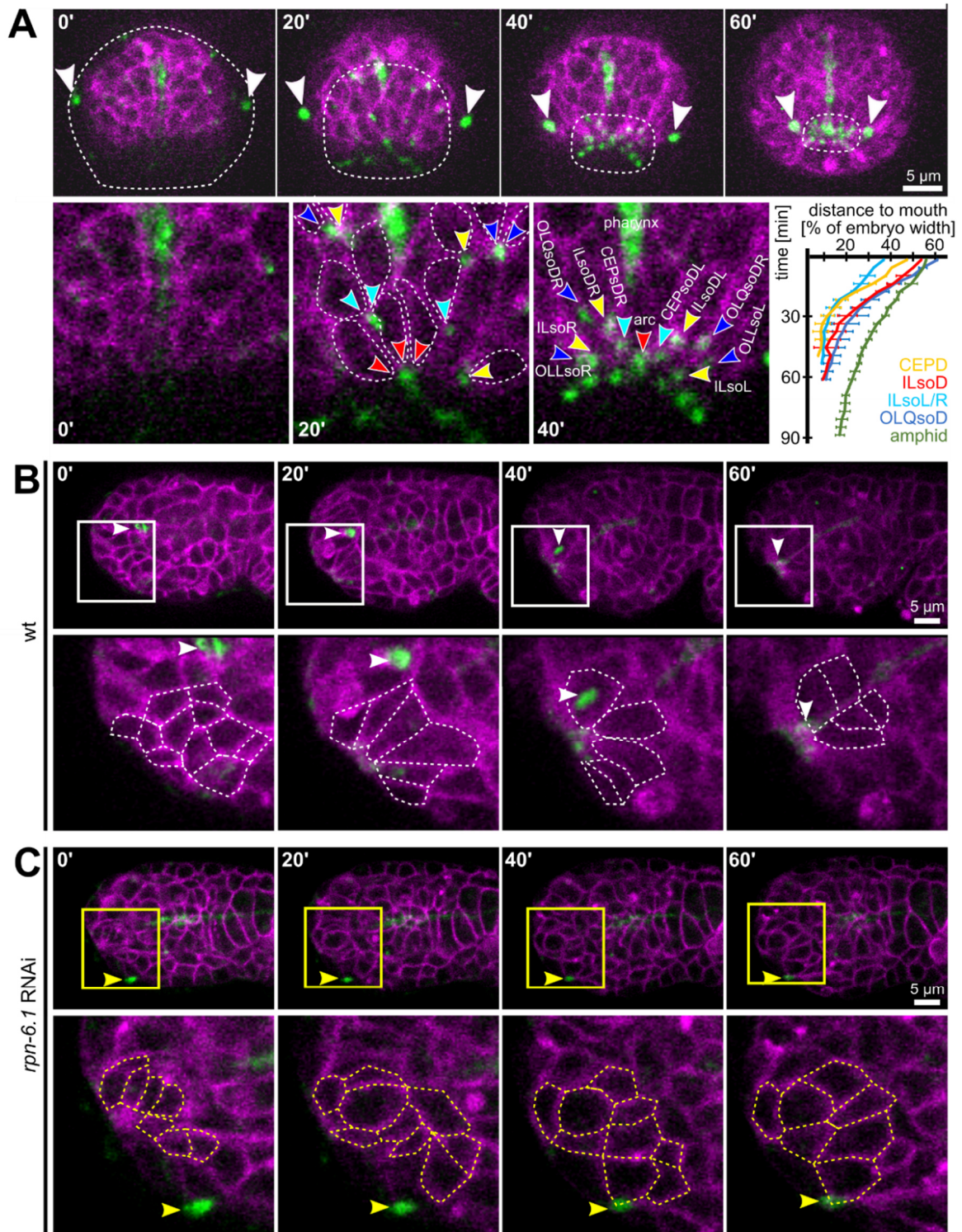
Figure 3.9: Apical constriction, sensory organ pore movement and the role of RPN-6.1

A: Top: Maximum intensity projections of stacks of confocal images from time lapse recordings of a representative wt embryo imaged from anterior. The edge of the epidermis was tracked based on cell membranes and is highlighted by a dashed line. The AM pores are highlighted by white arrowheads. Bottom left: Magnified views of cell shape changes and identification of individual sensory organ socket cells. Anterior apical tips of cells are marked with arrowheads. Bottom right: Quantification of sensory organ pore (socket cell) movement (n = 5). **B**: Top: Maximum intensity projections of stacks of confocal images from time lapse recordings of a representative wt embryo imaged from the left side. Bottom: Magnified single z-stacks from the boxed area above. Arrowheads mark the AM pore, individual neuronal and arcade cells are outlined to illustrate their shape change. **C**: Same depiction as in (B), however, for a representative, moderately RPN-6.1 depleted embryo. Modified from (Kunz, P. et al., 2021).

Besides investigating the events driving the positioning of sensilla pores, further analysis of the early development of the pharynx and constriction within neural trajectories was conducted (**Figure 3.11**). Therefore, the pharyngeal marker *Ppha-1::GFP::CAAX* was used, which highlights pharyngeal cell membranes through farnesylated GFP, and examination of the subdivisions of the alimentary tract, arcade tissue, pharynx and intestine was performed (**Figure 3.11A**). Importantly, arcade cells showed apical shrinkage and acquisition of funnel shape, which seems to interconnect the prospective mouth opening to the pharynx. At the same time, the results show accumulation of NMY-2 and collective constriction of cells at the anterior most part of the embryo's head (**Figure 3.11B**). Moreover, apical constriction of diverse ciliated neurons (*Punc-119::GFP*) within the head region was observed, which leads to a placement of their dendritic tips close to the prospective mouth (**Figure 3.11C**).

In conclusion, the results reveal co-occurrence of bottle-shaped cells and accumulation of non-muscle-myosin components at the anterior tip of the embryo. From these results, this study concludes that apical constriction could be the driving force for anterior translocation of IL/OL/CEP sensilla. Additionally, collective *de novo* apical constriction within arcade cells creates a funnel which connects the prospective mouth to the pharynx. Interestingly, also neuronal cells exhibit apical constriction followed by positioning of their dendritic tips surrounding the prospective mouth.

All in all, the results strongly indicate that AM morphogenesis is driven by epidermal head enclosure, whereby coupling between epidermis, AM pores and AM dendrite tips is a crucial precondition for AM dendrite elongation. Additionally, the results suggest that apical constriction could be a driving force in the translocation of sensilla pores of additional head sensilla. Apical constriction also seems to be of importance for early pharynx development. The two morphogenetic events of AM morphogenesis and development of other head sensilla are separable by dosage-dependent inactivation of the proteasomal factor RPN-6.1. Additionally, RPN-6.1 seems be important for AM pore morphogenesis, cell-cell attachment at AM pore dendrite tips, for interconnecting pharynx and mouth, and for a coherent apical lumen of the intestine.
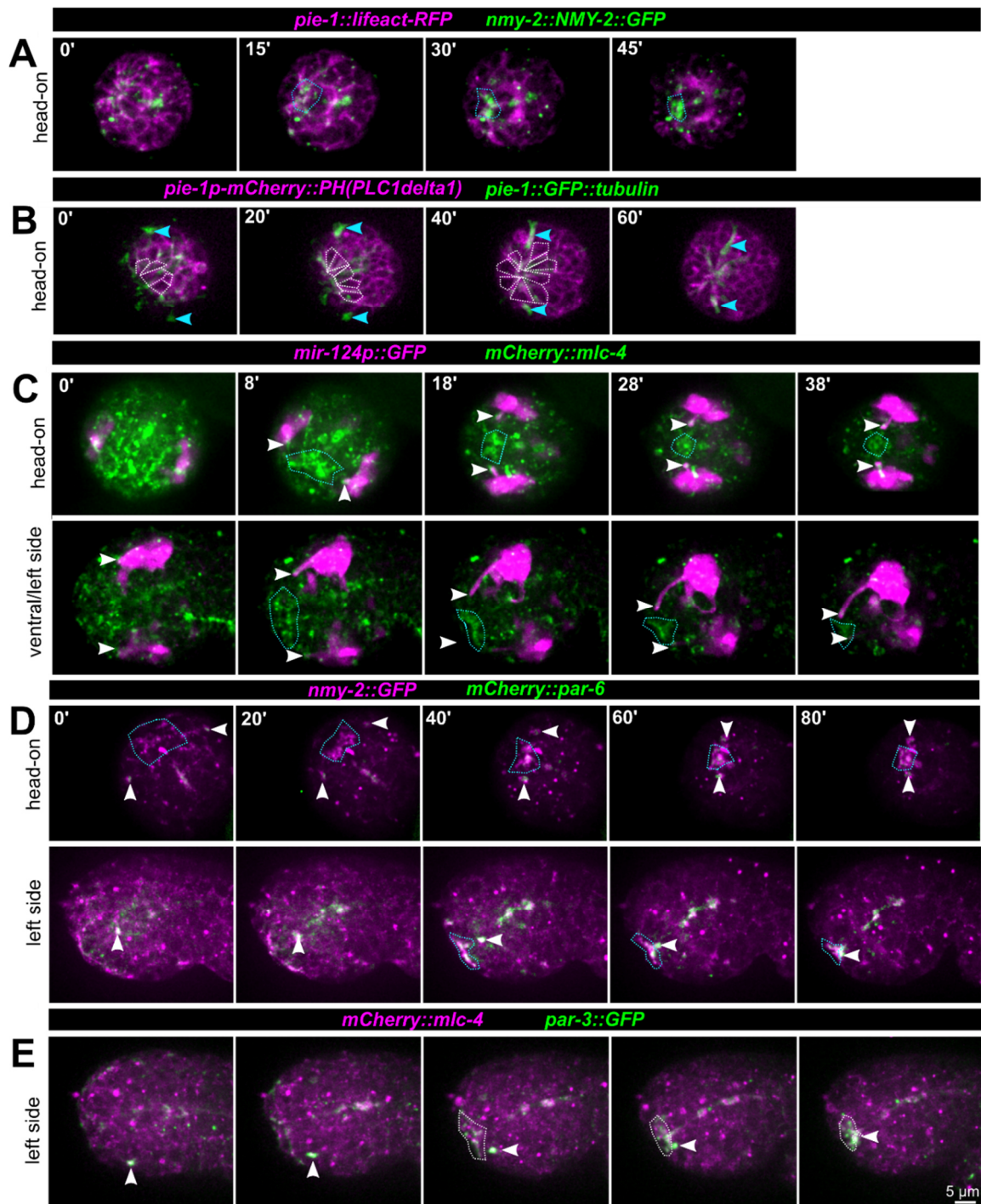
Figure 3.10: Additional markers highlighting collective apical polarity and constriction in the anterior head region

A: Head on view of wt embryo between lima-bean and 1.5-fold stage illustrating the accumulation of non-muscle myosin (green, NMY-2) together with the membrane (magenta, PIE-1). **B**: Same depictions as in panel A but tubulin (green) highlighted. Cell membranes of anterior most cells are highlighted in magenta. **C**: View of head-on (top) and ventral/left side wildtype embryos illustrating myosin (green, MLC-4) and elongation of the AM dendrites (magenta, *pmir-124*). **D**: same depictions as panel (C) but with marked myosin (magenta, NMY-2) and amphid pores (green, PAR-6). **E**: Same depiction as in (D) bottom panels, however with PAR-3 marker (green). White dashed lines highlight bottle-shaped wt cells. Light blue dashed lines frame myosin accumulation. White arrowheads point to wildtypic amphid pores. Light blue arrowheads mark prominent tubulin. All fluorescence images are maximum intensity projections of stacks or single layer confocal images from time lapse recordings. Scale bar = 5 µm. Modified from (Kunz, P. et al., 2021).
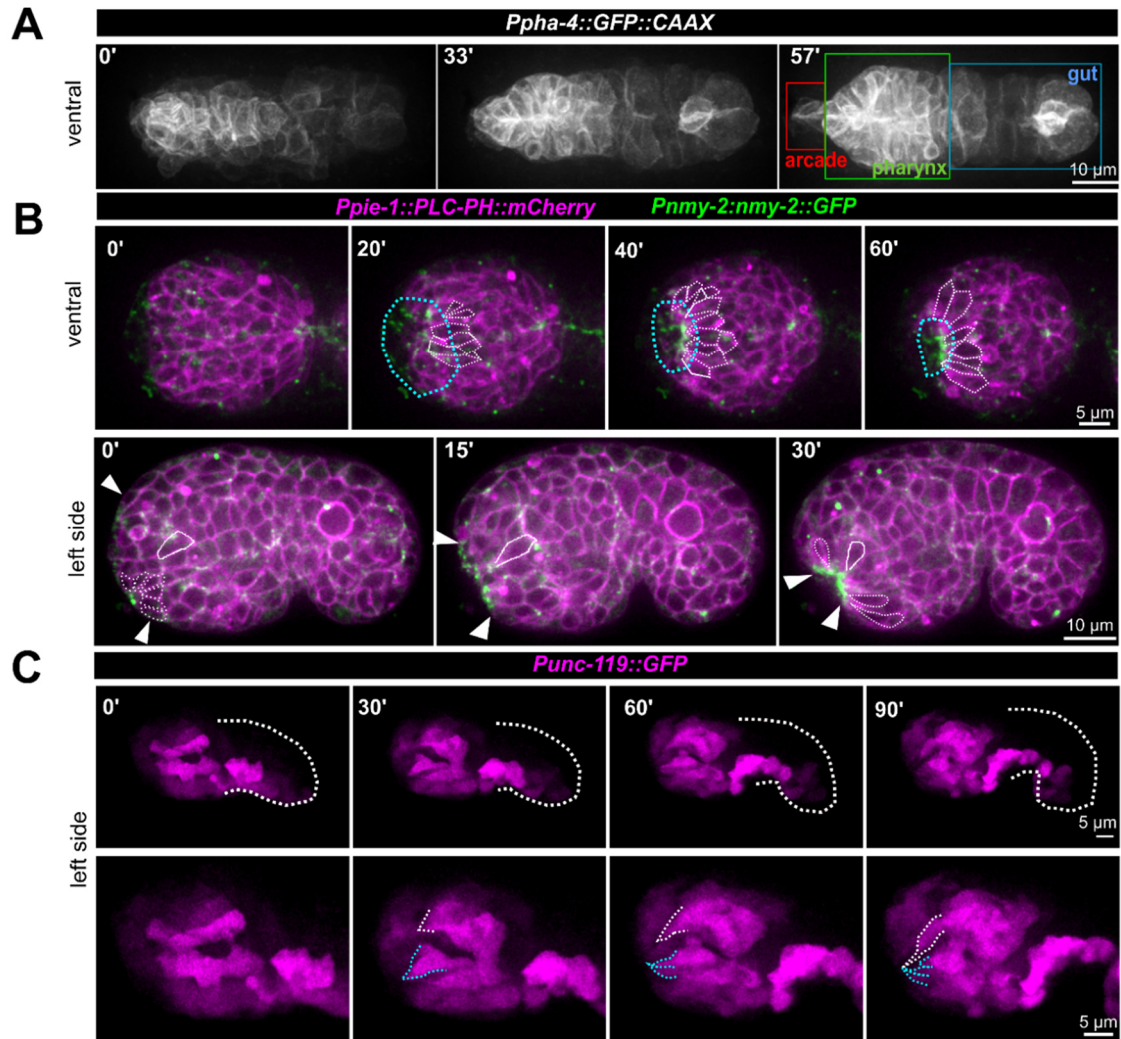
Figure 3.11: Apical constriction of anterior cells

A: Maximum intensity projections of stacks of confocal images from time lapse recordings of a representative wt embryo expressing a membrane-localized GFP under the control of the pha-4 promotor imaged from the ventral side. The individual compartments of the alimentary system are highlighted in the right panel. **B**: Top: Maximum intensity projections of stacks of confocal images from time lapse recordings of representative wt embryo imaged from the ventral side. Bottom: Central confocal plane from time lapse recordings of a representative wt embryo imaged from the left side. White arrowheads and blue dashed lines mark the anterior cell surfaces that acquire and accumulate NMY-2. The dashed white line highlights cells that have undergone apical constriction. The solid white line traces a cell that undergoes apical constriction and thereby moves juxta-orally. **C**: Maximum intensity projections of stacks of confocal images from time lapse recordings of a representative wt embryo imaged from the left side. Top: whole embryo shown. White dashed lines mark the outlines of the embryo. Bottom: Close-up view of the head region showing apical constriction in anterior neurites which are tracked by blue and white dashed lines. Modified from (Kunz, P. et al., 2021).

4. Discussion

This study reveals how *C. elegans* sensory organs are gaining their unique elongated shape during embryonic development. It unveils a coupling of multiple morphogenetic events; epidermal migration, dendrite towing, apical constriction and tissue invagination and discusses aspects of their molecular regulation. Overall, this dissertation provides a plausible cellular model how these aspects contribute to the interconnected morphogenesis of the *C. elegans* head.

4.1. Towing drives AM dendrite elongation

The data clearly exhibit the concomitant occurrence of multiple morphogenetic events during embryonic head development from lima-bean to 1.5-fold embryonic stages: (1) anterior covering of the head region by epidermal sheet (**Figure 3.2, Figure 3.3**), which is termed head enclosure (reviewed in (Chisholm, A. D. and Hardin, J., 2005)), anterior translocation of the AM pores (**Figure 3.1, Figure 3.2**) and simultaneous elongation of the AM dendrites (**Figure 3.3, Figure 3.4, Figure 3.5**). The findings unveil the importance of sustained coupling between AM pores and the epidermal sheet during head enclosure. The dissertation reveals this physical attachment as crucial for correct final positioning of the AM pores at the prospective mouth, due to the fact that AM pore translocation is impaired after ablating the connection to the epidermal sheet (**Figure 3.2**). Additionally, the data shows that AM dendrite tips translocate collectively with the migrating epidermal leading edge (**Figure 3.3, Figure 3.4**). The author of this study concludes that AM dendrite tips are attached to the anterior migrating AM pores, whereby the dendrite tips are pulled anteriorly. Moreover, this study shows through lineage-tracing of AM (AMsoL, AMshL, ASEL) and epidermal cells (hyp5, XXXL), that AM neuronal cell bodies (ASEL) are not moving actively but remain stationary at their initial position, even when the epidermal cells, or glial cells (AMsoL, AMshL) translocate anteriorly (**Figure 3.1**). The author conjectures that hereby AM dendrites can get stretched into their elongated shape, while the AM neural cell bodies stay stationary at posterior position as abutments.

To gain deeper understanding on how coupling of head enclosure, AM pore migration and AM dendrite extension can coordinate AM morphogenesis, possible dendrite elongation modes and the importance of junctional components for neural morphogenesis is discussed in the following section.

Firstly, this study is subdividing neuronal morphogenesis into active and passive neurite elongation modes (**Figure 1.12**). Active neurite elongation modes are driven by neuronal aspects and passive neurite elongation occurs without active neuronal contribution. Examples of active neurite elongation modes are growth cone advancement ((Tessier-Lavigne, M. and Goodman, C. S., 1996), reviewed in (Huber, A. B. et al., 2003) **Figure 4.1**, bottom panels) or retrograde extension ((Heiman, M. G. and Shaham, S., 2009) **Figure 4.1**, middle panels). In these cases, neurites extend through an advancing neuronal growth cone or via migration of the neural cell bodies. Examples of passive neurite extension include neurite elongation through migrating target tissues, like during towing (Gilmour, D. et al., 2004). Towing occurs during the development of the lateral line organ in zebrafish ((Metcalfe, 1985), (Gilmour, D. et al., 2004)) and most likely during spicule morphogenesis in *C. elegans* (Jiang, L. I. and Sternberg, P. W., 1999). Also, recent work on axon stretch-growth *in vitro* suggests that tension created by expansion of the body during development could be a trigger for neuronal growth, which was found to be distinguishable from injury driven neuronal growth (Loverde, J.R. and Pfister, B.J., 2015). During *C. elegans* embryonic development, it has been reported that sensory dendrite tips attach to the nose (Heiman, M. G. and Shaham, S., 2009). Their study also proposes that retrograde extension drives neuronal elongation, whereby "… the presumptive dendritic tip remains stationary while the cell body migrates away …" ((Heiman, M. G. and Shaham, S., 2009) **Figure 4.1**, middle panels). In extreme contrast to this statement, the same authors very recently suggested that "…the initial extension of the amphid dendrites is driven by the migrating skin through physical attachment" (Fan, L. et al., 2019). Importantly, the data of the study in hands show co-occurrence of dendrite elongation with epidermal head enclosure, which is reaffirmed by very recent findings from (Grimbert, S. et al., 2020). The data of this dissertation additionally unveil the coupling between epidermal migration and AM morphogenesis. Accordingly, the results of this dissertation and the findings from (Fan, L. et al., 2019) closely resemble towing (Gilmour, D. et al., 2004). However, in the study in hands dendrite and not axon towing transpires, because the actively moving epidermis is attached to neurons regulating their extension by pulling force (**Figure 4.1**, top panels).

Secondly, a fundamental anatomical prerequisite for the morphogenesis of AM neurons is the physical connection of AM sensory endings to the epidermis via apical junctions (CeAJ) ((Ward, S. et al., 1975), (Perkins, L. A. et al., 1986), (Low, I. I. et al., 2019)). Since dendrite tips are attached to the AMsh glia cell, which itself is linked to the AMso glia and this pore is connected to the epidermis, the AM sensory endings are completely embedded within the epidermal sheet through glial cells acting as support cells. Recent findings strongly suggest that "these neurons and glia can be viewed as part of an epithelium continuous with the skin and are shaped by mechanisms shared with other epithelia" (Low, I. I. et al., 2019). The findings from Low et al. additionally highlight apical-basal polarity and junctional components within the AM as epithelial properties and suggest that the apical extracellular matrix (ECM) factor DYF-7 (abnormal DYe Filling), which contains a zona pellucida-like protein, contributes to AM integrity within the epidermis.

Taken together, the findings of this dissertation unveil coupled anterior migration of epidermal sheet, AM pores and thereby AM dendrite extension with AM neural cell bodies staying stationary. Importantly, AM pores are attached to both the migrating epidermis and the AM dendritic tips by CeAJs ((Ward, S. et al., 1975), (Perkins, L. A. et al., 1986), reviewed in (Altun, Z. F. and Hall, D. H., 2010)). Hence, the conclusion is made that head enclosure and coupled AM pore migration drive elongation of the AM dendrites through stretching due to interconnection of all AM cells with the epidermis via CeAJ with AM neural cell bodies staying stationary. Thus, the mode of AM sensilla morphogenesis is categorized as passive dendrite towing according to (Gilmour, D. et al., 2004), because AM dendrites elongate via epidermally-derived pulling forces while neuronal cell bodies stay passive (**Figure 4.1**, top panels).
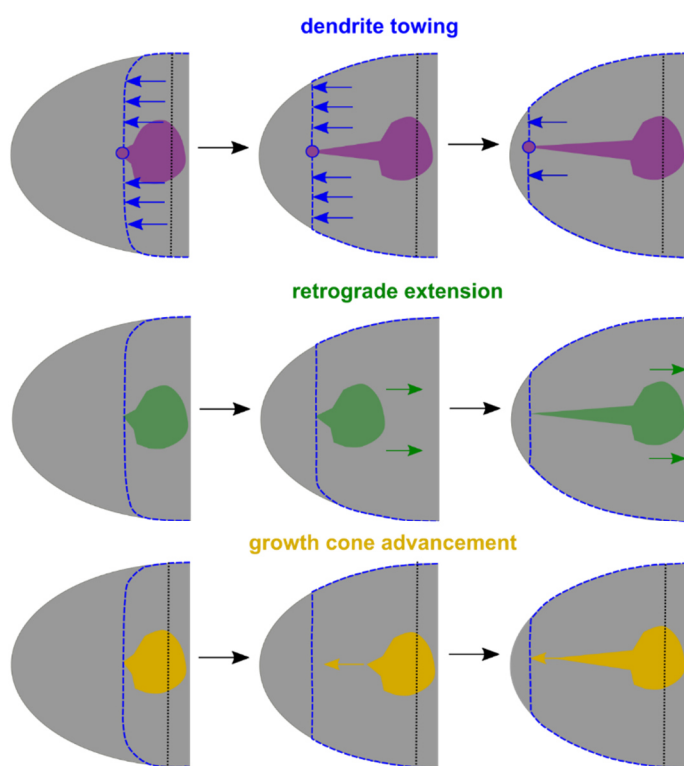
Figure 4.1: Summary of neural elongation modes

Schematic illustration depicting neural morphogenesis driven by diverging morphogenetic events. Top: Head enclosure-driven passive dendrite elongation facilitated by coupling of epidermis and sensilla cells coined dendrite towing (blue). Middle: Active neural cell body driven dendrite elongation through retrograde extension (green). Bottom: Active growth cone driven neural elongation through growth cone advancement. Modified from (Kunz, P. et al., 2021).

4.2. Apical constriction in OL/IL/CEP and pharynx development

Besides investigating the morphogenetic events driving AM sensilla development, this work also elucidates developmental aspects of additional head sensory sensilla (IL/OL, CEP). The findings show that the socket cells (glial pores) of these sensilla migrate concomitantly with epidermal cells, but anterior to the epidermal leading edge (**Figure 3.1A, Figure 3.2, Figure 3.4, Figure 3.9A**). Hereby, the OL/IL/CEP sensory pores are migrating simultaneously to their final juxta-oral position, while AM pores arrive there only later (**Figure 3.1A, Figure 3.9A**). Importantly, even after moderate and strong RPN-6.1 depletion, when AM pore migration is strongly impaired, the OL/IL/CEP head sensilla pores still translocate to the prospective mouth (**Figure 3.6B, Figure 3.7B**). The author of this study thereby suggests that the morphogenesis of the IL/OL/CEP sensilla is not driven by dendrite towing but otherwise. Essentially, the findings reveal bottle-shaped cells (**Figure 3.9B, Figure 3.10B, Figure 3.11B**), *de-novo* enrichment of the apical polarity markers PAR6 and PAR-3 (**Figure 3.9A, Figure 3.10D, E**) and presence of the apical cytoskeletal components NMY-2 and MLC-4 (**Figure 3.10, Figure 3.11B**) at the anterior most part of the head during lima-bean to 1.5-fold stage.

Bottle-shaped cells indicate tissue remodeling through apical constriction in *Xenopus* gastrulation ((Hardin, J. and Keller, R., 1988), (Lee, J. Y. and Harland, R. M., 2007)) or wound healing (Davidson, L. A. et al., 2002b) and throughout mammalian neural tube formation (Moore, D. C. P. et al., 1987). Apical constriction is known to be driven by force generation through the cytoskeletal motor non-muscle myosin II (NMY-2, MLC-4) and actin (reviewed in (Sawyer, J. M. et al., 2010)). The resulting cell shape changes drive tissue invagination enabled through linkage with neighboring cells by junctional components (reviewed in (Sawyer, J. M. et al., 2010), (Martin, A. C. and Goldstein, B., 2014)).

This study concludes that apical constriction is a driving force facilitating head sensilla morphogenesis, because bottle-shaped cells, accumulated polarity factors and force generators at the anterior most part of the head occur concomitantly with collective head sensilla pore migration (**Figure 4.2A**). The author of this dissertation suggests that acquisition of bottle-shape rather than proposed rosettes (Fan, L. et al., 2019) are important for head sensory morphogenesis. Apical cell boundaries of combined constricting cells indeed resemble rosettes described by (Fan, L. et al., 2019). However, a rosette is a mere kinematic description of a cell arrangement and does neither explain forces nor transitions. Nonetheless, the author of this dissertation admits that apical constriction may be just one of many morphogenetic events facilitating head sensilla morphogenesis, because after RPN-6.1 depletion, bottle shape was just slightly impaired in some cases. A deeper investigation to clarify which additional events might facilitate the morphogenesis of OL, IL and CEP sensilla organs is recommended.

In addition to sensilla development during lima-bean to 2-fold stages, multiple other cells traverse migration events at the anterior part of the embryo's developing head ((Sulston, J. E. et al., 1983), reviewed in (Altun, Z.F. and Hall, D.H., 2011)), the most relevant for this study being cellular re-arrangements during the early development of the pharynx (reviewed in (Altun, Z. F. and Hall, D. H., 2009B)). The findings of the study in hands suggest that apical constriction within anterior most cells of the embryo could contribute to mouth invagination and early pharynx development. This suggestion originates from observing a co-occurrence of bottle-shaped cells at the anterior most part of the head (**Figure 3.9B, Figure 3.10B, Figure 3.11B**), accumulation of apical force creating factors (NMY-2, MLC-4, **Figure 3.10, Figure 3.11B**) and enriched apical polarity markers (PAR-6, PAR-3, **Figure 3.10D,E**) at the position of the prospective mouth opening. Remarkably, the findings exhibit the establishment of an arcade-pharynx funnel, which seems to gain its shape by apical constriction within the arcade cells (**Figure 3.11A**). It is thereby assumed that the connection between mouth opening and pharynx is most likely established through apical constriction within the arcade cells. Very recent findings confirm the conclusion that embryonic head morphogenesis includes the anterior positioning of pharyngeal cells (through apical constriction) and epidermal cells (through head enclosure), adding a role for neuroblasts (Grimbert, S. et al., 2020). Moreover, this dissertation suggests that RPN.6.1 might play a role for successful interconnection of the mouth opening to the pharynx via arcade cells, since the results show lack of pharynx-mouth connection after RPN-6.1 depletion (**Figure 3.8**). Also, the interfacial epithelial arcade cells connect the pharynx to hyp1 epithelial cells and contribute to early pharynx development including pharyngeal extension ((Portereiko, M. F. and Mango, S. E., 2001), (Mango, 2007), reviewed in (Altun, Z. F. and Hall, D. H., 2009B)). The author of this study assumes that the development of the AM sensory endings and the establishment of a pharynx-mouth connection might share underlying morphological aspects, because both show impaired cell-to cell attachment after RPN-6.1 depletion. Furthermore, a function of DEX-1 for pharynx development is taken into account, since recent findings described DEX-1 expression in the pharynx and a Pin (pharynx ingressed) phenotype in *dex-1* mutant embryos (Cohen, J. D. et al., 2018). Finally, besides apical constriction driving head sensilla pore migration and mouth to pharynx connection, also anterior neuronal cells showed apical constriction (**Figure 3.11C**). This study thus concludes that during embryonic head morphogenesis, head sensory organ trajectories are surrounding an arcade-pharynx funnel (**Figure 4.2B**).

Taking the findings of the dissertation in hands, classical work and morphological descriptions of the pharynx together ((Sulston, J. E. et al., 1983), reviewed in (Altun, Z. F. and Hall, D. H., 2009B)), the author of this study hypothesizes that the mouth-pharynx connection might resemble the morphology of the AM sensilla opening: The mouth opening is composed of a tubular pore (like the AM pore) created by an arcade cell funnel (like AMso/AMsh creating the AM channel). Also, the mouth-opening interconnects the outer space to the pharynx, resembling the AM channel creating a continuous lumen enabling the AM dendrites to get in contact with the outer space.
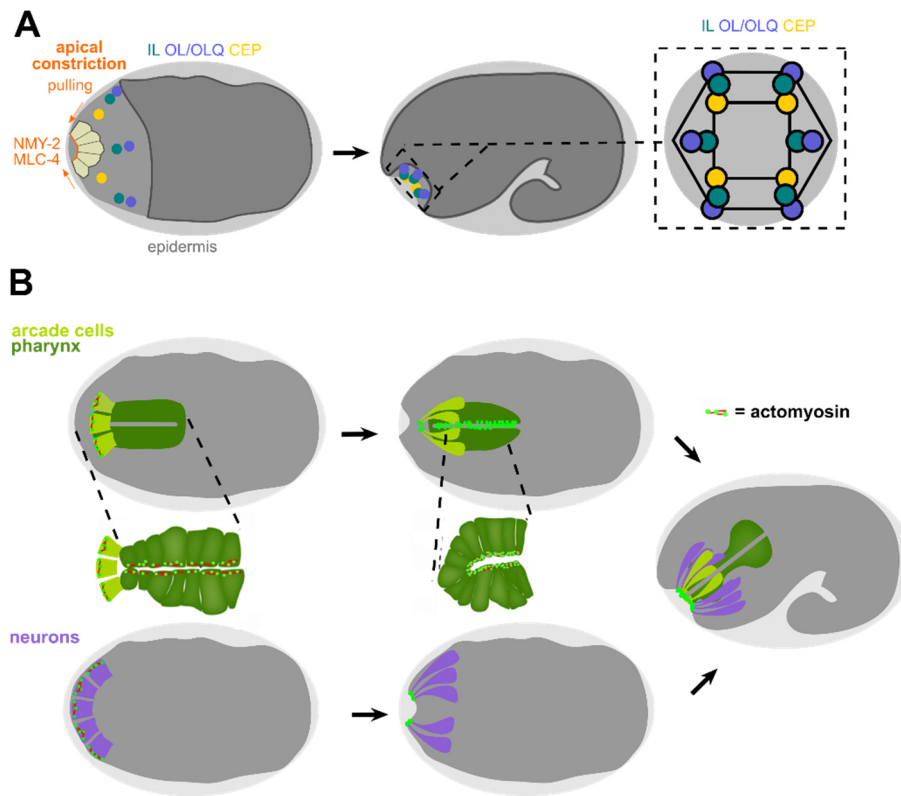
Figure 4.2: Apical constriction contributes to sensilla morphogenesis and pharynx development

Scheme depicting roles of apical constriction for sensilla (IL/OL/CEP) und pharynx development. **A:** Apical constriction contributes to pore migration of inner labial (IL), outer labial (OL) and cephalic (CEP) sensilla. Right panel shows head-on view of symmetric arrangement of sensilla endings. **B**: Top panels: Apical constriction creates a funnel and facilitates early pharynx development. Bottom panels: Apical constriction during morphogenesis of anterior neurons which get positioned surrounding the pharynx (right panel). Modified from (Kunz, P. et al., 2021).

4.3. Embryonic head morphogenesis

The findings of the study in hands are consistent with embryonic lineage analysis implemented by (Sulston, J. E. et al., 1983), clearly demonstrating how different types of cells migrate during the morphogenesis of the embryo's head region between lima-bean and comma stages (**Figure 4.4**). Epidermal cells migrate anteriorly until they encase the anterior region during head enclosure (Grimbert, S. et al., 2020). Remarkably, OL, IL and CEP head sensilla pores migrate ahead of the epidermal leading edge until they reach their final position neighboring the prospective mouth (**Figure 4.2A**), whereby their neural cells are proposed to translocate in anterior direction following their pores (**Figure 4.4**, top panels). Crucially, AM socket cells are migrating in anterior direction embedded within the epidermal leading edge, but AM neural cell bodies are staying stationary at their initial posterior position (**Figure 3.1B, Figure 4.4**, bottom panels, **Figure 4.1**). Besides the development of the head sensilla, the nerve ring (NR) establishment begins at lima-bean/comma stage and proceeds until late embryogenesis (**Figure 4.3, Figure 4.4**, top panels (reviewed in (Altun, 2017)). Importantly, not only neural migration events occur throughout head morphogenesis, but also the pharyngeal cyst develops into the pharyngeal tube ((Portereiko, M. F. and Mango, S. E., 2001), (Mango, 2007) **Figure 4.3, Figure 4.4**, top panels). Thereby, the establishing pharynx is proposed to be shoving the head neurons sideways (reviewed in (Altun, Z.F. and Hall, D.H., 2011)). Eventually, labial and AM sensilla endings localize with a specific symmetry (AM 2-fold, labial 6-fold, reviewed in (Altun, Z. F. and Hall, D. H., 2010)) and mouth and pharyngeal cells locate in their midst (**Figure 4.3**). Moreover, some initially anterior positioned non-sensory neural cells (e.g. RME, AVA, AVE, AVD) translocate in more posterior direction (**Figure 4.4**, top panels).
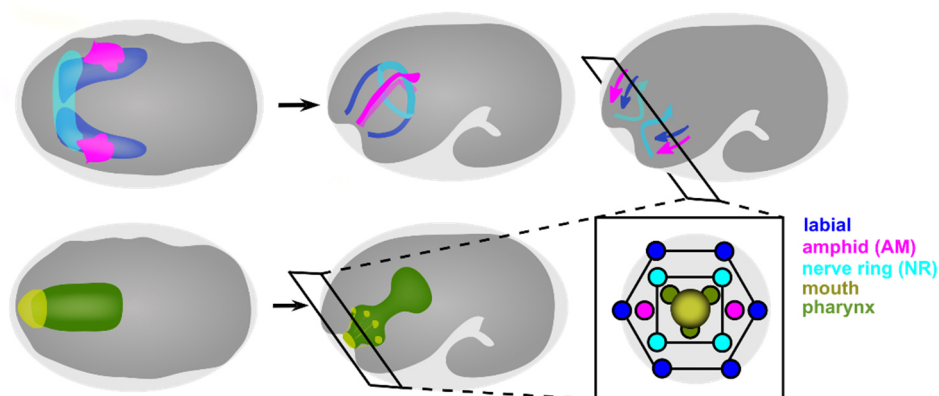

Figure 4.3: Coherent development of diverse tissues within the embryos head between lima-bean and 1.5-fold stage

Schematic illustration depicting the coherent development of multiple tissues in the embryo's head during lima-bean to 1.5-fold stages. Top: Development of amphid and labial sensilla and the nerve ring. Bottom: Early development of the pharynx. Bottom right: head-on view showing symmetric arrangement of amphid and labial sensilla endings, the nerve ring surrounding the pharynx and mouth opening at the center. Mofidied from (Kunz, P. et al., 2021).
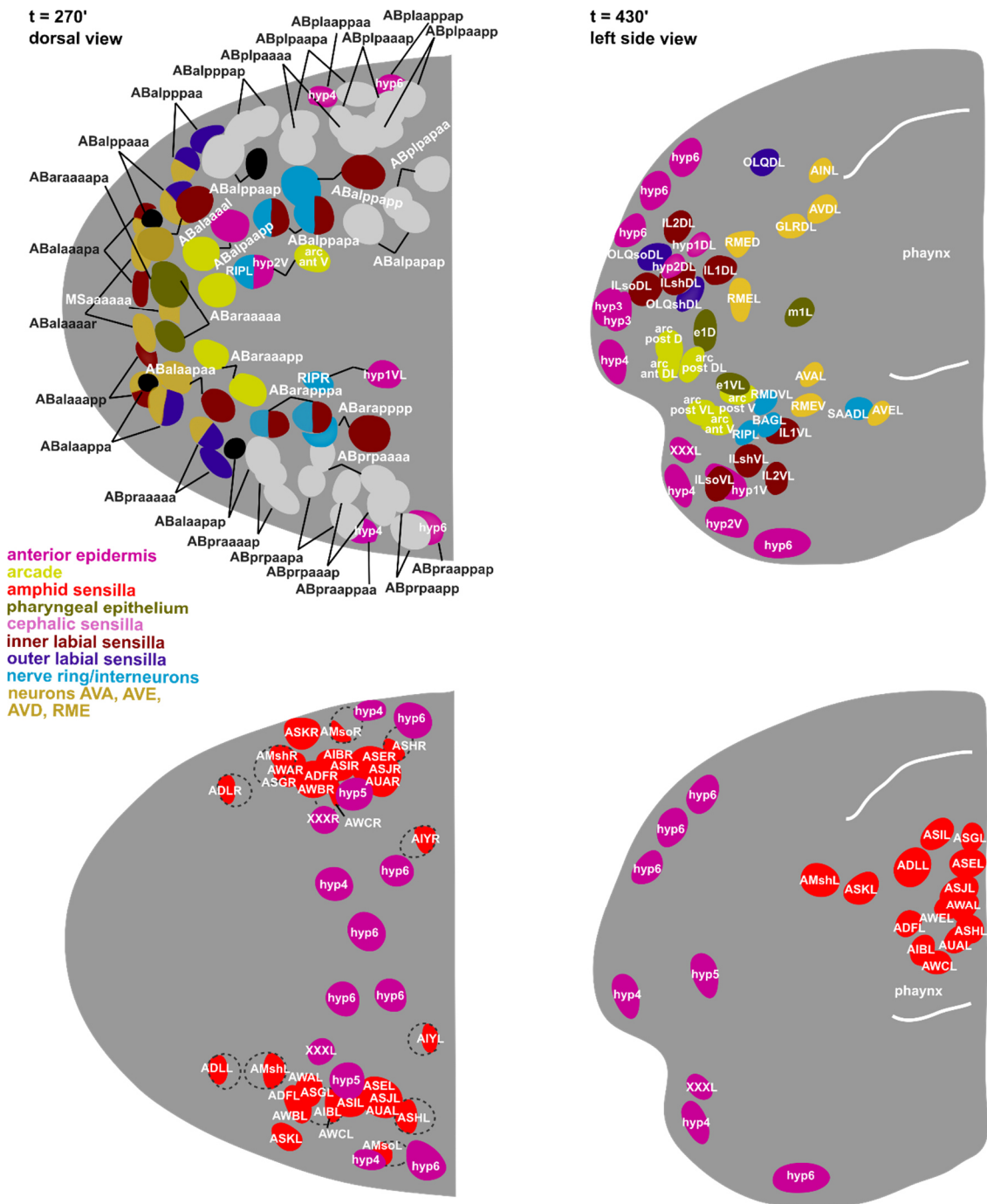
Figure 4.4: Annotated cell migration events during embryonal head morphogenesis
Modified from (Kunz, P. et al., 2021), based on (Sulston, J. E. et al., 1983).

4.4. Molecular view on AM sensilla morphogenesis

Multiple factors were recently suggested in having diverse functions during embryonal sensory organ development ((Heiman, M. G. and Shaham, S., 2009), (Cohen, J. D. et al., 2018), (Fan, L. et al., 2019), (Low, I. I. et al., 2019), (Cheerambathur, D. K. et al., 2019)). This study in hands mainly focuses on the proteasomal component RPN-6.1, which has been shown to act as an important proteasome activator (Pathare, G. R. et al., 2012). Furthermore, additional cell-cell adhesion and apicobasal polarity factors as well as molecules of the kinetochore-microtubule coupling machinery (KMN network) have been implicated to contribute to AM morphogenesis. Finally, a model is depicting the multiple morphological and possible molecular events which contribute to embryonic head morphogenesis (**Figure 4.5**).

a. RPN-6.1 activity is required for AM towing and enables separation from apical constriction-driven events

The findings show pleiotropic dosage-dependent phenotypes in embryos after RPN-6.1 depletion, including impaired AM pore morphogenesis (stretched, torn apart, loss), incorrect AM pore migration (arrest) and disturbed attachment of dendrite tips to AM pores, which clearly affect AM dendrite elongation (**Figure 3.6B**). Likewise, the data exhibit that after moderate RPN-6.1 downregulation the AM pore is partially dissociating from the migrating epidermis and partially arresting (**Figure 3.7B**). Thus, more evidence is added to the proposed mechanism that the AM pore is crucial for correct AM dendrite elongation. In this context, the pore needs a precisely tuned spatio-temporal attachment to AM dendrite tips and maintained coupling to the epidermis. Remarkably, the findings show that even after strong RPN-6.1 depletion, when AM sensilla morphogenesis is highly impaired, IL, OL and CEP head sensilla pores still migrate to their juxta-oral positions (**Figure 3.6B**). Also, bottle-shaped cells at the anterior most part of the head appeared in some cases are just slightly affected (**Figure 3.9C**). In addition to impaired AM sensilla development after RPN-6.1 depletion, the data show intestinal defects, including lack of connection between pharynx and mouth (**Figure 3.8B**). Thus, RPN-6.1 seems to contribute to AM pore morphogenesis and the attachment of AM pore to both dendrite tips and epidermis, thereby facilitating correct AM sensilla morphogenesis through AM dendrite towing. Additionally, RPN-6.1 seems to function in mouth-pharynx connection, apical polarization and lumen formation within the alimentary system. Thereby, dosage-dependent RPN-6.1 depletion enables the separation of AM dendrite towing from apical constriction-driven IL/OL/CEP sensilla morphogenesis: only the first strongly depends on RPN-6.1 activity. Moreover, RPN-6.1 seems to be more important for AM sensilla morphogenesis than for intestinal morphogenesis (**Figure 3.8C**). As follows, it is discussed in greater detail how RPN-6.1 might function on molecular level in combination with other factors to facilitate AM sensilla morphogenesis.

b. Cell-cell adhesion molecules contribute to AM morphogenesis

Possibly the most noted factors contributing to sensilla development in *C. elegans* are "…acting together in the extracellular space, DEX-1 and DYF-7 anchor dendritic tips…" (Heiman, M. G. and Shaham, S., 2009). DYF-7, which contains a zona pellucida (ZP) like domain, and DEX-1, comprising a zonadhesin like domain, are apical extracellular matrix (aECM) components potentially resembling α- and β-tectorins. It was suggested that "sensory neurons are born near the presumptive nose, polarize toward it, and express DYF-7. DYF-7 is trafficked toward this polarization; is released from the membrane …" (Heiman, M. G. and Shaham, S., 2009). Thus, especially DYF-7 seems to be of importance for sensory neuron development. Very recently and of interest for this work, more details were added to the role of DYF-7 for sensilla development ((Low, I. I. et al., 2019), (Fan, L. et al., 2019)). Firstly, loss of DYF-7 seems to harm correct AM pore morphology and also affects the continuity of the AM channel lumen between AMsh and AMso cells (Low, I. I. et al., 2019). In addition, the suggestion was made that "DYF-7 also plays a role in the attachment between epidermal cells and dendrite tips during the initial anterior extension of dendrites" (Fan, L. et al., 2019). Remarkably, DYF-7 resembles ZP domain proteins, which are undergoing proteolytic cleavage (reviewed in (Bokhove, M. and Jovine, L., 2018)) and their loss leads to disruption of tubular structures during their morphogenesis ((Ja´zwi´nska, A. et al., 2003), (Gill, H. K. et al., 2016)). For instance, "… Piopio (Pio) and Dumpy (Dp), containing a zona pellucida (ZP) domain, are essential for the generation of the interconnected tracheal network in *Drosophila melanogaster*." (Ja´zwi´nska, A. et al., 2003). Also, for *C. elegans* excretory duct tube development, the ZP domain glycoprotein LET-653 is crucial to prevent lumen fragmentation (Gill, H. K. et al., 2016). Accordingly, recent findings showed "... DYF-7 undergoes CFCS-dependent (consensus furin cleavage site) proteolysis *in vivo*" (Low, I. I. et al., 2019) and "… the ZP domain of DYF-7ecto localized with exquisite precision to caps at dendrite endings" (Low, I. I. et al., 2019). Moreover, DYF- 7 was found to be required for creation of fibrils, which are originating close to the AM dendrite tips, reaching throughout the AM channel and terminating at the aECM of the embryo (Low, I. I. et al., 2019). Furthermore, also the aECM factor DEX-1 was reported to be essential for embryonic development and of importance for sensilla development ((Heiman, M. G. and Shaham, S., 2009), (Cohen, J. D. et al., 2018)). Besides the DEX-1 expression near the nose tip (Heiman, M. G. and Shaham, S., 2009), it's expression also occurs within excretory cells (pore and duct lumen) (Cohen, J. D. et al., 2018). Since the usage of loss-of-function *dex-1 (cs201)* mutants exhibited strong phenotypes (Cohen, J. D. et al., 2018) in comparison to findings shown before (Heiman, M. G. and Shaham, S., 2009), the author of this study in hands assumes DEX-1 could have significant functions for head sensilla morphogenesis.

Remarkably, DEX-1 was found to be one of many apical ECM factors functioning during epithelial-, pharynx and excretory tissue morphogenetic events (Cohen, J. D. et al., 2018). For instance, *dex-1(cs201)* L1 larvae showed impaired excretory pore morphology and alteration of its auto-cellular junctions/ring shaped junctions. Thus, DEX-1 seems to facilitate morphogenesis of the excretory pore (Cohen, J. D. et al., 2018) (resembling the AM pore) and might contribute to correct pharynx morphogenesis.

Recent findings suggest that the adhesion molecules SAX-7 (Sensory AXon guidance; an ortholog of human NRCAM (neuronal cell adhesion molecule)) and HMR-1 (HaMmeRhead embryonic lethal; *C. elegans* ortholog of E-cadherin) might contribute to attaching the epidermis to AM dendrites (Fan, L. et al., 2019). HMR-1, SAX-7 and DLG-1 (Drosophila Discs LarGe homolog) are localized at epithelial junctions, but additionally HMR-1 and DLG-1 are expressed at dendritic tips and SAX-7 expression also occurs throughout the dendrite length. SAX-7 is also required for correct AM dendrite fasciculation ((Sasakura, H. et al., 2005), (Yip, Z. C. and Heiman, M. G., 2018)) and contributes to patterning, growth and branching of PVD dendrites trough skin-derived signaling in combination with other factors ((Salzberg, Y. et al., 2013), (Dong, K. et al., 2013)). SAX-7 and HMR-1 are assumed to act redundantly with DYF-7 (see above) in connecting migrating epidermis and sensory dendrite tips (Fan, L. et al., 2019). Moreover, SAX-7 might contribute to AM pore to dendrite tip attachment, because it's expression occurs at dendrite tips and throughout the dendrite length (Fan, L. et al., 2019) and SAX-7 may also assist dendrite morphogenesis in AM sensilla regarding its known roles for PVD development ((Salzberg, Y. et al., 2013), (Dong, K. et al., 2013) **Figure 4.5**, top panels). Since DLG-1 and HMR-1 are well known components of the CeAJ (reviewed in (Labouesse, 2006) **Figure 4.5**, top and middle panels), which are interconnecting AM dendrite tips, AMsh, AMso and the epidermis ((Ward, S. et al., 1975), (Perkins, L. A. et al., 1986)), the author of this study assumes that they could assist AM dendrite towing.

c. Polarity factors and KMN-components contribute to AM morphogenesis

Besides the adhesion molecules mentioned above, the polarity factor PAR-6 is also proposed to contribute to AM morphogenesis (Fan, L. et al., 2019). The PAR-6 expression pattern was found to be similar to DYF-7 expression. Remarkably, also some cases of *par-6* mutant embryos with expanded DYF-7 expression at dendritic tips were observed. According to the authors' suggestion, PAR-6 could act upstream of DYF-7, thereby contributing to connecting dendrite tips and epidermis. The findings clearly show stretched AM pores (highlighted by PAR-6) after moderate RPN-6.1 depletion (**Figure 3.6B**), which seems to resemble the altered DYF-7 pattern shown in *par-6* mutants by (Fan, L. et al., 2019). PAR-6 is part of the aPAR-complex, which is crucial for epithelial apicobasal cell polarity in tissues of diverse organisms (reviewed in (Chen, J. and Zhang, M., 2013), (Von Stetina, S. and Mango, S. E., 2015)) and vital for establishment of neural polarity (reviewed in (Takano, T. et al., 2019)).

The data exhibit impaired pore morphogenesis and incorrect spatio-temporal attachment of AM pores to AM dendrite tips after RPN-6.1 depletion using PAR-6 as a marker for apical polarity (**Figure 3.6B**). Thus, RPN-6.1 in some way impinges on PAR-6 to establish the apical lumen of the AM pore. Since multiple UPS factors have diverse influence on neural polarity (e.g. dendrite and axon extension) (reviewed in (Hamilton, A. M. and Zito, K., 2013)), RPN-6.1 may possibly function accordingly, potentially in removing factors that would prevent the *de novo* polarization which were observed in this study.

Furthermore, elegant work unveiled that sensory neuron morphogenesis is influenced by components of the kinetochore-microtubule coupling machinery (Knl1/Mis12/Ndc80-complex, KMN network) (Cheerambathur, D. K. et al., 2019). The authors discovered the positioning of KMN network components within head sensory neurons: Their findings show that KNL-1 (Kinetochore NuLl) is expressed throughout the microtubule-rich sensory neurites and GIP-2 (a subunit of the microtubule-nucleating γ-tubulin complex) is localized at the dendrite tips from comma to 2.5-fold stage embryos. They suggest, that "... the microtubule coupling function of the KMN network is required for the initial stages of dendritic extension during embryogenesis…" and that "… the KMN network is critical for proper extension of microtubule-rich dendrites" (Cheerambathur, D. K. et al., 2019). They also hypothesize, that the KMN network might assist neural development through microtubule stabilization.

Taken together, this study hypothesizes that RPN-6.1 might contribute to correct AM pore apical lumen establishment and attachment of the AM pore to dendrite tips (**Figure 4.5**, top panel). Moreover, the findings showing tubulin cables within anteriorly translocating sensory dendrites (**Figure 3.10B**) and the findings from (Cheerambathur, D. K. et al., 2019), allow the author of the dissertation to presume that KMN components (KNL-1, GIP-2) might aid in stabilizing microtubule-rich AM dendrites during their elongation process (**Figure 4.5**, middle panel), which might again be influenced by RPN-6.1. Notably, it is currently unclear how the initial rearrangement of dendrite microtubules during the start of towing is taking place, a very fascinating question to be tackled in future experiments.

4.5. A working model for embryonic head sensilla and pharynx morphogenesis

This study unveils an interplay of coordinated force-creating events driving separable morphogenetic aspects and identifies possible contributions of multiple factors on distinct levels. To summarize these aspects of this study and further aspects from recent studies discussed above, a model for the morphogenesis of the embryo's head is proposed below (**Figure 4.5**).

First and foremost, this dissertation defines the event of AM dendrite elongation as dendrite towing (**Figure 4.1**, top panels, **Figure 4.5**). This includes the anterior migration of the epidermal cells (head enclosure), coupled migration of embedded AM pores (target tissue) which are attached to AM dendrite tips, hereby exerting pulling forces on AM dendrite bundles. These events eventually facilitate passive elongation of AM dendrites. Importantly, towing occurs while AM neural cell bodies are stationery. Additionally, this study concludes that *de novo* apicobasal polarization and collective apical constriction within anterior most cells at the tip of the embryo's head could facilitate anterior translocation of OL, IL and CEP head sensilla pores, which are finally positioned adjacent to the prospective mouth (**Figure 4.2A, Figure 4.5**, top and middle panels). Also, the conclusion is made that apical constriction within arcade cells drives the formation of an arcade funnel, which seems to connect the mouth opening to the developing pharynx (**Figure 4.2B, Figure 4.5**). The author assumes this funnel is encircled by dendrite bundles of head sensory organs.

Importantly, besides the fact that dosage-dependent depletion of RPN-6.1 effects AM sensilla morphogenesis, it enabled the separation of AM dendrite towing from apical constriction. Thus the findings lead to the suggestion that the UPS factor RPN-6.1 plays specific roles for correct AM pore morphogenesis and precise spatio-temporal cell-cell attachment between AM pores and dendrite tips (**Figure 4.5**, top panel). RPN-6.1 thereby facilitates AM sensilla morphogenesis through supporting AM dendrite towing, and RPN-6.1 plays a role in connecting the mouth opening and the pharynx. Taken together, the author was able to separate two different morphogenetic forces for facilitating head sensilla development – dendrite towing and apical constriction – differentially affected by the UPS activator RPN-6.1.

Taking all conclusions discussed above together, the author of this dissertation proposes the following sequence of events and key molecular factors for each event: Firstly, the AM pore is established and spatio-temporally precisely interconnected to the AM dendrite tips, the AM sheath and the migrating epidermis by adherens junctions (DLG-1/HMR-1) (**Figure 4.5**, top panels). In addition, DYF-7 and DEX-1 seem to contribute to the correct AM pore morphogenesis and its attachment to the AM dendrite tips. Additional cell-cell adhesion molecules like SAX-7 may contribute to pore-dendrite attachment and possibly AM dendrite stabilization. Due to progressing anterior epidermal migration (head enclosure), the embedded AM pore translocates anteriorly while the AM neural cell bodies stay behind. This creates a pulling force in attached AM dendrite tips which is driving their passive elongation (AM dendrite towing) (**Figure 4.5**, top and middle panels). Hereby, microtubule-connected KMN-components like KNL-1 and CAM molecules like SAX-7 might contribute to the stabilization of AM dendrites to prevent their rupture during dendrite towing (**Figure 4.5**, middle panel). Additionally, pore shape and correct linkage to AM dendrites and likewise to the migrating epidermis need to be maintained. Besides efficient AM dendrite towing, also *de novo* apico-basal polarity establishment (NMY-2/MLC-4) and apical constriction events occur at the anterior most part of the head, whereby anterior translocation of CEP, IL, OL and OLQ sensilla pores proceeds (**Figure 4.5,** top and middle panel). At the same time, apical constriction within arcade cells creates a shallow funnel.

Moreover, between comma and 1.5-fold stage also multiple additional migration events occur within the embryonic head. For example, the pharynx extends anteriorly until it is attached to the mouth opening and develops into a pharyngeal tube (**Figure 4.5**, middle and bottom panel), the nerve ring is developing and non-sensory neural cells (e.g. RME, AVA, AVE, AVD) translocate posteriorly. The author of this study suggests that these developing tissues within the head might push the AM neural cell bodies slightly in posterior direction. Thus, AM dendrites move passively while several other cells at this stage actively migrate posteriorly, which has been wrongly described as retrograde extension (Heiman, M. G. and Shaham, S., 2009), since no efforts of lineage tracing had been undertaken by these authors. In contrast, this dissertation demonstrates by lineage tracing and usage of appropriate, early markers for the entire AM organ, that AM morphogenesis occurs by dendrite towing.
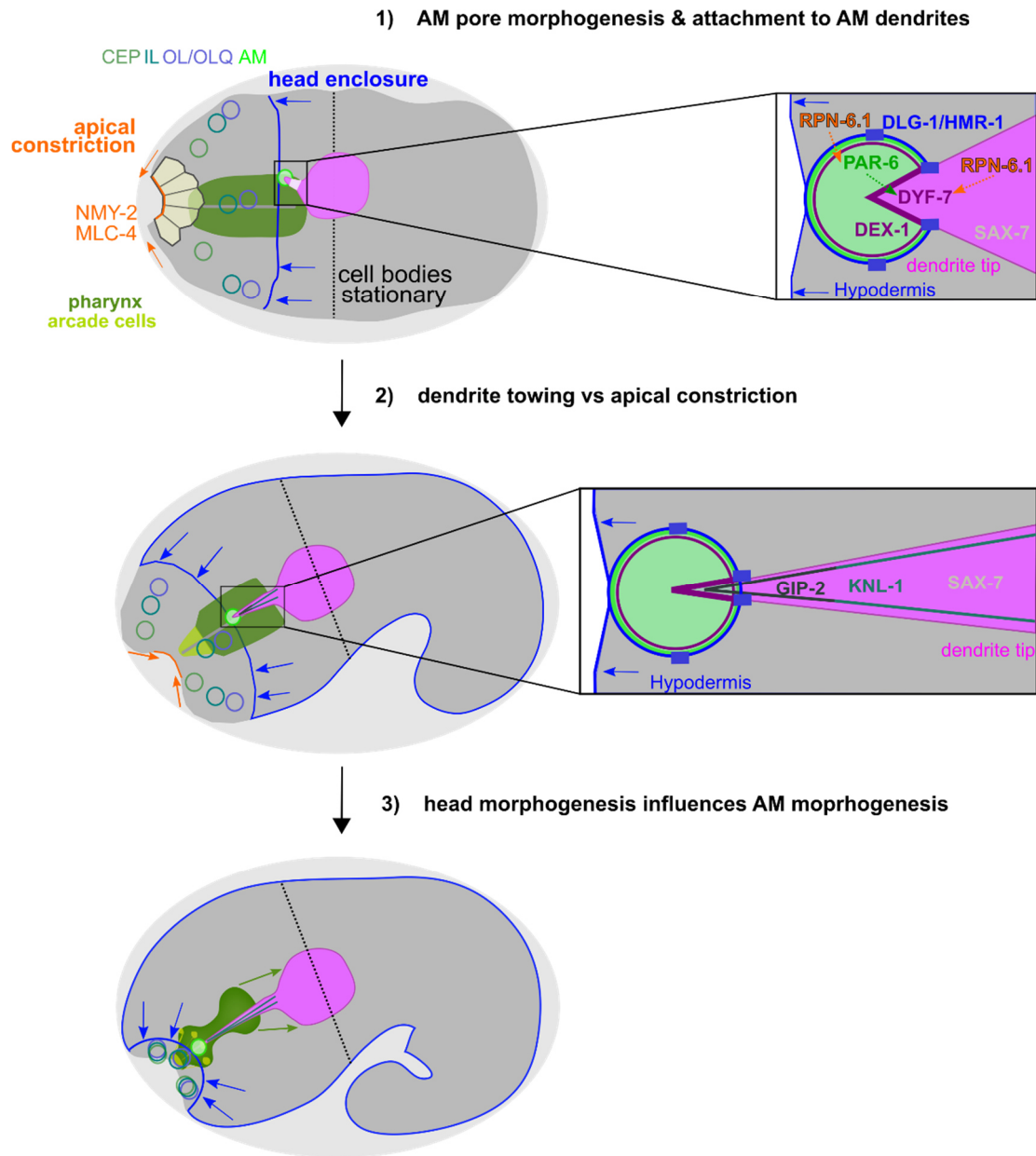
Figure 4.5: Working model for morphogenetic and possible molecular interactions facilitating AM sensilla development

Proposed schematic model depicting multiple coupled morphogenetic and molecular aspects which might contribute to embryonic AM sensilla development.

5. Outlook

With the main focus of this study laying on investigating the morphogenesis of AM sensilla (AM dendrite towing), the author additionally was able to show that apical constriction plays a role for translocation of IL/OL/CEP sensilla pores. The findings unveil that IL/OL/CEP pores translocate collectively, anterior of the epidermal leading edge, coherent with *de novo* apically polarizing constricting cells and independently from AM pores (**Figure 4.2A**). Also, RPN-6.1 depletion allowed the separation of apical constriction-driven translocation of the other head sensilla from head enclosure-driven AM dendrite towing (**Figure 4.1**, top panels). Additionally, using the an *unc-119* marker (highlighting all ciliated neurons), the results showed apical constriction of neuroblasts with their tips encircling the prospective mouth (**Figure 3.11C, Figure 4.2B**). However, during these stages, a substantial number of neuronal cell migration events occur within the head region, which is strongly impairing precise analysis of IL, OL and CEP neuronal cells. The author of this study thus recommends the usage of specific markers for IL, OL or CEP neural cells in combination with the *mir-124* AM specific markers and PAR-6 markers used in this study, to gain more detailed insight into their morphogenesis. Additionally, lineage tracing of all IL/OL/CEP cells (socket, sheath, neural cell bodies) and epidermal cells, like performed for AM cells in this study ((Sulston, J. E. et al., 1983), **Figure 3.1**, **Figure 4.4**) would allow to precisely visualize all migration events during morphogenesis of those sensilla. The author believes that a more detailed analysis of all head sensilla cell movements (not just AMso translocation) would strengthen the assumption that IL/OL/CEP sensilla morphogenesis is dissimilar from AM dendrite towing. Furthermore, based on the presented findings, the author concludes that *de novo* apical constriction in arcade cells *(pha-4* marker) creates a funnel, which seems to be facilitating mouth and pharynx linkage (**Figure 3.11C, Figure 4.2B**). Also, bottle-shaped cells were apparent at the anterior tip of the embryo concurrent with NMY-2 accumulation (**Figure 3.11B**). The author hypothesizes, that apical constriction might not just contribute to interconnection of mouth opening and arcade cells but could also facilitate invagination of the mouth opening. To confirm this assumption, investigation of mouth-opening development in the embryo in greater detail is recommended. This could be accomplished by combining pharynx markers (e.g. *pha-4*) with either non-muscle-myosin (NMY-2), membrane (*Ppie-1::PLC-PH*) or epidermal markers (VAB-10) in head-on view imaging. To further characterize the role of RPN-6.1 for pharynx to mouth attachment and mouth-invagination, depletion of RPN-6.1 in embryos with these markers would need to be analyzed in even greater detail. To validate the proposed possible molecular functions of RPN-6.1, cell-cell adhesion (DYF-7, DEX-1, SAX-7, DLG-1, HMR-1), polarity PAR-6 and KMN components (KNL-1) should be analyzed in experiments that combine these markers. First and foremost, the molecular interactions concerning RPN-6.1 have to be defined more clearly in future experiments, for instance by ubiquitome profiling of embryos.

The findings of this study lead to the conclusion that RPN-6.1 is important for AM pore morphogenesis and attachment of AM pores to AM dendrites (**Figure 3.6, Figure 4.5**, top panels). The author executed first observations on RPN-6.1 expression within the embryo (using an RPN-6.1::GFP CRISPR strain), but it was not possible to detect specific RPN-6.1 signals. Creation of further RPN-6.1 marker constructs to visualize RPN-6.1 expression patterns is recommended. Furthermore, to gain more evidence about DYF-7 and DEX-1 function during AM dendrite towing, precise observation of DYF-7 and DEX-1 markers should be analyzed in concert with the specific AM markers used in this study (*pmir-124::GFP; pmir-124::mCherry*) or with PAR-6 markers and RPN-6.1 RNAi. Additionally, the author suggests that embryos with the loss-of-function *dex-1 (cs201)* (Cohen, J. D. et al., 2018) should be investigated for occurrence of possible phenotypes in AM sensilla pore morphogenesis. Also, DYF-7 positioning is suggested to be influenced by PAR-6, based on findings showing spread DYF-7 signal at dendrite tips in *par-6 (m/z)* mutant embryos (Fan, L. et al., 2019). Remarkably, the stretched AM pore phenotype (PAR-6) after RPN-6.1 depletion shown in this study (**Figure 3.6B**) resembles the phenotype shown by (Fan, L. et al., 2019). It is suggested that observing DYF-7 expression after PAR-6 depletion might provide insights into a possible interaction of all three factors (RPN-6.1, PAR-6, DYF-7), which could facilitate correct morphogenesis of the AM pore and thus efficient AM dendrite towing. Furthermore, possible roles of the cell adhesion molecules SAX-7, DLG-1 and HMP-1 for AM dendrite towing need to be analyzed more closely, which could be performed by examination of their expression pattern in combination with the specific AM marker used in this study (pmir-124::GFP/mCherry) and highlighting of the AM pores (PAR-6). Especially the CeAJ factors DLG-1 and HMP-1 should be of great importance for efficient AM dendrite towing, because of their known function of attaching AM cells to epidermis (reviewed in (Labouesse, 2006)). The author also believes that the KMN-component KNL-1 might be of importance for stabilizing AM dendrites during their extension via pulling force due to findings from (Cheerambathur, D. K. et al., 2019), thus a deeper investigation is recommended. Since pharynx extension (one of multiple migration events) occurs at the same time span as AM development, combined observation of both would be shedding more light onto mutual regulatory principles.

References

Acconcia, F. et al. (2009). "Ubiquitin in trafficking: the network at work". *Experimental Cell Research, 315*(9), 1610–1618.

Adler, C. E. et al. (2006). "UNC-6/Netrin induces neuronal asymmetry and defines the site of axon formation". *Nat Neurosci, 9*, 511–518.

Alqadah, A. et al. (2016). "Stochasticleft-right neuronal asymmetry in Caenorhabditis elegans". *Phil.Trans.R.Soc.B, 371*.

Altun, Z. (2017). "Nervous system in the embryo, development of the nerve ring". *WormAtlas*. doi:10.3908/wormatlas.4.2

Altun, Z. F. and Hall, D. H. (2009). "Introduction". *WormAtlas*. doi:10.3908/wormatlas.1.1

Altun, Z. F. and Hall, D. H. (2009A). "Epithelial system, hypodermis". *WormAtlas*. doi:10.3908/wormatlas.1.13

Altun, Z. F. and Hall, D. H. (2009B). "Epithelial system, interfacial cells". *WormAtlas*. doi:10.3908/wormatlas.1.15

Altun, Z. F. and Hall, D. H. (2009C). "Epithelial system, atypical cells". *WormAtlas*. doi:10.3908/wormatlas.1.16

Altun, Z. F. and Hall, D. H. (2009D). "Epithelial system, seam cells". *WormAtlas*. doi:10.3908/wormatlas.1.14

Altun, Z. F. and Hall, D. H. (2010). "Nervous system, neuronal support cells". *WormAtlas*. doi:10.3908/wormatlas.1.19

Altun, Z.F. and Hall, D.H. (2011). "Nervous system, general description". *WormAtlas*. doi:10.3908/wormatlas.1.18

Altun, Z.F. et al. (2009). "High resolution map of Caenorhabditis elegans gap junction proteins". *Dev.Dyn., 238*, 1936-1950.

Anderson, D. C. et al. (2008). "Polarization of the C. elegans embryo by RhoGAP-mediated exclusion of PAR-6 from cell contacts". *Science*(320), 1771-1774.

Aratyn-Schaus, Y. et al. (2011). "Dynamic and structural signatures of lamellar actomyosin force generation". *Mol.Biol.Cell, 22*, 1330-1339.

Baas, P. W. and Lin, S. (2011). "Hooks and comets: the story of microtubule polarity orientation in the neuron". *Dev. Neurobiol., 71*, 403-418.

Baas, P. W. et al. (1988). "Polarity orientation of microtubules in hippocampal neurons: uniformity in the axon and nonuniformity in he dendrite". *Proc. Natl. Acad. Sci. USA, 85*, 8335-8339.

Bacaj, T. et al. (2008). "Glia are essential for sensory organ function in C. elegans". *Science, 322*(5902), 744–747.

Baker, P. C. and Schroeder, T.E. (1967). "Cytoplasmatic filaments and morphogenetic movement in the amphibian neural tube". *Dev. Biol., 15*, 432-450.

Bargmann, C. (2006). "Chemosensation in C. elegans". *WormBook (ed. The C. elegans Research Community), WormBook*. doi:doi/10.1895/wormbook.1.123.1

Bargmann, C.I and Horvitz, H.R. (1991). "Control of larval development by chemosensory neurons in Caenorhabditis elegans". *Science, 251*, 1243-1246.

Bargmann, C.I. and Mori, I. (1997). "Chemotaxis and thermotaxis". In *C. elegans II (ed. D.L. Riddle et al.)* (pp. 717–737). Cold Spring Harbor, New York, from altun & hall, 2010: Cold Spring Harbor Laboratory Press.

Bender, K.J. and Tussel, L.O. (2012). "The physiology of the axon initial segment". *Annu. Rev. Neurosci., 35*, 249-265.

Benjamini et al. (2006). "Adaptive linear step-up procedures that control the false discovery rate". *Biometrika, 93*(3), 491–507.

Bergamasco, C. and Bazzicalupo, P. (2006). "Chemical sensitivity in C. elegans". *Cell Mol. Life Sci., 63*, 1510-1522.

Bingol, B. and Schuman, E.M. (2005). "Synaptic protein degradation by the ubiquitin proteasome system". *Curr. Opin. Neurobiol., 15*, 536–541.

Bloom, A.J. et al. (2007). "The requirement for Phr1 in CNS axon tract formation reveals the corticostriatal boundary as a choice point for cortical axons". *Genes and Development, 21*(20), 2593–2606.

Bokhove, M. and Jovine, L. (2018). "Structure of zona pellucida module proteins". *Curr. Top. Dev. Biol., 130*, 413-442.

Brenner, S. (1973). "The genetics of behavior". *Br. Med. Bull, 29*, 269-271.

Brenner, S. (1974). "THE GENETICS OF CAENORHABDZTZS ELEGANS". *Genetics, 77*, 71-94.

Brodu, V. and Casanova, J. (2006). "The RhoGAP crossveinless-c links trrachaeless and EGFR signaling to cell shape remodeling in Drosophila tracheal invagination". *Genes.Dev., 20*, 1817-1818.

Bush, K. T. et al. (1990). "Neural tube formation in the mouse: a morphometric and computerized three-dimensional reconstruction study of the relationship between apical constriction of neuroepithelial cells and the shape of the neuroepithelium". *Anat. Embryol(Berl), 181*, 49-58.

Byerly, L. et al. (1976). "The life cycle of the nematode Caenorhabditis elegans". *Dev. Biol., 51*, 23-33.

Chatzigeorgiou, M. and Schafer, W.R. (2011). "Lateral facilitation between primary mechanosensory neurons controls nose touch perception in C. elegans". *Neuron, 70*, 299-309.

Cheerambathur, D. K. et al. (2019). "The Kinetochore-Microtubule Coupling Machinery Is Repurposed in Sensory Nervous System Morphogenesis". *Developmental Cell, 48*, 1-9. doi:https://doi.org/10.1016/j.devcel.2019.02.002

Chen, J. and Zhang, M. (2013). "The Par3/Par6/aPKC complex and epithelial cell polarity". *Experimental Cell Research, 319*, 1357-1364.

Chisholm, A. D. and Hardin, J. (2005). "Epidermal morphogenesis". *WormBook, ed. The C. elegans Research Community*. doi:doi/10.1895/wormbook.1.35.1

Chisholm, A. D. and Hsiao, T. I. (2012). "The C.elegans epidermis as a model skin. I: development, patterning and growth". *Wiley Interdiscip Rev Dev Biol., 1*(6), 861-878. doi:10.1002/wdev.79.

Clark, A. M. et al. (2010). "The microRNA miR-124 controls gene expression in the sensory nervous system of Caenorhabditis elegans". *Nucleic Acids Research, 38*(11), 3780-3793.

Cohen, J. D. et al. (2018). "Epithelial shaping by diverse apical extracellular matrices required the nidogen protein DEX-1 in C. elegans". *Genetics*. Retrieved from 10.1534/genetics.118.301752

Conde, C. et al. (2010). "Evidence for the Involvement of Lfc and Tctex-1 in Axon Formation". *The Journal of Neuroscience, 30*(19), 6793–6800.

Costa, M. et al. (1997). "The role of actin filaments in patterning the Caenorhabditis elegans cuticle". *Dev.Biol., 184*, 373-384.

Da Silva, J.S. et al. (2003). "RhoA/ROCK regulation of neuritogenesis via profilin IIa- mediated control of actin stability". *J. Cell. Biol., 162*, 1267–1279.

Daskalaki, A. et al. (2011). "Distinct intracellular motifs of Delta mediate its ubiquitylation and activation by Mindbomb1 and Neuralized". *The Journal of Cell Biology, 195*(6), 1017–1031.

Davidson, L. A. et al. (2002b). "Embryonic wound healing by apical contraction and ingression in Xaenopus laevis". *Cell. Motil. Cytoskeleton, 53*(3), 163-176. doi:10.1002/cm.10070

de Vrij, F.M. et al. (2004). "Protein quality control in Alzheimer's disease by the ubiquitin proteasome system". *Prog. Neurobiol., 74*, 249–270.

Ding, M. et al. (2004). "The cytoskeleton and epidermal morphogenesis in C.elegans". *Exp. Cell Res., 301*, 84-90.

Dong, K. et al. (2013). "An extracellular adhesion molecule complex patterns dendritic branching and morphogenesis". *Cell, 155*, 296-307.

Dong, X. et al. (2013). "An Extracellular Adhesion Molecule Complex Patterns Dendritic Branching and Morphogenesis". *Cell, 155*, 296-307. doi:http://dx.doi.org/10.1016/j.cell.2013.08.059

Doroquez, D. B. et al. (2014). "A high-resolution morphological and ultrastructural map of anterior sensory cilia and glia in Caenorhabditis elegans". *eLife*, 1-35. doi:10.7554/eLife.01948

Driscoll, M. and Kaplan, J. (1997). "Mechanotransduction". In *C. elegans II (ed. D.L. Riddle et al.)* (pp. 645–677). Cold Spring Harbor, New York, fromk altun and hall, 2010: Cold Spring Harbor Laboratory Press.

Dutta, P. et al. (2019). "Planar cell polarity in the C. elegans embryo emerges by differential retention of aPARs at cell-cell contacts". *Frontiers in Cell and Developmental Biology, 7*(209).

Dwyer, N. D. et al. (2001). "Polarized Dendritic Transport and the AP-1 !1 Clathrin Adaptor UNC-101 Localize Odorant Receptors to Olfactory Cilia". *Neuron, 31*, 277–287.

Evans, T. C. (2006). "Transformation and microinjection". *WormBook, ed. The C. elegans Research Community, WormBook*. doi:doi/10.1895/wormbook.1.108.1

Fan, L. et al. (2019). "A multicellular rosette-mediated collective dendrite extension". *eLIFE, 8:e38065*. doi:doi: 10.7554/eLife.38065

Forscher, P. and Smith, S.J. (1988). "Actions of cytochalasins on the organization of actin filaments and microtubules in a neuronal growth cone". *J Cell Biol, 107*, 1505–1516.

Ghysen, A. and Dambly-Chaudière, C. (2004). "Development of the zebrafish lateral line". *Current Opinion in Neurobiology, 14*, 67-73.

Gill, H. K. et al. (2016). "Integrity of Narrow Epithelial Tubes in the C.elegans Excretory System Requires a Transient Luminal Matrix". *PLOS Genetics*, 1-32. doi:10.1371/journal.pgen.1006205

Gilmour, D. et al. (2004). "Towing of sensory axons by their migrating target cells in vivo". *Nature Neuroscience, 7*(5), 49-492.

Goodwin, P.R. et al. (2012). "Cyclin-dependent kinase 5 egulates the polarized trafficking of neuropeptide-containing dense-core vesicles in aenorhabditis elegans motor neurons". *J. Neurosci., 32*, 8158-8172.

Grill, B. et al. (2007). C. elegans RPM-1 regulates axon termination and synaptogenesis through the Rab GEF GLO-4 and the Rab GTPase GLO-1". *Neuron, 55*(4), 587–601.

Grimbert, S. et al. (2020, April 28). "Multi-tissue patterning drives anterior morphogenesis of the C. elegans embryo". doi:https://doi.org/10.1101/2020.04.27.064469

Hall, D.H. et al. (2017). "Introduction to C. elegans Embryo Anatomy". *WormAtlas*. doi:doi:10.3908/wormatlas.4.1

Hamilton, A. M. and Zito, K. (2013). "Breaking it Down: The Ubiquitin Proteasome System in Neural Morphogenesis". *Hindawi Publishing Corporation, Neural Plasticity*. doi:http://dx.doi.org/10.1155/2013/196848

Hamilton, A.M. et al. (2012). "Activity dependent growth of new dendritic spines is regulated by the proteasome". *Neuron, 74*(6), 1023–1030.

Hao, J. C. et al. (2001). "C. elegans slit acts in midline, dorsal-ventral, and anterior-posterior guidance via the SAX-3/Robo receptor". *Neuron, 32*, 25–3.

Hardin, J. and Keller, R. (1988). "The behaviour and function of bottle cells during gastrulation of Xenopus laevis". *Development, 103*, 211-230.

Hegde, A.N. and Upadhya, S.C. (2007). "The ubiquitin–proteasome pathway in health and disease of the nervous system". *TRENDS in Neurosciences, 30*(11), 588-595. doi:10.1016/j.tins.2007.08.005

Heiman, M. G. and Shaham, S. (2009). "DEX-1 and DYF-7 Establish Sensory Dendrite Length by Anchoring Dendritic Tips during Cell Migration". *Cell, 137*, 344-355.

Hilliard, M. A. and Bargmann, C. L. (2006). "Wnt Signals and Frizzled Activity Orient Anterior-Posterior Axon Outgrowth in C. elegans". *Dev Cell, 10*, 379–390.

Hirokawa, N. et al. (2010). " Molecular motors in neurons: transport mechanisms and roles in brain function, development, and disease". *Neuron, 68*, 610-638.

Hohenester, E. and Yurchenco, P. D. (2013). "Laminins in basement membrane assembly". *Cell Adhes. Migr., 7*, 56-63.

Hoopfer, E.D. et al. (2006). "Wlds protection distinguishes axon degeneration following injury from naturally occurring developmental pruning". *Neuron, 50*, 883–895.

Huber, A. B. et al. (2003). "Signaling at the growth cone: Ligand-Receptor Complexes and the Control of Axon Growth and Guidance". *Annu. Rev. Neurosci., 26*, 509-563.

Itoh, M. et al. (2003). "Mind bomb is a ubiquitin ligase that is essential for efficient activation of Notch signaling by Delta". *Developmental Cell, 4*, 67–82.

Ja´zwi´nska, A. et al. (2003). "Epithelial tube morphogenesis during Drosophila tracheal development requires Piopio, a luminal ZP protein". *Nature Cell Biology, 5*(10), 895-901.

Jiang, L. I. and Sternberg, P. W. (1999). "Socket Cells Mediate Spicule Morphogenesis in Caenorhabditis elegans Males". *Developmental Biology, 211*, 88-99.

Jovine, L. et al. (2002). "The ZP domain is a conserved module for polymerization of extracellular proteins". *Nat.Cell Biol., 4*, 457-461.

Kaplan, J. M. and Horvitz, H. R. (1993). "A dual mechanosensory and chemosensory neuron in Caenorhabditis elegans". *Proc. Natl. Acad. Sci., 90*, 2227-2231.

Kapustina, M. et al. (2013). "Compression and dilation of the membrane-cortex layer generates rapid changes in cell shape". *The Journal of Cell Biology, 200*(1), 95-108.

Kawabe, H. et al. (2010). "Regulation of Rap2A by the ubiquitin ligase Nedd4-1 controls neurite development". *Neuron, 65*(3), 358–372.

Keith, S. A. et al. (2016). "Graded proteasome dysfunction in Caenorhabditis elegans activates an adaptive response involving the conserved SKN-1 and ELT-2 transcription factors and the autophagy-lysosome pathway". *PLoS Genet.*

Kelliher, M.T. et al. (2019). "Microtubule control of functional architecture in neurons". *Current Opinion in Neurobiology, 57*, 39-45.

Kemphues, K. et al. (1988). "Identification of genes required for cytoplasmic localization in early C. elegans embryos". *Cell, 52*, 311–320.

Kim, A.H. et al. (2009). "A centrosomal Cdc20-APC pathway controls dendrite morphogenesis in post-mitotic neurons". *Cell, 136*(2), 322–336.

Klompstra, D. et al. (2015). "An instructive role for C.elegans E-cadherin in translating cell contact cues into cortical polarity". *Nature Cell Biology, 17*(6), 726-735. doi:10.1038/ncb3168

Kunz, P. et al. (2021). "Differential Thresholds of Proteasome Activation Reveal Two Separable Mechanisms of Sensory Organ Polarization in C. elegans". *Frontiers in Cell and Developmental Biology, 9*. doi:10.3389/fcell.2021.619596

Kuo,C.T. et al. (2005). "Dendrite-specific remodelingof Drosophila sensory neurons requires matrix metalloproteases, ubiquitin-proteasome, nd ecdysone signaling". *Proc. Natl. Acad. Sci. U. S. A., 102*, 15230-15235.

Kwok, S.F. et al. (1999). "Characterization of two subunits of Arabidopsis 19S proteasome regulatory complex and its possible interaction with the COP9 complex". *J Mol Biol, 285*, 85–95.

Labouesse, M. (2006). "Epithelial junctions and attachments". *WormBook, ed. The C. elegans Research Community, WormBook*. doi:doi/10.1895/wormbook.1.56.1

Lecuit, T. et al. (2011). "Force generation, transmission, and integration during cell and tissue morphogenesis". *Annu.Rev.Cell Dev.Biol., 27*, 157-184.

Ledent, V. (2002). "Postembryonic development of the posterior lateral line in zebrafish". *Development, 129*, 597-604.

Lee, J. Y. and Harland, R. M. (2007). "Actomyosin contractility and microtubules drive apical constriction in Xenopus bottle cells. *Developmental Biology, 311*, 40-52.

Lee, J.-Y and Harland, R. M. (2010). "Endocytosis Is Required for Efficient Apical Constriction during Xenopus Gastrulation". *Current Biology, 20*(3), 253-258.

Lee, J.-Y. and Goldstein, B. (2003). "Mechanisms of cell positioning during C. elegans gastrulation". *Development, 130*, 307-320.

Lefcort, F. and Bentley, D. (1989). "Organization of cytoskeletal elements and organelles preceding growth cone emergence rom an identified neuron in situ". *J. Cell Biol., 108*, 1737–1749.

Legan, P.K. et al. (1997). "The mouse tectorins. Modular matrix proteins of the inner ear homologous to components of the sperm-egg adhesion system". *J. Biol. Chem., 272*, 8791–8801.

Lehmann, C. (2018). "Regulation of Epithelial Morphogenesis in Caenorhabditis elegans". *Dissertation, Faculty of Biological Sciences of the Johann Wolfgang Goethe University, Frankfurt am Main, Germany*.

Lewis, J. A. and Fleming, J. T. (1995). "Basic culture methods". In *Caenorhabditis elegans, Modern biological analysis of an organism (ed. Epstein, H.F. and Shakes, D.C.)* (pp. 4-27). California: Academic Press.

Li, H. et al. (2008). "RPM-1, a Caenorhabditis elegans protein that functions in presynaptic differentiation, negatively regulates axon outgrowth by controlling SAX-3robo and UNC-5/UNC5 activity". *Journal of Neuroscience, 28*(14), 3595–3603.

Lier, S. and Paululat, A. (2002). " The proteasome regulatory particle subunit Rpn6 is required for Drosophila development and interacts physically with signalosome subunit Alien/CSN2". *Gene, 298*, 109-119.

Loverde, J.R. and Pfister, B.J. (2015). "Developmental axon stretch stimulates neuron growth while maintaining normal electrical activity, intracellular calcium flux, and somatic morphology". *Frontiers in Cellular Neuroscience, 9*(308), 1-15.

Low, I. I. et al. (2019). "Morphogenesis of neurons and glia within an epithelium". *Development, 146*.

Macara, I. G. (2004). "Parsing the polarity code". *Nat. Rev. Mol. Cell Biol.*(5), 220-231.

Mango, S. E. (2007). "The C. elegans pharynx: A model for organogenesis". *Wormbook (ed. The C. elegans Research Community)*. doi:doi/10.1895/wormbook.1.129.1

Marston, D. J. et al. (2016). "MRCK-1 Drives Apical Constriction in C. elegans by Linking Developmental Patterning to Force Generation". *Current Biology, 26*, 2079-2089.

Martin, A. C. (2009). "Pulsed contractions of an actin-myosin network drive apical constriction". *Nature, 457*, 495-499.

Martin, A. C. and Goldstein, B. (2014). "Apical constriction: themes and variations on a cellular mechanism driving morphogenesis". *Development, 141*, 1987-1998. doi:10.1242/dev.102228

Martin, A. C. et al. (2009). "Pulsed contractions of an actin-myosin network drive apical constriction". *Nature, 457*, 495-499.

Massaly, N. et al. (2015). "Roles of the ubiquitin proteasome system in the effects of drugs of abuse". *Frontiers in Molecular Neuroscience, 7*(99), 1-11.

Matilainen, O. et al.;. (2013). "Insulin/IGF-1 signaling regulates proteasome activity through the deubiquitinating enzyme UBH-4". *Cell Rep., 3*, 1980–1995.

McLachlan, I.G. and Heiman, M.G. (2013). "Shaping dendrites with machinery borrowed from epithelia". *Current Opinion in Neurobiology, 23*, 1005-1010.

Ménager, C. et al. (2004). "PIP3 is involved in neuronal polarization and axon formation". *Journal of Neurochemistry, 89*, 109–118.

Metcalfe, W. K. (1985). "Sensory Neuron Growth Cones Comigrate With Posterior Leteral Line Primordial Cells in Zebrafish". *The Journal of Comperative Neurology, 238*, 218-224.

Michaux, G. et al. (2000). "CHE-14, a protein with sterol-sensing domain, is required for apical sorting in C. elegans ectodermal epithelial cells". *Curr. Biol., 10*, 1098-1107.

Mikkonen, E. et al. (2017). "Immunohistochemical analysis reveals variations in proteasome tissue expression in C. elegans". *PLoS One*.

Mizeracka, K. and Heiman, M. G. (2015). "The many glia of a tiny nematode: studying glial diversity using Caenorhabditis elegans". *WIREs Dev Biol, 4*, 151–160. doi:10.1002/wdev.171

Moore, D. C. P. et al. (1987). "Morphometric analyses of changes in cell shape in the neuroepithelium of mammalian embryos". *J. Anat., 155*, 87-99.

Mori, I. (1999). "Genetics of chemotaxis and thermostaxis in the nematode Caenorhabditis elegans". *Annu. Rev. Genet., 33*, 399-422.

Mukhopadhyay, S. et al. (2008). "Sensory signaling-dependent remodeling of olfactory cilia architecture in C. elegans". *Developmental Cell, 14*, 762–774.

Nakata, K. et al. (2005). "Regulation of a DLK-1 and p38 MAP kinase pathway by the ubiquitin ligase RPM-1 is required for presynaptic development". *Cell, 120*(3), 407-420.

Namba, T. et al. (2015). "Extracellular and intracellular signaling for neuronal polarity". *Physiol.Rev., 95*, 995–1024.

Nance, J. and Zallen, J. A. (2011). "Elaborating polarity: PAR proteins and the cytoskeleton". *Development, 138*, 799-809.

Nance, J. et al. (2003). "C.elegans PAR-3 and PAR-6 are required for apicobasal asymmetries associated with cell adhesion and gastrulation". *Development, 130*(22), 5339-5350.

Nelson, W. J. et al. (2013). "Roles of cadherins and catenins in cell-cell adhesion and epithelial cell polarity". *Prog. Mol. Biol.Transl. Sci., 116*, 3-23.

Nishimura, T. et al. (2005). "PAR-6–PAR-3 mediates Cdc42-induced Rac activation through the Rac GEFs STEF/Tiam1". *Nature Cell Biology, 7*(3), 270-277.

Ou, C.-Y. and Shen, K. (2010). "Neuronal Polarity in C. elegans". *Developmental Neurobiology, 71*, 554-566.

Owaribe, K. and Masuda, H.;. (1982). "Isolation and characterization of circumferential microfilament bundles from retinal pigmented epithelial cells". *J.Cell Biol., 95*, 310-315.

Pan, C. et al. (2006). "Multiple Wnts and frizzled receptors regulate anteriorly directed cell and growth one migrations in Caenorhabditis elegans". *Dev Cell, 10*, 367–377.

Pathare, G. R. et al. (2012). "The proteasomal subunit Rpn6 is a m9olecular clamp holding the core and regultory subcomplexes together". *PNAS, 109*(1), 149-154.

Perens, E.A. and Shaham, S. (2005). ""C.elegans daf-6 Encodes a Patched-Related Protein Required for Lumen Formation". *Developmental Cell, 8*, 893-906.

Perkins, L. A. et al. (1986). "Mutant Sensory Cilia in the Nematode Caenorhabditis elegans". *Developmental Biology, 117*, 456-487.

Plaza, S. et al. (2010). "From A to Z: apical structures and zona pellucida-domain proteins". *Trends Cell Biol., 20*, 524-532.

Podbilewicz, B and White, J. G. (1994). "Cell fusions in the developing epithelia of C. elegans". *Dev. Biol., 161*, 408-424.

Pohl, C. et al. (2012). "Actomyosin-based Self-organization of cell internalization during C. elegans gastrulation". *BMC Biology, 10*(94), 1-16. Retrieved from http://www.biomedcentral.com/1741-7007/10/94

Portereiko, M. F. and Mango, S. E. (2001). "Early morphogenesis of the Caenorhabditis elegans pharynx". *Dev. Biol., 233*, 482-494.

Portereiko, M.F. and Mango, S.E. (2001). "Early morphogenesis of the Caenorhabditis elegans pharynx". *Dev Biol., 233*(2), 482-94.

Prasad, B. C. and Clark, S. G. (2006). "Wnt signaling establishes anteroposterior neuronal polarity and requires retromer in C. elegans". *Development, 133*, 1757–1766.

Priess, J. R. and Hirsh, D. I. (1968). "Caenorhabditis elegans morphogenesis: the role of the cytoskeleton in elongation of the embryo". *Dev.Biol., 117*, 156-173.

Quinn, C. C. et al. (2006). "UNC-6/netrin and SLT-1/slit guidance cues orient axon outgrowth mediated by MIG-10/RIAM/lamellipodin". *Curr Biol, 16*, 845–853.

Roh-Johnson, M. et al. (2012). "Triggering a Cell Shape Change by Exploiting Pre-Existing Actomyosin Contractions". *Science, 335*(6073), 1232–1235.

Rolls, M. M. and Jegla, T. J. (2015). "Neuronal polarity: an evolutionary perspective". *The Journal of Experimental Biology, 218*, 572-580.

Rual, J-F. et al. (2004). "Toward Improving Caenorhabditis elegans Phenome Mapping With an ORFeome-Based RNAi Library". *Genome Research, 14*, 2162-2168. doi:10.1101/gr.2505604

Saito, A. et al. (1997). "cDNA cloning and functional analysis of p44.5 and p55, two regulatory subunits of the 26S proteasome". *Gene, 203*, 241–250.

Sakaguchi-Nakashima, A. et al. (2007). "LRK-1, a C. elegans PARK8-Related Kinase, Regulates Axonal-Dendritic Polarity of SV Proteins". *Curr Biol, 17*, 592–598.

Salbreux, G. et al. (2012). "Actin cortex mechanics and cellular morphogenesis". *Trends Cell Biol, 22*, 536-545.

Salzberg, Y. et al. (2013). "Skin-derived cues control arborization of sensory dendrites in Caenorhabditis elegans". *Cell, 155*, 308-320.

Salzberg, Y. et al. (2013). "Skin-Derived Cues Control Arborization of Sensory Dendrites in Caenorhabditis elegans". *Cell, 155*, 308-320. doi:http://dx.doi.org/10.1016/j.cell.2013.08.058

Sapède, D. et al. (2002). "Cell migration in the postembryonic development of the fish lateral line". *Development, 129*, 605-615.

Sasakura, H. et al. (2005). "Maintenance of neuronal positions in organized ganglia by SAX-7, a Caenorhabditis elegans homologue of L1". *EMBO J, 24*, 1477-1488.

Sawin, E.R. et al. (2000). "C.elegans locomotory rate is modulated by the environment through a dopaminergic pathway and by experience through a serotonergic pathway". *Neuron, 26*, 619-631.

Sawyer, J. M. et al. (2010). "Apical constriction: A cell shape change that can drive morphogenesis". *Developmental Biology, 341*, 5-19. doi:10.1016/j.ydbio.2009.09.009

Schaefer, A.M. et al. (2000). "rpm-1, a conserved neuronal gene that regulates targeting and synaptogenesis in C. elegans". *Neuron, 26*(2), 345–356.

Schaeffer, C. et al. (2009). "Analysis of uromodulin polymerization provides new insights into the mechanisms regulating ZP domain-mediated protein assembly". *Mol. Biol. Cell, 20*, 589-599.

Schindelin, J. et al. (2012). "Fiji: an open-source platform for biological-image analysis". *Nature Methods, 9*(7), 676-682.

Schwarz, L.A. and Patrick, G.N. (2012). "Ubiquitin-dependent endocytosis, trafficking and turnover of neuronal membrane proteins". *Molecular and Cellular Neuroscience, 49*(3), 387–393.

Sengupta, P. (2007). "Generation and modulation of chemosensory behaviors in C. elegans". *Pflugers Arch - Eur J Physiol, 454*, 721-734. doi:10.1007/s00424-006-0196-9

Shi, S. et al. (2003). "Hippocampal Neuronal Polarity Specified by Spatially Localized mPar3/mPar6 and PI 3-Kinase Activity". *Cell, 112*, 63–75.

Shin, J.E. and DiAntonio, A. (2011). "Highwire regulates guidance of sister axons in the Drosophila mushroom body". *The Journal of Neuroscience, 31*(48), 17689–17700.

Shum, A.S. and Copp, A.J. (1996). "Regional differences in morphogenesis of the neuroepithelium suggest multiple mechanisms of spinal neurulation in the mouse". *Anatomy and Embryology (Berl)., 194*, 65-73.

Solecki, D. J. et al. (2006). "Neuronal polarity in CNS development". *Genes & Development, 20*, 2639-2647.

Sugiyama, Y. et al. (2008). "Symmetrically dividing cell specific division axes alteration observed in proteasome depleted C. elegans embryo". *Mech. Dev., 25*, 743–755.

Sulston, J. E. et al. (1980). "The Caenorhabditis elegans male: Postembryonic development of nongonadal structures". *Dev.Biol., 78*(2), 542–576. doi: 10.1016/0012-1606(80)90352-8

Sulston, J. E. et al. (1983). "The Embryonic Cell Lineage of the Nematode Caenorhabditis elegans". *Developmental Biology, 100*, 64-119.

Sulston, J. et al. (1975). "Dopaminergic neurons in the nematode Caenorhabditis elegans". *J.Comp.Neurol., 163*, 215-226.

Sulston, J.E. and Horvitz, H.R. (1977). "Post-embryonic cell lineages of the nematode Caenorhabditis elegans". *Dev. Biol., 56*, 110-156.

Szu-Yu Ho, T. and Rasband, M.N. (2011). "Maintenance of neuronal polarity". *Dev. Neurobiol., 71*, 474-482.

Tabuse, Y. et al.;. (1998). "Atypical protein kinase C cooperates with PAR-3 to establish embryonic polarity in Caenorhabditis elegans". *Development, 125*, 3607-3614.

Tahirovic, S. and Bradke, F. (2009). "Neural Polarity". *Cold Spring Harb Perspect Biol, 1*, 1-17. doi:10.1101/cshperspect.a001644

Takano, T. et al. (2017). "Discovery of long-range inhibitory signaling to ensure single axon formation". *Nature Communications, 8*(33).

Takano, T. et al. (2019). "Neuronal Polarity: Positive and Negative Feedback Signals". *Frontiers in Cell and Developmental Biology, 7*(69), 1-10.

Tessier-Lavigne, M. and Goodman, C. S. (1996). "The Molecular Biology of Axon Guidance". *Science, 274*(5290), 1123-1133. Retrieved from http://www.jstor.org/stable/2891572

Tessier-Lavigne, M. and Goodman, C. S. (1996). "The Molecular Biology of Axon Guidance". *Science, 274*, 1123-1133.

Totong, R. et al. (2007). "PAR-6 is required for junction formation but not apicobasal polarization in C. elegans embryonic epithelial cells". *Development*(134), 1259-1268.

Troemel, E.R. et al. (1997). " Reprogramming chemotaxis responses: sensory neurons define olfactory preferences in C. elegans". *Cell, 91*, 161-169.

Upadhya, S.C. and Hegde, A.N. (2005). "Ubiquitin-proteasome pathway components as therapeutic targets for CNS maladies". *Curr. Pharm. Des., 11*, 3807–3828.

Vicente-Manzanares, M. et al. (2009). "Non-muscle myosin II takes centre stage in cell adhesion and migration". *Nature Reviews. Molecular Cell Biology, 10*, 778-790. doi:10.1038/nrm2786

Von Stetina, S. and Mango, S. E. (2015). "PAR-6, but not E-cadherin and !!!-integrin, is necessary for epithelial polarization in C. elegans". *Developmental Biology, 403*, 5-14.

Wadsworth, W. G. et al. (1996). "Neuroglia and pioneer neurons express UNC-6 to provide global and local netrin cues for guiding migrations in C.elegans". *Neuron, 16*, 35-46.

Ward, S. et al. (1975). "Electron microscopical reconstruction of t5he anterior sensory anatomy of the nematode C. elegans". *J.Comp.Neurol., 160*, 313-337.

Ware, R.W. et al. (1975). "The nerve ring of the nematode C.elegans: Sensory input and motor output". *J.Comp.Neurol., 162*, 71-110. Retrieved 05 07, 2021, from https://www.wormatlas.org/Ware_build0.2/Ware_build0.2.1.html

Way, J.C. and Chalfie, M. (1989). "he mec-3 gene of Caenorhabditis elegans requires its own product for maintained expression and is expressed in three neuronal cell types". *Genes Develop., 3*, 1823-1833.

Wes, P.D. and Bargmann, C.I. (2001). "C. elegans odour discrimination requires asymmetric diversity in olfactory neurons". *Nature, 410*, 698-701.

White, J. (1988). "The Anatomy". In *The nematode C. elegans (ed. W.B. Wood)* (pp. 81-122). Cold Spring Harbor, New York, citation from Altun & hall, 2009, hypodermis: Cold Spring Harbor Laboratory Press.

White, J. G. et al. (1986). "The Structure of the Nervous System of the Nematode Caenorhabditis elegans". *Philosophical Transactions of the Royal Society of London. Series B, Biological Sciences, 314*(1165), 1-340. Retrieved from http://www.jstor.org/stable/2990196

Wood, W. B. (1988a). "Introduction to C. elegans biology". In *The nematode C. elegans (ed. W.B. Wood)* (pp. 1-16). Cold Spring Harbor, New York: Cold Spring Harbor Laboratory Press.

Wood, W. B. (1988b). "Embryology". In *The nematode C. elegans (ed. W.B. Wood)* (pp. 215-241). Cold Spring Harbor, New York: Cold Spring Harbor Laboratory Press.

Wright, K. A. and Thomson, J. N. (1981). " The buccal capsule of C. elegans (Nematoda: Rhabditoidea): An ultrastructural study". *Canad. J. Zool., 59*, 1952-1961. doi:10.1139/z81-266

Yi, J.J. et al. (2010). "TGF-β Signaling Specifies Axons During Brain Development". *Cell, 142*(1), 144–157.

Yip, Z. C. and Heiman, M. G. (2018). "Ordered arrangement of dendrites within a C. elegans sensory nerve bundle". *eLIFE, 7*(e35825), 1-26. doi:https://doi.org/10.7554/eLife.35825

Yoshimura, S. et al. (2008). "mls-2 and vab-3 Control glia development, hlh-17/Olig expression and glia-dependent neurite extension in C. elegans". *Development, 135*(13), 2263–2275.

Yoshimura, T. et al. (2006). "Ras regulates neuronal polarity via the PI3-kinase/Akt/GSK-3beta/CRMP-2 pathway". *Biochem. Biophys Res. Commun., 340*, 62–68.

Yun, C. (2008). "Proteasomal adaptation to environmental stress links resistance to proteotoxicity with longevity in Caenorhabditis elegans". *Proc. Natl. Acad. Sci. U.S.A., 105*, 7094–7099.

Zhang, X. et al. (2007). "Dishevelled promotes axon differentiation by regulating atypical protein kinase C". *Nature Cell Biology, 9*(7), 743-754.

List of Abbreviations

AM	amphid
a/b	apical/basal
a/p	anterior/posterior
ADE	anterior deirid
aECM	apical Extra-Cellular-Matrix
AIS	axon initial segment
AMsh	amphid sheath cell
AMso	amphid socket cell
arc	arcade cells
ATP	adenosin Tris phosphat
C. elegans	*Caenorhabditis elegans*
CAM	cell adhesion molecules
CeAJ	*C.elegans*Apical Junction
CEP	cephalic sensilla
d/v	dorsal/ventral
DEX	Dendrite EXtension defective
DLG	Discs Large
DUB	deubiquinating enzymes
DYF	abnormal DYe Filling
GFP	green fluorescent protein
GIP	Gamma-tubulin Interacting Protein
HMR	HaMmeRhead embryonic lethal
hyp	hypodermal cells
IL	inner labial sensilla
KMN	kinetochore-microtubule coupling machinery
KNL	Kinetochore NuLl
L	lateral
L/R	left/right
L1-L4	larval stages 1 to 4
LLP	Lateral line primordium
mCherry	red fluorescent protein
miRNA	micro RNA
MLC	Myosin Light Chain
NM II/NMY-2	Non-muscle MYosin
NR	nerve ring
OL	outer labial sensilla
P cells	pocket cells
PAR	abnormal embryonic PARtitioning of cytoplasm
PDE	posterior deirid
RNAi	RNA interference
RPN-6	proteasome Regulatory Particle, Non-ATPase-like
SAX	Sensory AXon guidance
TZ	transition zone

Ub	ubiquitin
UPS	ubiquitin proteasome system
UV	ultra violet
v	ventral
VAB-10	Variable ABnormal morphology
wt	Wild type
ZP	zona pellucida

List of Figures

List of Tables